FINAL REPORT
U.S. Department of Energy

INTERFACIAL REDUCTION-OXIDATION MECHANISMS GOVERNING FATE AND TRANSPORT OF CONTAMINANTS IN THE VADOSE ZONE

Principal Investigator: Baolin Deng
Institution: Department of Civil and Environmental Engineering
University of Missouri-Columbia
DengB@missouri.edu

Co-Principal Investigator: Edward C. Thornton
Institution: Environmental Technology Division
Pacific Northwest National Laboratory
edward.thornton@pnl.gov

Co-Principal Investigator: Kirk J. Cantrell
Institution: Environmental Technology Division
Pacific Northwest National Laboratory

Co-Principal Investigator: Khris B. Olsen
Institution: Environmental Technology Division
Pacific Northwest National Laboratory

Co-Principal Investigator: James E. Amonette
Institution: Environmental Molecular Sciences Laboratory (MSEL)
Pacific Northwest National Laboratory

Project Number: EMSP-70088
Grant Number: DE-FG07-99ER15011
Grant Project Officers: Roland Hirsch and Mark Gilbertson
Project Duration: 9/15/1999 – 9/14/2001

Table Of Contents

EXECUTIVE SUMMARY

Immobilization of toxic and radioactive metals (e.g., Cr, Tc, and U) in the vadose zone by *In Situ* Gaseous Reduction (ISGR) using hydrogen sulfide (H_2S) is a promising technology for soil remediation. Earlier laboratory and field studies have shown that Cr(VI) can be effectively immobilized by treatment with dilute gaseous H_2S. The objective of this project is to characterize the interactions among H_2S, the metal contaminants, and soil components. Understanding these interactions is needed to assess the long-term effectiveness of the technology and to optimize the remediation system. Proposed research tasks include: (A) Evaluation of the potential catalytic effect of mineral surfaces on the rate of Cr(VI) reduction by H_2S and the rate of H_2S oxidation by air; (B) Identification of the reactions of soil minerals with H_2S and determination of associated reaction rates; (C) Evaluation of the role of soil water chemistry on the reduction of Cr(VI) by H_2S; (D) Assessment of the reductive buffering capacity of H_2S-reduced soil and the potential for emplacement of long-term vadose zone reactive barriers; (E) Evaluation of the potential for immobilization of Tc and U in the vadose zone by reduction and an assessment of the potential for remobilization by subsequent reoxidation. Through a collaborative effort in the last three years, Tasks A, B, C, and E have been completed, resulting in a much improved understanding of reaction kinetics and mechanisms involved in the Cr(VI)-H_2S-O_2-Soil System and the treatability for Tc and U. Research on Task C will continue in the one-year period of no-cost extension granted to this project. The result will be submitted to the Department of Energy by October 2003 as a supplement to this report.

Chromium (VI) Reduction by Hydrogen Sulfide in Aqueous Media: Aqueous phase Cr(VI) reduction is being examined as a function of pH, Cr(VI) concentration, sulfide concentration, temperature, and ionic strength. Experiments with excess [Cr(VI)] over $[H_2S]_T$ indicated that the molar amount of sulfide required for the reduction of one molar of Cr(VI) was 1.5, suggesting the following stoichiometry: $2CrO_4^{2-} + 3H_2S + 4H^+ \rightarrow 2Cr(OH)_{3(S)} + 3S_{(S)} + 2H_2O$. Further study with Transmission Electron Microscopy (TEM) and Energy-Dispersive X-Ray Spectroscopy (EDS) confirmed that chromium hydroxide and elemental sulfur were the stable products under the anaerobic condition.

The kinetics of Cr(VI) reduction by hydrogen sulfide was measured under various initial concentrations of Cr(VI) and sulfide, as well as pHs controlled by HEPES, phosphate, and borate buffers. Results showed that the overall reaction was second order, i.e., first order with respect to Cr(VI) and first order to sulfide. The reaction rate increased as pH was decreased, and the pH dependence correlated well with the fraction of fully protonated sulfide (H_2S) in the pH range of 6.5 to 10. The nature of buffers didn't influence the reaction rate significantly in the homogeneous system. A three-step mechanism was proposed for the reaction: formation of an inner sphere chromate-sulfide complex formation, intramolecular electron transfer to form intermediate Cr(IV) species, and subsequent fast reactions leading to the formation of Cr(III). Kinetic data under various pHs, ionic strengths, and concentrations of [Cr(VI)] and $[H_2S]_T$ agreed with this mechanism.

Catalysis of Elemental Sulfur Product on Cr(VI) Reduction by sulfide: Through well-controlled batch experiments performed in an anaerobic chamber, it is observed that while Cr(VI) reduction by sulfide can be described by a pseudo first order kinetics with respect to [Cr(VI)] initially, the rate was largely accelerated at the later stage of the reaction. Such an acceleration is likely due to the formation of some reaction intermediates and products. The Cr(III) species, mainly in the form of $Cr(OH)_{3(s)}$ under the experimental condition, didn't demonstrate any discernible effect on the reaction kinetics. Elemental sulfur is believed to be the main compound causing the accelerated Cr(VI) reduction.

Effect of Various Soil Minerals on Cr(VI) Reduction by Sulfide: Effects of mineral surfaces on Cr(VI) reduction by sulfide were investigated at pH range from7.67 to 9.07 buffered by borate under the anaerobic condition. Results showed that the minerals examined can be categorized into three groups. Illite exhibited dramatic catalytic effect on the reduction of Cr(VI) by sulfide. Al_2O_3 showed no obvious effect on the reaction. The third group, which includes kaolin, montmorillonite, SiO_2 and TiO_2, inhibited the reduction of Cr (VI) as compared to the control without minerals being present. In the illite system, low concentration of ferrous iron produced from the mineral dissolution is believed to be responsible for the rate acceleration by serving as an electron shuttle. The reaction rate increases with increasing Fe(II) concentration and at the later stage, the effect of elemental sulfur produced can be observed. When a strong Fe(II) chelating agent such as phenanthroline is added into the system, the effect of soluble iron from illite disappears. The inhibitive behavior observed for the third group is likely due to the uptake of elemental sulfur product on the mineral surfaces, so the catalytic effect from elemental sulfur is hindered.

Oxidation of H_2S by Iron Oxides: Iron oxides are well-known oxidizing reagents and oxidation catalysts for H_2S. It is thus expected that the quantity of H_2S required to remediate a site and the rate of treatment will typically be dependent upon the quantity and form of the iron oxides in the soils and not on the amount of contaminants present. A detailed experimental and modeling study was conducted to understand the interactions among hydrogen sulfide and iron oxides coated onto the quartz sand. The results illustrate that the reactions involving the ferric oxide ferrihydrite with H_2S under anaerobic and aerobic conditions can be largely understood from a mechanistic standpoint. The modeling effort provided significant insights on the processes controlling the H_2S breakthrough.

Immobilization of Cr, Tc, and U in Soils from Hanford Site: Preliminary tests were conducted to determine (i) if Tc and U in contaminated sediments can be effectively immobilized by exposure to diluted hydrogen sulfide gas and (ii) if H_2S-treated sediments can effectively retard the migration of Cr, Tc, and U in solutions that may potentially infiltrate through the treated zone. The results showed that the H_2S treatment resulted in about 50% of Tc being immobilized, but no significantly immobilization for U. Soils treated with H_2S could generate certain reductive capacity in soils and thus can be used as a permeable reactive barrier (PRB) for effective immobilization of Cr and to a lesser

degree, for Tc. Uranium was also immobilized in the soil columns, but the mechanism was unclear.

A long-term test lasting 835 days was conducted to provide information regarding whether or not reoxidation of chromium can occur after Cr(VI) is reduced in a contaminated sediment by gas treatment. No Cr(III) reoxidation was observed for the experimental time period.

ACKNOWLEDGMENTS

This project is supported by the Environmental Management Science Program (EMSP) of the Office of Science and Technology of the U.S. Department of Energy. The research was conducted at the Pacific Northwest National Laboratory (Richland, Washington), New Mexico Institute of Mining and Technology (Socorro, NM), and the University of Missouri-Columbia (Columbia, MO).

I. INTRODUCTION

Chromium contamination in the vadose zone has been identified at a number of DOE sites (e.g., Hanford, Pantex, and the Chemical Waste Landfill), as well as numerous nonfederal sites. Subsurface contamination with radionuclides such as technetium (Tc) and uranium (U) also takes place. For example, Tc is a constituent of the underground waste storage tanks at the Hanford Site and is present in the vadose zone owing to tank leakage. When surface water infiltrates through or groundwater level rises to the contaminated zone, Cr and the radionuclides leached out from the soil could serve as a constant source for groundwater contamination.

A promising technology for metal immobilization in the vadose zone, In-Situ Gaseous Reduction (ISGR), is developed by PNNL staff for the U.S. Department of Energy (DOE) (Thornton et al., 1999). Laboratory investigations have shown that Cr(VI) in soil samples can be effectively immobilized by treatment with diluted H_2S. A field test at White Sand Missile Range, New Mexico, has also been completed that resulted in 70% immobilization of Cr(VI). The field demonstration has further shown that H_2S gas can be handled safely for field application and residual H_2S gas can be recovered, so no secondary contamination takes place (ASME,1999). There are, however, many related scientific questions that need to be addressed. The exact immobilization kinetics and mechanism, including the reaction stoichiometry between Cr(VI) and hydrogen sulfide, are unknown. It is unclear whether the reduced chromium will remain in the stabilized form in the long term. Similar to chromium, Tc and U demonstrate substantially lower mobility in their reduced forms than in their oxidative species, and thus, may be immobilized by H_2S treatment. A sound mechanistic understanding of the geochemical processes as related to this process is critical to ensure successful deployment of ISGR for Cr and to explore whether this technology can be applied to other contaminants.

The primary objective of this study is to improve our understanding of the complex interactions among the contaminant metals, hydrogen sulfide (H_2S), and various soil constituents. Critical areas include the reaction kinetics and mechanisms for Cr(VI) reduction, assessment of potential catalysis by soil matrices, interaction of H_2S with iron oxides, and treatability of Tc and U by the gaseous H_2S.

The approach employed in this study consisted of conducting batch and column experiments to collect kinetic information, coupled with microscopic and spectroscopic studies and modeling effort, for acquiring a much better understanding of the reaction mechanisms. Aqueous batch tests were performed under well-controlled systems, including the use of pure oxides (e.g., Al_2O_3, SiO_2, FeOOH, Fe_2O_3) as surrogates of soil components, to obtain information regarding the major reactions and their associated rates and products. Soil column tests were conducted to obtain information regarding catalytic processes associated with H_2S oxidation and the consumption of H_2S by soil minerals, and the changes in soil reduction capacity associated with H_2S treatment. This was needed to predict the longevity of a reduced permeable barrier in the vadose zone.

Substantial progress has been made to better understand the interactions among Cr(VI), sulfide and soil minerals, as being summarized in the Sections II – V. Preliminary studies on the contaminant immobilization in the Hanford soil samples are described in Section VI.

II. CHROMIUM(VI) REDUCTION BY HYDROGEN SULFIDE IN AQUEOUS MEDIA: STOICHIOMETRY AND KINETICS

(Chulsung Kim, Qunhui Zhou, Baolin Deng, Edward C. Thornton, Huifang Xu)

INTRODUCTION

Chromium contamination has been found in many industrial and federal sites in the United States, due to accidental leakages and improper disposals associated with its widespread usage (Nriagu and Nieboer, 1988; Katz and Salem, 1994; Thornton and Amonette, 1999). Since some chromium chemicals are known to be toxic and carcinogenic (Costa, 1997), site remediation is often needed in order to reduce the risk to humans and ecosystems. Chromium exists as either Cr(VI) or Cr(III) species in natural water and soils and is redox active. The mobility of chromium in the environment largely depends on its oxidation states. Generally, Cr(VI) is quite mobile in soils and aquifers, whereas Cr(III) is mostly precipitated as hydroxides and adsorbed onto mineral surfaces. As a result, Cr(VI) could be immobilized and become less bioavailable when reduced to Cr(III).

Reduction of Cr(VI) could be coupled with the oxidation of numerous reductants including zero valent iron (Blowes et al., 1997; Pratt et al., 1997), divalent iron (Eary and Rai, 1988; 1989; Fendorf and Li, 1996; Sedlak and Chan, 1997; Pettine et al., 1998; Buerge and Hug, 1997; 1998; 1999; Seaman et al. 1999), Fe(II)-bearing minerals (Eary and Rai, 1989; Anderson et al., 1994; Ilton and Veblen, 1994; Ilton et al., 1997; Peterson et al., 1997), organic compounds (James and Bartlett, 1983; Goodgame and Hayman, 1984; Eary and Rai, 1991; Wittbrodt and Palmer, 1995), and H_2S (Schroeder and Lee, 1975; Smillie et al., 1981; Saleh et al., 1989; Pettine et al., 1994; 1998; Thornton and Amonette, 1999). Cr(VI) reduction is strongly pH dependent and subject to catalysis by dissolved and surface-bound metals (Deng and Stone, 1996a, b; Buerge and Hug, 1999).

Hydrogen sulfide is one of the strongest reductants that is capable of reducing Cr(VI). The reduction of Cr(VI) by H_2S has been demonstrated in a number of studies (Schroeder and Lee, 1975; Saleh et al., 1989; Fude et al., 1994) and may explain Cr(VI) reduction in the marine environment under sulfate-reducing conditions (Smillie et al., 1981). Pettine and co-workers (1994, 1998) reported that the kinetics of Cr(VI) reduction by H_2S under seawater conditions could be described by the following equation:

$$\frac{d[Cr(VI)]}{dt} = -k[Cr(VI)]^x[H^+]^y[H_2S]_T^z \qquad (1)$$

and according to their experiments, the reaction was pseudo first-order with respect to [Cr(VI)], total hydrogen sulfide, and proton activity. They also showed that Pb^{2+}, Cu^{2+}, Cd^{2+}, and Ni^{2+} at micromolar concentrations caused large increases of the reduction rates, while ionic strength had no effect on the reaction. Nevertheless, significant uncertainties in the reaction stoichiometries, kinetics, and mechanism still exist. Based on the large amount of sulfate production in the Cr(VI)-sulfide system, Pettine et al. (1994, 1998) suggested that sulfate was the major final product during the oxidation of sulfide by Cr(VI), but the exact reaction stoichiometry was not established. In fact, the amount of sulfate detected was much higher than the stoichiometric amount allowed via the reaction with Cr(VI) alone, which indicated the presence of other parallel reactions such as sulfide oxidation by oxygen.

Recently, the In Situ Gas Reduction (ISGR) approach has been under development for metal

immobilization in the vadose zone (Thornton and Amonette, 1999), in which hydrogen sulfide is used as a reductant for Cr(VI) and other contaminant metals. Laboratory investigations have shown that 90% of Cr(VI) in soil samples can be immobilized by treatment with diluted H_2S (Thornton and Amonette, 1997). A field test at White Sand Missile Range, New Mexico, has resulted in 70% immobilization of Cr(VI) (Thornton and Amonette, 1997). The field demonstration has further shown that H_2S gas can be handled safely for field application and residual H_2S gas can be recovered, so no secondary contamination takes place. There are, however, significant data gaps that needs to be addressed in order to properly evaluate the effectiveness of the technology.

As part of our overall effort to better understand the interactions among Cr(VI), H_2S, and soil minerals, this paper examined Cr(VI) reduction by H_2S in homogeneous aqueous phases. Reaction stoichiometry was investigated by monitoring the degree of reaction and the analysis of solid reaction products with Transmission Electron Microscopy (TEM). Reaction kinetics was measured in a pH range of 6.5 – 10 and a reaction mechanism was proposed to explain the reaction kinetics and the observed pH dependence.

MATERIALS AND METHODS

Milli-Q water (Millipore Corp., with resistivity of 18.2 MΩ-cm) was used for all experiments and the glassware was cleaned using 10 N HNO_3 and rinsed with Milli-Q water before use. Chemicals used were at least reagent grade and were from Sigma Chemicals (HEPES) and Fisher Scientific ($K_2Cr_2O_7$, $Na_2S{\cdot}9H_2O$, H_3BO_3, KH_2PO_4). Sulfide stock solution was prepared by dissolving $Na_2S{\cdot}9H_2O$ crystal in degassed water after rinsing to remove the oxidized surface layer. Sulfide stock solution was prepared anew immediately before the initiation of each experiment. Cr(VI) stock solution was prepared with $K_2Cr_2O_7$ in an amber bottle with degassed water.

Solution pH was controlled by various buffers including HEPES (N-[2-hydroxyethyl] piperazine-N′-[2-ethanesulfonic acid]) buffer (pH 6.6 to 8.2), phosphate buffer (pH 6.5 – 8.2), and borate buffer (pH 8.2 - 10.5). The concentration of each buffer was 0.08 M. Preliminary tests showed that there was no reactions between the buffers and Cr(VI) or buffers and sulfide.

Experimental procedures. Cr(VI) reduction in HEPES buffer solution followed the following procedure: 1000 ml of water was transferred into an amber bottle and purged with nitrogen gas to decrease oxygen content for 1 hr. Crystal sodium sulfide was then introduced into the aqueous phase and the bottle was covered with a Teflon dispenser screwed cap. Once sodium sulfide was dissolved, sulfide concentration was standardized by iodometric titration. An adequate amount of sulfide stock solution was transferred into acid washed amber vials containing Cr(VI) stock solution, degassed Milli-Q water, and buffer solution. The vials were closed immediately with Teflon-lined septa and crimp-sealed with aluminum caps. Each vial contained a total of 14.0 ml solution with a headspace less than 1% of the total volume. A typical reaction system had 20 μM Cr(VI), 200-800 μM total sulfide, and 0.08M buffer with a target pH range of 6.6-8.2. Several tests contained 200 μM Cr(VI) and 100μM sulfide, which were designed to investigate the stoichiometric amount of sulfide required for Cr(VI) reduction. The prepared vials were mounted onto the rotating shaker (Bellco. Glass Inc.) at 10 rpm. All tests were conducted in a temperature controlled room at 23.5±0.5 ^{o}C.

For Cr(VI) reduction in phosphate and borate buffers, 60-ml polypropylene syringes were used as

reactors. Preliminary experiments using different types of reaction vessels, including 60 ml polypropylene syringes, 14 ml amber glass bottles sealed with Teflon-lined septa, and 250 ml polypropylene bottles, gave the same kinetic results under otherwise the same experimental conditions. Preliminary experiments also showed that purging of Q-H_2O with N_2 gas for one hour prior to use did not affect Cr(VI) reduction kinetics. This implied that either the dissolved oxygen was still present even in the N_2-purged water in the experimental system or the oxidation of H_2S by oxygen didn't significantly affect the reduction of Cr(VI). This reaction vessel was a closed system to air after the system setup. Generally, reagents were prepared and added into the reaction vessel following the order: (1) preparing pH-buffered solution; (2) dissolving $Na_2S{\cdot}9H_2O$ crystals rinsed with Milli-Q water in the pH-buffered solution; (3) splitting pH-buffered Na_2S solution into polyethylene beakers; (4) adding the Cr(VI) stock solution, (5) withdrawing the solution into a 60 ml syringe, and (6) mixing on the rotor drum at 10 rpm and sampling as a function of time. This procedure will be adapted to investigate Cr(VI) reduction in the presence of minerals.

Ionic strength was not controlled in this study because our preliminary experiments and the literature (Pettine et al., 1994) all indicate that the effect of ionic strength is negligible when it is between 0.0 and 1.0 M. In this study, the ionic strength was always less than 0.1 M.

Analytical Methods. Aqueous Cr(VI) concentration was determined using the diphenylcarbazide colorimetric method (APHA, 1992). The absorbance was measured in a 1-cm cell at 540 nm on a spectrophotometer (Spectronic 20 Genesys, Spectronic Instruments). The method had a detection limit of 0.1 μM. Preliminary experiments showed that under the experimental concentration condition, the interference of reaction products such as elemental sulfur did not interfere with Cr(VI) analysis. Total H_2S in the stock solution was standardized with the standard iodometric titration method (APHA, 1992), and sulfide concentration during the reaction was monitored as a function of time by the methylene blue method (APHA, 1992). Sulfate in the samples was analyzed using turbidimetric method (APHA, 1992). For selected samples, sulfite and thiosulfate were analyzed by high-performance liquid chromatography (HPLC) after derivatization Rethmeier et al., 1997). A Perkin-Elmer HPLC system with an LC 410 pump and a LS 40 fluorescence detector was employed to perform this measurement. The detection limits for sulfite and thiosulfate was 5 and 1μM, respectively. A UV spectrophotometer (Genesys 5, Milton Roy Company) was used to detect qualitatively the presence of polysulfide at the wavelength of 290nm (Chen and Morris, 1972). An Orion 420A pH meter was used to measure pH after a 2-point calibration.

In order to detect elemental sulfur formation without the interference from oxygen, a set of experiments was performed in an anaerobic chamber (Models 855-AC, Plas-Labs Inc.). Samples were prepared with 400 μM of Cr(VI) and 200 μM of sulfide at pH of 7.4 in HEPES buffer, following the same procedures as mentioned before. After 2 weeks of reaction, the solid products were analyzed with Transmission Electron Microscopy (TEM) and associated Energy-Dispersive X-ray Spectroscopy (EDS). The solution containing colloidal particles of the reaction products was dropped on a holey Cu grids coated with carbon and allowed to dry. The grids were then placed in a specimen holder for analysis. All TEM and EDS results were carried out on a JEOL 2010 high-resolution TEM and an Oxford Link ISIS EDS system at the University of New Mexico. Mineral standards were used for quantification of collected EDS data (Xu and Wang, 2000).

RESULTS AND DISCUSSION

Reaction Stoichiometry. While it is known that the reduction of Cr(VI) results in the production of Cr(III) species (Deng, 1995), oxidation of sulfide could potentially generate sulfur species in several oxidation states including $S_2O_6^{2-}$, SO_3^{2-}, SO_4^{2-}, S^0, and polysulfides. To illustrate, below are two possible stoichiometries corresponding to elemental sulfur and sulfate production:

$$2CrO_4^{2-} + 3H_2S + 4H^+ \rightarrow 2Cr(OH)_{3(S)} + 3S_{(S)} + 2H_2O \quad (2)$$

$$8CrO_4^{2-} + 3H_2S + 10H^+ + 4H_2O \rightarrow 8Cr(OH)_{3(S)} + 3SO_4^{2-} \quad (3)$$

The equilibrium constants for the reactions (2) and (3) at pH 7.00 are log K = 91, and 323, respectively (calculated from data in 37), so both reactions are energetically favorable. Based on the reactions (2) and (3), the stoichiometric ratio of sulfide to Cr(VI) is 1.5 when elemental sulfur is stable in the system, and 0.38 when sulfate is the final product.

Earlier studies suggested that sulfate was the major product based on the very high concentration of sulfate detected during Cr(VI) reduction by H_2S (Pettine et al. 1994). This was not nearly conclusive, however, since sulfate concentration was significantly higher than the amount required by the reaction stoichiometry (Eq. 3). Similar results were observed in our experiments where high concentration of sulfate was detected after 2 hours of reaction. In addition, non-negligible concentration of thiosulfate and low concentration of sulfite were also detected in the solution. Because sulfate, sulfite, and thiosulfate were known products of sulfide oxidation by oxygen (Cline & Richards, 1969; O'Brien & Birkner, 1977; Zhang & Millero, 1993), these three sulfur species identified in our samples could be derived from the oxidation of sulfide with oxygen present in the reactor. These different forms of sulfur products therefore do not provide proof for sulfate as a final product of sulfide oxidation by Cr(VI).

In order to establish the correct reaction stoichiometry, we monitored the reaction between 200 μM of Cr(VI) and 106 μM of sulfide in the HEPES buffer system (pH 8.2) until all sulfide was consumed. As shown in Fig. 2-1, the reduction of 200μM of Cr(VI) by 106μM of sulfide indicated that after sulfide was used up, aqueous Cr(VI) concentration remained constant at 128 μM. The total amount of Cr(VI) reduced in the experiment is approximately 72 μM. Thus, the ratio of consumed [H_2S] to reduced [Cr(VI)] is about 1.5. Experiments at pH 7.8 similarly generated stoichiometry ratios ranging from 1.44 to 1.60 with average value of 1.51 (data not shown). The results suggest that the appropriate reaction stoichiometry between Cr(VI) and sulfide is Eq. 2, in which elemental sulfur serves as the stable oxidation product of sulfide. Fig. 2-1 also shows that sulfide concentration in the control is decreased by approximately 4% at 1-hr, and 10% at 2-hr in the absence of Cr(VI). Thus, the loss of sulfide, possibly due to evaporation or oxidation with oxygen, is not significant during the first 1 to 2 hrs of kinetic data collection for most of the tests conducted in this study. The loss of sulfide through these processes under high Cr(VI) over sulfide as used for assessing the reaction stoichiometry should be even less due to the rapid oxidation by Cr(VI).

Fig. 2-2a is a TEM image of the stabilized final products of Cr(VI) reduction by sulfide. There are two distinct regions, area A with amorphous structure and area B consisting of particles with 100 nm in diameter. EDS spectra (Fig. 2-2b) shows that sulfur is the major species in area A, while in area B, sulfur, chromium, and oxygen coexist and chromium appears to be present as coatings of the sulfur layer. It is important to notice that the peak for oxygen is not associated with the sulfur peak as in area A, thus, the sulfur must be mainly in the form of elemental sulfur. Elemental sulfur as the oxidation product of sulfide by Cr(VI) has not been reported before. Direct detection of elemental sulfur here supports the conclusion that the overall reaction for

Cr(VI) reduction by sulfide primarily follows the stoichiometry represented by Eq. 2.

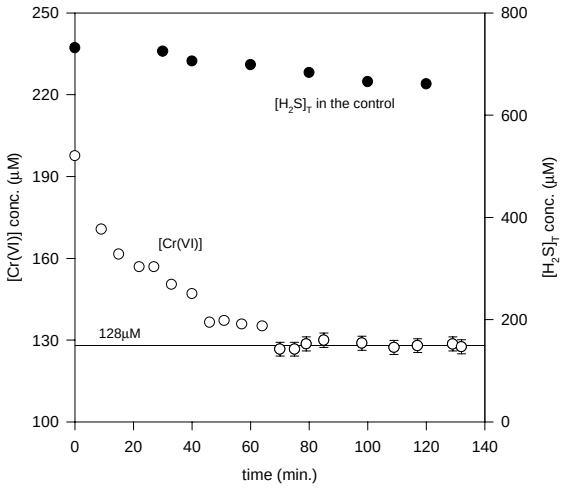

Figure 2-1. Reaction between 200 μM Cr(VI) reduction with 106 μM sulfide showed that the ratio of sulfide in the system to the amount of Cr(VI) consumed is close to 1.5. The figure also indicated that sulfide in the control was stable during the time period tested. (pH 8.2 controlled by HEPES buffer).

Reaction Kinetics. Kinetics of Cr(VI) reduction by hydrogen sulfide depends on reactant concentrations and pH. The rate equation by Pettine et al. (1994, 1998) (see Eq. 1) was based on experiments at very low Cr(VI) (1.9 μM) and high H_2S (~ 400 - 1400 μM) concentrations in the pH range of 7.5 - 10.5. Our experiments used much higher Cr(VI) concentrations that are likely to be present at hazardous waste sites and over a wider pH range, aiming to see whether the kinetics remain the same. According to Eq. 1, the rates of Cr(VI) reduction at constant pH can be expressed as:

$$d[\mathrm{Cr(VI)}]/dt = -k[\mathrm{Cr(VI)}]^x[\mathrm{H_2S}]^y \qquad (4)$$

where x and y are the reaction order and k is the overall rate constant. When sulfide concentration is much higher than Cr(VI) concentration, the rate equation can be simplified to:

$$d[\mathrm{Cr(VI)}]/dt = -k_{obs}[\mathrm{Cr(VI)}]^x \qquad (5)$$

with $k_{obs} = k[\mathrm{H_2S}]^y$.

Rates of Cr(VI) reduction under various initial concentrations of Cr(VI) are presented in Fig. 2-4. Since Cr(VI) concentrations used (20 - 40 μM) are much less than the sulfide concentration (~ 800 mM), sulfide concentration will remain near constant during the initial stage of the reaction. It is clear that plots of log[Cr(VI)] versus time are linear ($0.979 < r^2 < 0.983$) under various initial Cr(VI) concentrations (Fig. 2-4), suggesting a first order reaction with respect to Cr(VI). This result agrees with the earlier studies (Pettine et al., 1994, 1998). The rate constants k_{obs} obtained from our experimental results are 0.0305 min^{-1} (S.D.: 0.00057) in this HEPES buffered system at pH 7.4.

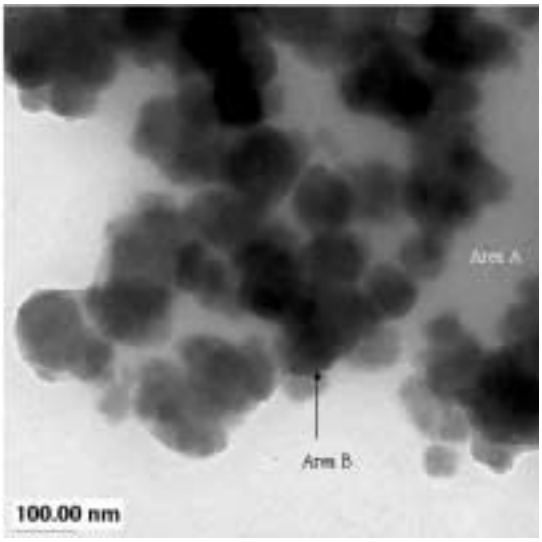

Figure 2-2. (a) Bright-field TEM image of the reaction products showing aggregates of elemental S (area A) and amorphous Cr-hydroxide (area B). It is proposed that the reduced Cr is amorphous $Cr(OH)_3$.

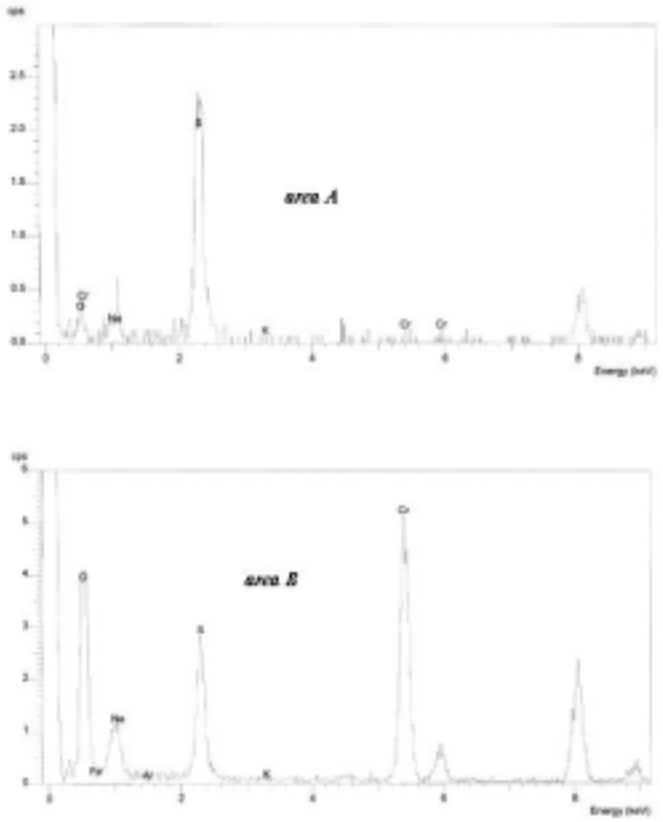

Figure 2-3. EDS spectra from area A and area B of the TEM image in Figure 2-2. The spectrum from area B shows Cr, O, and S peaks. The S peak results from elemental S coating Cr-hydroxide particles. All Cu peaks (both K and L lines) result from Cu grid holding the specimen.

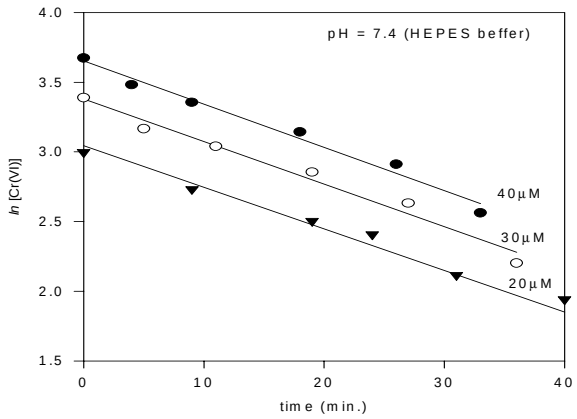

Figure 2-4. The log [Cr(VI)] versus t plots under different initial Cr(VI) concentrations at pH 7.4 (HEPES buffer). The reaction is pseudo-first order with respect to Cr(VI).

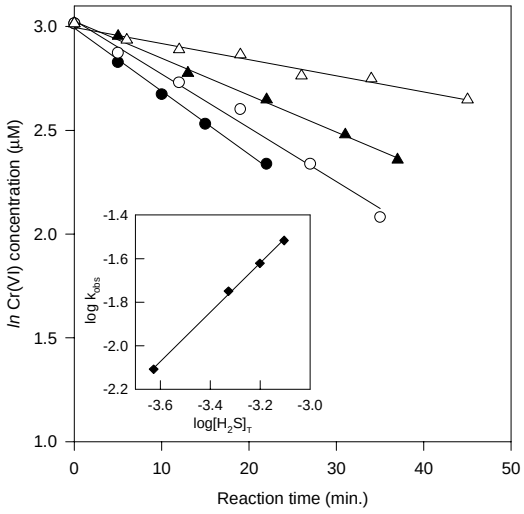

Figure 2-5. Effects of initial sulfide concentration on Cr(VI) reduction. The reaction is first-order with respect to the total sulfide concentration.

Effect of initial sulfide concentrations (236 – 790 μM) on the reduction of Cr(VI) (20μM) was also studied in HEPES buffered solutions with pH 7.4. As shown in Fig. 2-5, Cr(VI) reduction rate increases as initial sulfide concentration is increased. Linear plots of *ln*[Cr(VI)] vs. t are obtained under all sulfide concentrations. The inset is a plot of log k_{obs} versus log $[H_2S]_T$. The data can be fitted by a straight line with a slope of 1.13 (r^2 = 0.9988), suggesting a first order reaction with respect to H_2S. It is thus clear that Eq. 4 applies for Cr(VI) reduction in the concentration ranges used in this study.

Solution pH has a dramatic effect on Cr(VI) reduction by sulfide (Fig. 2-6). The reduction rate increased as pH was decreased. The linear plots of ln [Cr(VI)] vs. t indicate that the reaction was pseudo first order with respect to Cr(VI) in all buffer solutions. The slopes of these linear plots, i.e. the observed rate constants (k_{obs}), are shown in Fig. 2-7 as a function of pH. The results reveal that k_{obs} decreased significantly as pH was increased. It should be noted that the solid curve in the Fig. 2-6 is not the fitting curve of the data but the calculated mole fraction of hydrogen sulfide as a function of pH ($f = [H_2S]/([H_2S] + [HS^-] + [S^{2-}])$). The curve and the data agree well, suggesting that the rate dependence on pH can be explained by assuming that H_2S is the major species involved in Cr(VI) reduction.

The types of buffers seemed to have no effect on the reaction rate in the homogeneous aqueous system. The k_{obs} values of Cr(VI) reduction by H_2S at the same pH buffered with borate and

phosphate were the same (results not shown). Additionally, the changes of k_{obs} were smooth as a function of pH.

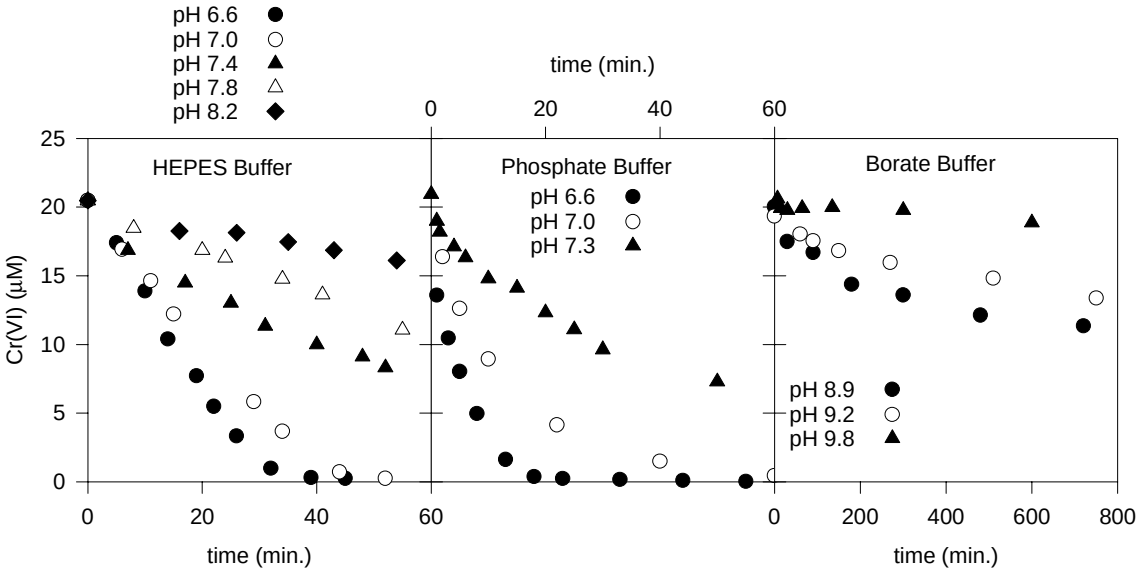

Figure 2-6. Effect of pH on Cr(VI) reduction in solutions buffered by HEPES (a), phosphate (b), and borate (c) buffers.

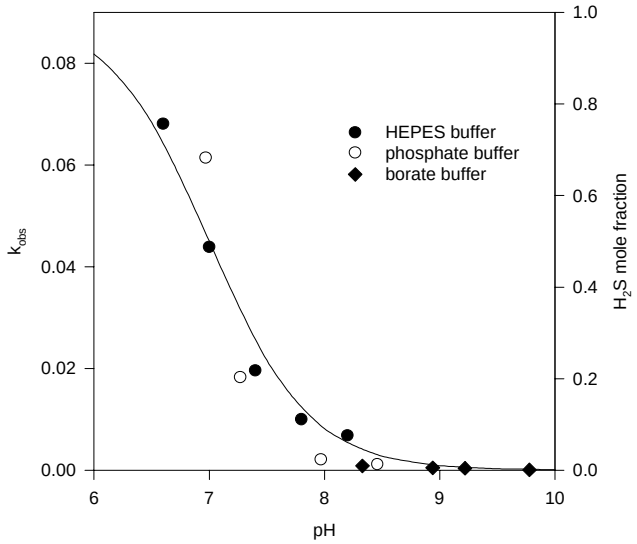

Figure 2-7. The change of k_{obs} as a function of pH. The dots are the experimental results and the curve is the mole fraction of H_2S species calculated based on the dissociation constants of hydrogen sulfide: $pK_1 = 7.05$ and $pK_2 = 19$.

Reaction Mechanism. The first-order reduction with respect to Cr(VI) and reductant concentrations are consistent with the previous studies of Cr(VI) reduction by H_2S (Pettine et al., 1994, 1998), ascorbate (Dixon et al., 1995), and thiol compounds (Connett and Wetterhahn, 1985; Shi et al., 1999). The studies on Cr(VI) reduction by thiols have shown that the reaction begins with the formation of a Cr(VI) thioester followed by either a redox reaction involving a second molecule of thiol or an unimolecular redox reaction of the thioester (Connett and Wetterhahn, 1985). The Cr(VI)-thioesters have been identified spectroscopically (e.g. with glutathione, cysteine, and thiolactate), suggesting that the reaction take place by an inner-sphere mechanisms.

The electron transfer step could take place faster or slower than the formation of the thioester, depending on the reductant. This thioester formation step limits Cr(VI) reduction by some reductants (e.g., thiolactate, thiomalate, and penicillamine), since the electron transfer step is faster than the rate of Cr(VI) ligand exchange, or Cr(VI)-thioester formation (Connett and Wetterhahn, 1985).

We propose that the attack of chromate by hydrogen sulfide also proceeds by the formation of a precursor. A three-step mechanism proposed for the reduction of Cr(VI) by H_2S is illustrated by Eq. 6-12. The first step (Eqs 6 and 7) involves the formation of a chromium-sulfur precursor like $\{H_2O_4CrS\}^{2-}$. The attack of chromate ion by a H_2S molecule (Eq 6) is most likely, considering the lock of an ionic strength effect on the reaction and the rate dependence on H_2S observed in this study (Fig 2-6). The effect of pH can be alternatively interpreted by a HS^- attack of $HCrO_4^-$ (Eq 7) since HS^- is the main species in most of the pH range examined, however, this mechanism is not supported by the fact that ionic strength does not affect the reaction. The second step involves either an intra-molecular electron transfer of the precursor complex (Eq 8) or the reaction of the precursor with a second H_2S (Eq 9). A two-electron transfer process is proposed since our experiments indicate the existence of elemental sulfur as a product. The third step accounts for the reactions of Cr(IV) and/or Cr(V), which are normally very fast and may not affect the overall reaction kinetics.

Step 1:

$$H_2S + CrO_4^{2-} \xleftrightarrow{k_1} \{H_2O_4Cr^{VI}S\}^{2-} \quad (6)$$

$$HS^- + CrO_4^{2-} + H^+ \xleftrightarrow{k_1'} \{H_2O_4Cr^{VI}S\}^{2-} \quad (7)$$

Step 2:

$$\{H_2O_4Cr^{VI}S\}^{2-} \xrightarrow{k_2} Cr^{IV}O_3^{2-} + S^0 + H_2O \quad (8)$$

$$\{H_2O_4Cr^{VI}S\}^{2-} + H_2S \xrightarrow{k_3} Cr^{IV}O_3^{2-} + HSSH + H_2O \quad (9)$$

Step 3:

$$Cr^{IV} + Cr^{VI} \xrightarrow{k_4} 2Cr^{V} \quad (10)$$

$$2Cr^{IV} \xrightarrow{k_5} Cr^{III} + Cr^{V} \quad (11)$$

$$Cr^{V} + S^{-II} \xrightarrow{k_6} Cr^{III} + S^0 \quad (12)$$

The precursor formation and the electron transfer proceed sequentially. If the formation of the intermediate thiol compounds is slower than the electron transfer processes and the overall reaction is limited by the slow step, the concentration of the precursor would reach a steady state. A rate law consistent with this mechanism is:

$$\frac{d[Cr(VI)]}{dt} = \frac{-k_1(k_3[H_2S] + k_2)}{k_{-1} + k_2 + k_3[H_2S]} [H_2S][CrO_4^{2-}] \quad (13)$$

where k_2 represents the electron transfer by Eq. 8 to form elemental sulfur and $k_3[H_2S]$ by Eq. 9 to form polysulfides. Polysulfides such as tetrasulfide and pentasulfide were detected in neutral and slightly basic solutions (O'Brien, and Birkner, 1977). Our experiments with HPLC and UV-visible spectroscopy, however, failed to show the presence of polysulfides, suggesting that the Eq. 8 is more important (i.e., $k_2 >> k_3[H_2S]$). Consequently, Eq. 13 can be simplified as:

$$\frac{d[Cr(VI)]}{dt} = \frac{-k_1k_2}{k_{-1} + k_2} [H_2S][CrO_4^{2-}] \quad (14)$$

In this equation, $[H_2S]$ is the concentration of the fully protonated species of sulfide, rather than the total concentration of sulfide $[H_2S]_T$ as monitored analytically as a function of time. $[H_2S]$ can be easily calculated based on the dissociation constants for hydrogen sulfide, pH, and $[H_2S]_T$ as shown in Eq. 15:

$$[H_2S] = [H_2S]_T \left\{\frac{[H^+]^2}{[H^+]^2 + [H^+]K_1 + K_1K_2}\right\} \quad (15)$$

where K_1 and K_2 are the dissociation constants for H_2S and HS^-, respectively. Combining Eq. 14 and 15, we have:

$$\frac{d[Cr(VI)]}{dt} = \frac{-k_1k_2[CrO_4^{2-}][H_2S]_T}{k_{-1} + k_2} \left\{\frac{[H^+]}{[H^+]^2 + [H^+]K_1 + K_1K_2}\right\} \quad (16)$$

$$= \frac{-k_1k_2Q[CrO_4^{2-}][H_2S]_T}{k_{-1} + k_2} \quad (17)$$

$$\text{where } Q = \left\{\frac{[H^+]^2}{[H^+]^2 + [H^+]K_1 + K_1K_2}\right\} \quad (18)$$

It is clear that the second order kinetics observed for Cr(VI) reduction by sulfide can be explained by this reaction scheme, with $k_1k_2Q / (k_{-1} + k_2)$ in equation 17 corresponding to the second order rate constant, k, of the equation 4. If the electron transfer step is much faster than the reversible step of the intermediate thiol compound ($k_2 >> k_{-1}$), the formation of the intermediate compound would be rate-limiting, resulting in an overall rate constant $k = k_1Q$. It should be noted that Q is a function of pH (Eq 18). As pH increases (approximately up to 11), the slope of log$Q$ versus pH goes toward –1 due to the ignorable values of the 1st and 3rd terms at denominator, while as pH decreases, the slope moves to 0. Such a pH dependence agrees well with the current experimental results (Fig. 2-6), i.e., the overall rate constant k of Cr(VI) reduction by sulfide is proportional to the mole fraction of H_2S species in the solution. The result, however, is not in conflict with the observation by Pettine et al (27), where a slope of 1 was obtained from a linear log k_{obs} vs. pH plot. The difference is resulted from the different pH ranges tested. When our data in the comparable pH range (pH 7 – 9.8) are also presented by the log k_{obs} vs. pH plot, we similearly obtain a straight line with a slope of –0.99. The linear log k_{obs} vs. pH plot is only valid under basic condition, not for the whole pH range tested in this study. Under strongly acidic conditions where sulfide exists mainly as H_2S, it is expected that k_{obs} will be pH-independent, but further research, suitable for measuring fast reduction kinetics under acidic condition, is needed to confirm the

prediction. Additionally, Cr(VI) acid/base speciation may affect the reaction rate and needs to be assessed.

CONCLUSIONS

This part of the work was to investigate the reaction stochiometry, kinetics, and mechanism for Cr(VI) reduction by hydrogen sulfide in the aqueous phase. Batch experiments with excess [Cr(VI)] over $[H_2S]_T$ indicated that the molar amount of sulfide required for the reduction of one molar of Cr(VI) was 1.5, suggesting the main product of sulfide oxidation be elemental sulfur. Further study with Transmission Electron Microscopy (TEM) and Energy-Dispersive X-Ray Spectroscopy (EDS) confirmed that chromium hydroxide and elemental sulfur were the stable products. Aqueous Cr(VI) reduction by sulfide is first order with respect to each of the two reactants. The effect of pH results from the speciation change of sulfide, since it appears that only the fully protonated sulfide species reacts with Cr(VI). Elemental sulfur is the main stable product during sulfide oxidation by Cr(VI). Such understanding provides insights as how to optimize the design of the ISGR approach for the remediation of chromium-contaminated sites and to predict and assess the system performance.

III. CHROMIUM(VI) REDUCTION BY SULFIDE UNDER ANAEROBIC CONDITIONS: CATALYSIS BY ELEMENTAL SULFUR PRODUCT

(Yeqing Lan, Chulsung Kim, Baolin Deng, Edward C. Thornton, and Huifang Xu)

INTRODUCTION

Chromium is one of the most frequently detected soil and groundwater contaminants (Riley and Zachara 1992; NRC 1994). In aquatic environments, chromium occurs mainly as species in the oxidation states of Cr^{VI} and Cr^{III}. Since Cr^{III} species are normally less mobile, the reduction of Cr^{VI} to Cr^{III} decreases chromium mobility and bioavailability. As a result, Cr^{VI} reduction is used as a main approach for chromium contamination site remediation.

Many chemicals are capable of reducing Cr^{VI} by directly providing electrons in the aquatic system, including zerovalent iron (Blowes et al. 1997; Puls et al. 1999), divalent iron (Eary and Rai 1988; Fendorf and Li 1996; Buerge and Hug 1997), hydrogen sulfide (Pettine et al. 1994; Thornton and Amonette 1999), and organic compounds (Elovitz and Fish 1994; Wittbrodt and Palmer 1995; Deng and Stone 1996a; Deng and Stone 1996b). Rates of Cr^{VI} reduction depend upon the types of reductants and solution pH. For example, Cr^{VI} reduction by Fe^{II} takes place rapidly, with the reaction rate decreasing from pH 1.5 to 4.5 and increasing from pH 5.5 to 8.7 (Buerge and Hug 1997; Pettine et al. 1998). The reduction by many organic compounds is slow near neutral pH but the rate normally increases as pH is decreased (Deng 1995). Once reduced, Cr^{III} species are quite stable. The only compounds known to oxidize Cr^{III} to Cr^{VI} are manganese oxides in the subsurface environment (Eary and Rai 1987; Fendorf and Zasoski 1992; Banerjee and Nesbitt 1999).

There are many other chemical constituents that may not directly reduce Cr^{VI}, but can alter the rate of Cr^{VI} reduction. Surface-catalyzed Cr^{VI} reduction on goethite (α-FeOOH), aluminum oxide (α-Al_2O_3) and titanium dioxide by various organic reductants has been observed, including α-hydroxyl carboxylic acids and their esters, α-carbonyl carboxylic acids, and substituted phenols (Deng and Stone 1996; Deng and Stone 1996). The research revealed that the rate of Cr^{VI} reduction could be increased by several orders of magnitude in the presence of some metal (hydr)oxides. In another study, Buerge and Hug (Buerge and Hug 1999) found that Cr^{VI} reduction by Fe^{II} was strongly enhanced by iron minerals including goethite and lepidocrocite. Dissolved metals such as Mn^{II}/Mn^{III} and Fe^{II}/Fe^{III} are also able to catalyze Cr^{VI} reduction (Huber and Haight 1976).

Cr^{VI} reduction by hydrogen sulfide takes place rapidly in a wide range of pH, with elemental sulfur as the main product of sulfide oxidation (Section II). This reaction has been explored as a remediation approach for chromium immobilization in the subsurface (Thornton and Amonette 1999) and may also contribute to Cr^{VI} reduction in natural water and sediments (Pettine et al. 1994). The objective of this paper is to evaluate whether the particulate elemental sulfur produced during the reaction can catalyze further Cr^{VI} reduction, similar to other mineral surfaces.

MATERIALS AND METHODS

Chemicals: Solutions were prepared by deionized Milli-Q water (Q-H_2O, with18.2 MΩ-cm resistivity, Millipore Corp.) after purging with high purity nitrogen gas for at least 20 min. Glassware was cleaned by soaking in 1M HCl for at least 3 hrs and then thoroughly rinsed by Q-H_2O. Potassium dichromate, elemental sulfur (S_8), diphenyl carbazide, acetone, and N, N-dimethyl-1,4-phenylene-diamine oxalate were purchased from Aldrich Chemical Company and boric acid, sodium phosphate, sodium hydroxide, sodium sulfide ($Na_2S\bullet 9H_2O$), sulfuric acid, ferric chloride, and diammonium hydrogen phosphate were from Fisher Scientific. The chemicals were at least ACS reagent grade and used without further purification, except that sodium sulfide crystals were rinsed with degassed Q- H_2O to remove the oxidized surface layer. Stock solutions of chromate and sulfide were stored in amber bottles placed in an anaerobic chamber (Models 855-AC, PLAS-LABS, INC.) prior to use. Elemental sulfur stock was prepared by crystalline elemental sulfur (S_8) powder dispersed in acetone.

Experimental Systems: Experiments reported in this study were mostly performed in the anaerobic chamber (N_2, balanced by 10% H_2), including experimental setup and chemical analyses. Solution pH was controlled by 0.10 M phosphate buffer (pH7.60) or 0.10 M borate buffer (pH 8.10). No strong electrolytes were applied to control ionic strength in this study, since the literature (Pettine et al. 1994; Pettine et al. 1998) and our preliminary experiments all indicated that the reaction was independent of ionic strength when it was between 0.0 and 1.0 M. The actual ionic strength in the experimental systems was determined mainly by the buffer solutions, which was less than 0.10 M.

To ensure no sulfide loss due to evaporation, adsorption, and oxygenation, we tested the stability of sulfide at pH=7.60 and 25 ^oC. First, approximately 40 ml of 0.10 M phosphate buffer was added into a 41 ml amber bottle and degassed with high purity N_2 for 20 minutes, then the bottle was moved into the anaerobic chamber. After sulfide stock solution was pippeted into the buffer solution, the bottle was closed by a screw cap with Teflon liner and mixed by hand. Samples (0.50 ml) were taken at 30-min interval with a 0.5 ml glass syringe for sulfide analysis. Sulfide stability was evaluated for 180 minutes at 200μM concentration level and 120 minutes at 800μM concentration level. Most kinetic experiments in this study followed this procedure with a sulfide concentration ranging from 200 to 800 μM.

Reaction stoichiometry between Cr^{VI} and S^{-II} was determined by monitoring the consumption of both reactants with different initial concentration ratios. The temperature was maintained at 15 ± 0.5 ^oC and 25 ± 0.5^oC using a water bath.

Kinetic experiments were conducted by monitoring Cr^{VI} concentration as a function of time in excess sulfide over Cr^{VI}. At pH 7.60, tests were performed with initial Cr^{VI} concentrations ranging from 10 to 60μM and initial sulfide concentrations from 300 to 800μM. The temperature varied from 5 to 35 ^oC. At pH 8.10, $[Cr^{VI}]_0$ and $[S^{-II}]_0$ were 40μM and 800μM, respectively.

Several types of experiments were performed to evaluate whether elemental sulfur produced during Cr^{VI} reduction by S^{-II} could alter the reaction rate. (1). After 40 μM Cr^{VI} was completely reduced in a system with 800 μM total sulfide, another 40 μM Cr^{VI} was re-spiked into the system. It is hypothesized that if elemental sulfur was involved in the Cr^{VI} reduction, the reduction rate of the re-spiked Cr^{VI} should be enhanced by the elemental sulfur produced in the earlier reaction. (2) After 40 μM Cr^{VI} was completely reduced in a system with 800 μM total sulfide, the supernatant was collected by centrifugation at 6000 rpm (IEC Clinical Centrifuge, International Equipment Company), followed by filtration through 0.40 μm Millipore membrane filters. The

supernatant was degassed with N_2 again and in the anaerobic chamber, spiked with certain amounts of Cr^{VI} and S^{-II}. (3). Colloidal elemental sulfur was added into the buffer solution prior to the additions of Cr^{VI} and S^{-II}. Elemental sulfur was prepared in acetone to allow proper dispersion and formation of elemental sulfur colloids. In the reaction systems, acetone concentration was always less than 2%. Control experiments showed that at this concentration level, acetone didn't alter the reaction rate between Cr^{VI} and S^{-II}.

Analytical Methods: Cr^{VI} concentration was determined by the diphenylcarbazide colorimetric method, using phosphoric buffer to control pH for the color development (Deng and Stone 1996). The absorbance was measured in a 1-cm cell at 540nm on a spectrophotometer (Spectronic 20 Genesys, Spectronic Instruments). The method detection limit was 0.05 μM and the precision was 5% rsd at Cr^{VI} concentrations in the range 0.5-2μM (Pettine et al. 1994; Pettine et al. 1998). Sulfide concentration in the stock solution was standardized with the standard iodometric titration method (APHA et al. 1998). Sulfide concentration during the reaction was monitored by the methylene blue colorimetric method with the absorbance measured at 664 nm (Allen et al. 1993; APHA et al. 1998).

To our surprise, the methylene blue method for sulfide analysis was significantly affected by the order of reagent additions (Table 1). If the reagents were added with the sequences of A (sulfide + 5 ml H_2O + amine-sulfuric acid solution + ferric chloride), B (sulfide + 5 ml H_2O + mixture of amine-sulfuric acid solution and ferric chloride), and C (5 ml H_2O + sulfide + amine-sulfuric acid solution + ferric chloride), the absorbance values were all similar. Adding the amine-sulfuric acid and ferric chloride stock solutions separately or adding the mixture of the two reagents didn't alter the absorbance. If other orders were followed as for D, E, and F, however, the absorbance values were significantly lower. Thus, following proper order of reagent addition was critical to maintain the sensitivity of the method and avoid erroneous results. In this study, we selected the following sequence for sulfide analysis: (1) adding 5 ml Milli-Q water; (2) injecting sulfide sample into the bottom of the water through a syringe; (3) adding the mixture of amine-sulfuric acid and ferric chloride solution for color development. Using the premixed amine-sulfuric acid and ferric chloride solution decreased time for reagent addition and increased analytic precision. This was similar to the procedure used for the analysis of acid volatile sulfur (AVS) in sediments (Allen et al. 1993). Additionally, it was noticed that the calibration curve for the methylene blue method did not follow a strict straight line for sulfide concentration ranging from 0 to 40μM, but two linear segments were observed (data not shown). To minimize the analytical error, a two-segment calibration curve was used for the concentration from 0 to 15 μM and from 15 to 40 μM, respectively.

Solution pH was measured prior to and after the redox reaction by an Orion 420A pH meter following a 2-point calibration. To evaluate how complete the oxygen was removed by N_2 purging, dissolved oxygen was analyzed in selected experiments using the HACH dissolved oxygen test kit (HACH company, Loveland, CO).

Transmission electron microscopy (TEM) was used for the imaging of elemental sulfur particles. A drop of solution containing the S particles was placed on a holey carbon coated Cu grid. The Cu grid was placed on TEM specimen holder after the Cu grid dried. All TEM observations were carried out with a JEOL 2010 high-resolution transmission electron microscope (HRTEM) with an attached Oxford LINK EDS system (Xu and Wang 2000).

Table 1. Effect of orders of reagent addition on the absorbance during sulfide analysis by the methylene blue colorimetric method.

Sequence	**A** 1. Sulfide 2. 5ml H_2O 3. amine-sulfuric acid 4. ferric chloride	**B** 1. sulfide 2. 5ml H_2O 3. mixture of amine - sulfuric acid + ferric chloride	**C** 1. 5ml H_2O 2. sulfide 3. amine-sulfuric acid 4. ferric chloride	**D** 1. sulfide 2. amine sulfuric acid 3. ferric chloride 4. 5ml water	**E** 1. amine sulfuric acid + ferric chloride 2. sulfide 3. 5ml water	**F** 1. amine sulfuric acid + ferric chloride 2. 5ml water 3. sulfide
Absorbance (triplicates)	1.890 1.854 1.910	1.906 1.962 1.930	1.926 1.890 1.894	1.421 1.458 1.446	0.776 0.840 0.825	1.666 1.620 1.699
Average	**1.885**	**1.933**	**1.903**	**1.442**	**0.815**	**1.662**
S^{-II} conc. (μM)	61.57	63.41	62.26	44.53	20.42	52.99

RESULTS AND DISCUSSION

Sulfide Stability: For the experiments designed to study sulfide oxidation kinetics, potential loss of sulfide due to its evaporation, adsorption, and oxygenation needs to be properly controlled. The stability of sulfide in the phosphate buffered aqueous solution was tested at initial concentrations of 200 and 800µM (pH=7.60 and 25°C), and the results indicated that sulfide was stable during a time period of 2 to 3 hrs (Figure 3-1), following the established experimental procedure. By minimizing the loss of sulfide through evaporation and oxygenation, we were able to investigate the reaction stoichiometry and kinetics by monitoring both Cr^{VI} and S^{-II}.

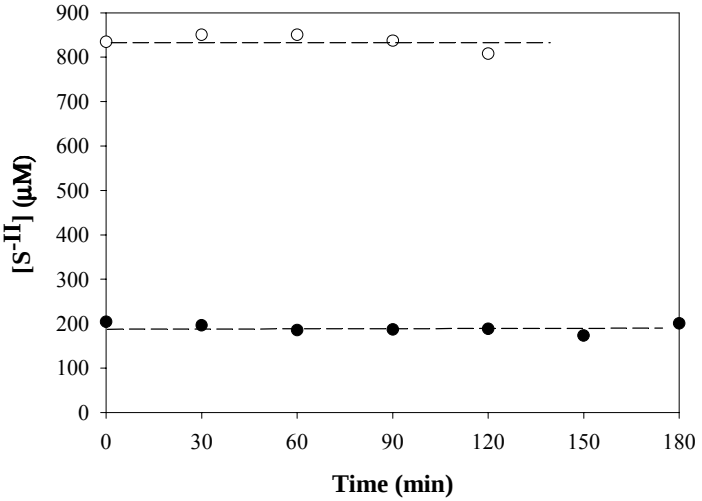

Figure 3-1. The stability of sulfide in the experimental systems (pH=7.60 and 25°C)

Reaction Kinetics: Through well-controlled batch experiments performed in an anaerobic chamber, it is observed that while Cr(VI) reduction by sulfide follows a pseudo first order kinetics with respect to [Cr(VI)] initially, as described in Section II, and the rate was largely accelerated at the later stage of the reaction (Figure 3-2). This discovery was not expected prior to the start of the project, and to our knowledge, it has not been reported in the literature.

Such acceleration is likely due to the formation of some reaction intermediates and products. Since elemental sulfur and chromium hydroxide are known to form in the experimental system, our working hypothesis was that the acceleration was due to elemental sulfur and chromium hydroxide. We examined Cr(VI) reduction in the presence of 40 μM of Cr(III) at pH 8.10. The Cr(III) species, mainly in the form of $Cr(OH)_{3(s)}$ under the experimental condition, didn't demonstrate any discernible effect on the reaction kinetics. Thus elemental sulfur produced during the reaction was proposed to be the main compound causing the accelerated Cr(VI) reduction.

Two types of experiments were conducted to see whether elemental sulfur could be involved in the rate acceleration observed. In the first type, we allowed 40 μM Cr(VI) to be completely reduced by 800 μM S^{-II}, and then additional Cr(VI) was re-spiked but no additional sulfide was added. To illustrate, the results at pH 8.10 (buffered by borate) are shown in Figure 3-3. Under this pH condition, it took 210 min for the complete reduction of the first batch of Cr(VI) (curve A), and only 56 min for the second batch (curve B). The acceleration was observed under even slightly lower reductant concentration than in the first batch since no sulfide was re-spiked. The results indicate that the products formed during the reaction catalyzed the Cr(VI) reduction processes.

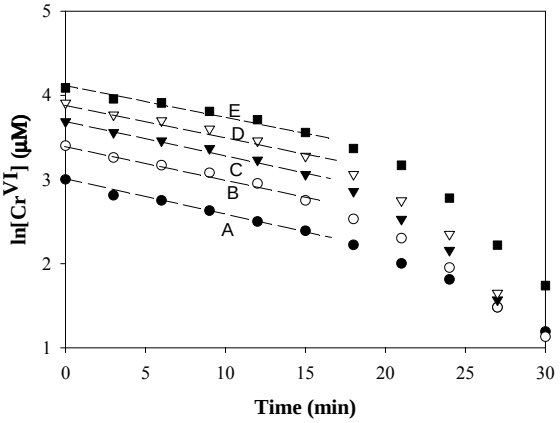

Figure 3-2. ln [Cr^{VI}] as a function of time in the systems with excess of sulfide (800 μM) at pH=7.60 and 25°C. Reaction rate for Cr(VI) was accelerated compared to first order kinetics. ($[Cr(VI)]_0$ (μM): A = 20; B=30; C=40; D=50; E=60.)

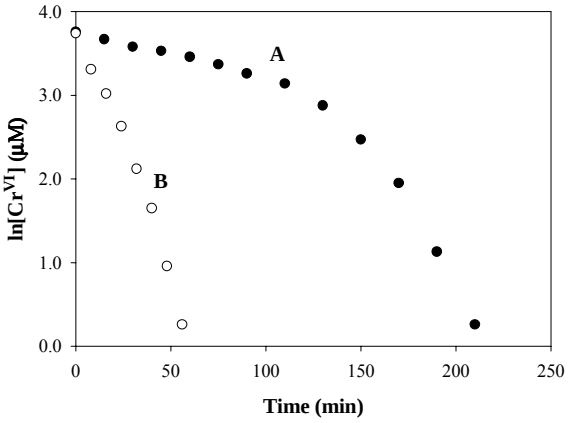

Figure 3-3. Rates of Cr(VI) reduction by sulfide at pH 8.10. Curve A is for the reduction of the first batch of Cr(VI) (40 μM) by (800 μM sulfide); Curve B is for the re-spiked Cr(VI) after the first batch is completed.

The second type of testing involved in the addition of various amounts of elemental sulfur into the system before the redox reaction was initiated. The results showed that the presence of elemental sulfur did increase the reaction rate significantly (Figure 3-4). The presence of elemental sulfur greatly decreased the time for complete Cr(VI) reduction. Higher concentrations of added sulfur particles resulted in faster Cr(VI) reduction. When the initial concentration of elemental sulfur was raised to 320μM, the time needed for completing the reaction was less than 30 min. In addition, in the presence of externally added sulfur colloids, the $ln[Cr^{VI}]$ vs. t plots are linear, suggesting a first order kinetics.

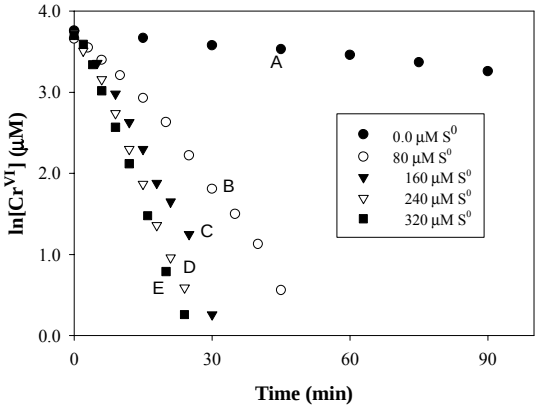

Figure 3-4. Effect of externally added elemental sulfur on Cr(VI) reduction in the systems with excess of sulfide (800 μM) at 25°C and pH 7.60 (Externally added $[S^0]$ (μM): A = 0; B= 80; C=160; D=240; E=320).

During the tests with crystalline sulfur particles, we observed that the colloidal system exhibited a milky white appearance typical of elemental sulfur. When sulfide was also added into the system, however, this milky white appearance disappeared and the colloidal system became almost as clear

as true solution (Figure 3-5). TEM study showed that without S^{-II} in the system, the elemental sulfur particles display an elongated shape, with an averaged width of 10 nm and length of 50 - 100 nm (Figure 3-6a). With S^{-II} being present, the elemental sulfur was in the form of much smaller nano particles with an average size of around 5 nm (Figure 3-6b). These nano S^0 particles were not amorphous, but in crystalline form because sharp diffraction rings in selected-area electron diffraction (SAED) patterns were observed. Apparently, interactions between S^0 and S^{-II}, or the sorption of S^{-II} onto the surface, have altered the crystalline behavior of the elemental sulfur.

It is believed that the rate acceleration at later stage of the reaction is caused by the S^0 produced in the system. Several lines of evidences support this hypothesis. First, re-spiked Cr^{VI} is reduced much faster than the Cr^{VI} originally present in the system. Between the two main reaction products in the system, $Cr(OH)_{3(s)}$ does not affect the reaction, so the other one, S^0, is most likely involved. Second, the presence of externally added S^0 increases the rate of Cr^{VI} reduction, and the higher the S^0 concentration, the faster the rate (Fig.3-4).

The catalytic kinetics for Cr^{VI} reduction caused by S^0 produced in the system is different from typical autocatalytic processes (Cappelos and Bielski 1980; Schwartz 1989). Rate of a typical autocatalytic reaction is slow initially, increases to a maximum, and decreases again due to the depletion of the reactants. For example, oxidation of organic compounds by MnO^-_4 follows this autocatalytic model, in which Mn^{2+} produced during the reaction acts as a catalyst (Schwartz 1989; Perez-Benito, Arias et al. 1990). The kinetic data on Cr^{VI} reduction by sulfide, however, can't be described by the typical autocatalytic model. Instead, the reaction follows first order at the initial stage of the reaction. The acceleration takes place only after a certain time period, e.g., 15 min at pH 7.8, and by that time, the amount of S^0 produced can be as high as 40μM.

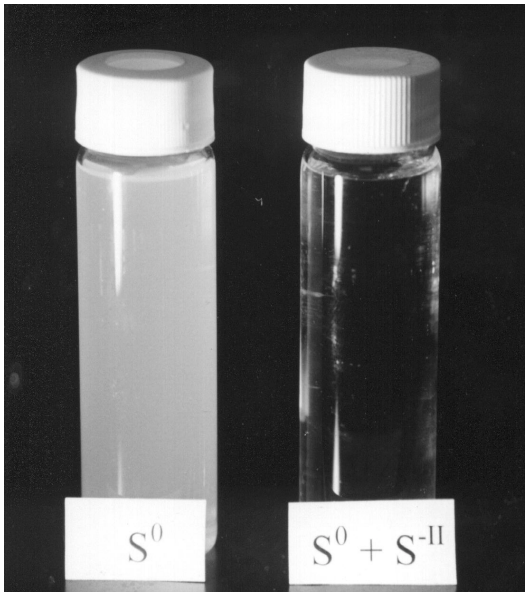

Figure 3-5. Photos of crystalline elemental sulfur particles (S_8) in the absence and presence of S^{-II}

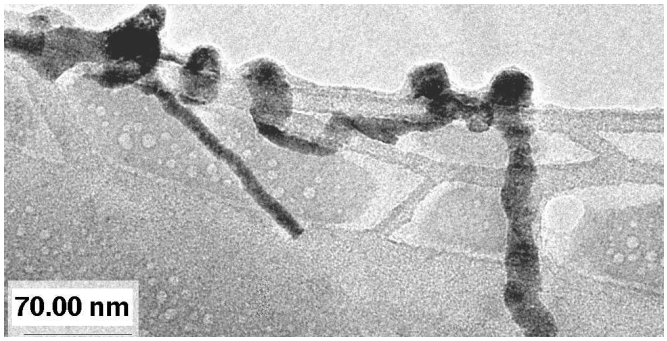

(a)

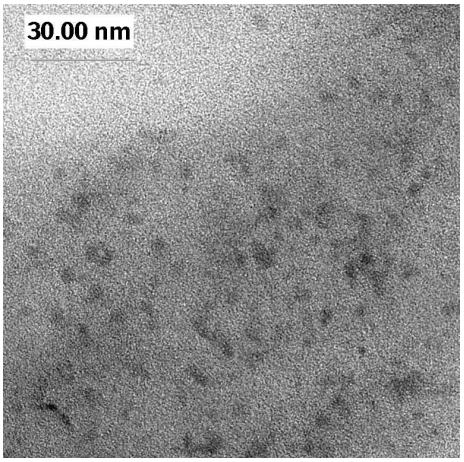

(b)

Figure 3-6. (a) S^0 particles from a sample without H_2S treatment. Most S particles display elongated shapes. Average width of the elongated S particles is about 10 nm. (b) S^0 nano particles from a sample with H_2S treatment. They are nano crystalline particles. Noise background is amorphous carbon film holding the S particles. Average size of the S nano-crystals is about 5 nm.

We propose that particulate form of elemental sulfur or S^0 colloids are the catalyst of Cr^{VI} reduction by sulfide. Amorphous S^0 molecules, when produced during the reaction, are dispersed in the aqueous system and are not capable of catalyzing the reaction. Only when nucleation occurs that eventually leads to the formation of crystalline S^0 colloids, the catalytic pathway becomes significant compared to the non-catalytic pathway. Thus, the reaction follows the pseudo first order kinetics at the initial stage when the colloidal form of elemental sulfur is not significant, even though S^0 is produced from the very beginning of the reaction. Once colloidal S^0 is formed, which provides reactive surface for reactant adsorption, the reaction is accelerated due to the high reactivity of sorbed reactants. Adsorption of Cr^{VI} onto amorphous elemental sulfur is insignificant (less than 3%). S^{-II} sorption onto nano-crystalline S^0 colloids, however, is highly likely due to the similar electronic structure of S^0 and S^{-II}. Particle size of elemental sulfur is significantly decreased due to the presence of S^{-II} as shown in Fig. 3-6, which indicates the existence of strong interactions between S^0 and S^{-II}. Effort of measuring S^{-II} sorption onto the elemental sulfur colloids was not successful because we were unable to separate solids with particle size around 5 nm.

CONCLUSION

Through well-controlled batch experiments performed in an anaerobic chamber, it is observed that while Cr(VI) reduction by sulfide follows a pseudo first order kinetics with respect to [Cr(VI)] initially, the rate was largely accelerated at the later stage of the reaction. It was known that elemental sulfur was the product of sulfide oxidation by Cr^{VI} under the anaerobic condition. The elemental sulfur produced can form particulate sulfur colloids capable of adsorbing sulfide and such adsorbed sulfide exhibits much higher reactivity towards Cr^{VI} reduction than the aqueous phase sulfide and is responsible for the accelerated Cr^{VI} reduction observed.

IV. EFFECT OF VARIOUS SOIL MINERALS ON Cr(VI) REDUCTION BY SULFIDE

(Yeqing Lan, Chulsung Kim, Baolin Deng)

INTRODUCTION

Release of toxic heavy metals into soils and water has been widespread. Chromium is one of the concerned heavy metals due to its high toxic and carcinogenic properties. Between the two common oxidation states of chromium in the aquatic environment, trivalent chromium usually has lower solubility and stronger affinity to soil components than hexavalent chromium, therefore, reduction of Cr(VI) to Cr(III) has been used as an important remediation technology for Cr(VI)-contaminated soils and water. Cr(VI) species can be reduced by many types of reductants such as zero valent iron (Blowes et al., 1997; Pratt et al., 1997; Ponder et al., 2000), ferrous iron (Eary and Rai, 1988; Fendorf and Li, 1996; Sedlak and Chan, 1997; Pettine et al., 1998; Buerge and Hug, 1997; 1998; 1999; Seaman et al. 1999), and naturally occurring organic compounds (James and Bartlett, 1983; Goodgame and Hayman, 1984; Eary and Rai, 1991; Wittbrodt and Palmer, 1995). The reaction kinetics is strongly dependent upon the nature of the reductants and pH.

Recently, hydrogen sulfide has been applied for reductive Cr(VI) immobilization that is particularly suitable for vadoze zone remediation. Facile reduction of Cr(VI) by sulfide in the aqueous phase has been demonstrated by a number of studies (Schroeder and Lee, 1975; Smillie et al., 1981; Saleh et al., 1989; Pettine et al., 1994; 1998; Thornton and Amonette, 1999). Under the anaerobic condition, elemental sulfur was identified as the major product of sulfide oxidation (Section II). The reaction was first order with respect to both Cr(VI) and H_2S and the kinetics was interpreted by a three step mechanism: formation of an inner sphere chromate-sulfide complex formation, intramolecular electron transfer to form Cr(IV) species, and subsequent fast reactions leading to the formation of Cr(III). It was further demonstrated that the produced elemental sulfur provided surface sites for sulfide sorption, and the sorbed sulfide possessed substantially higher reactivity towards Cr(VI) reduction than dissolved sulfide (Section III). Therefore, Cr(VI) reduction by sulfide in the aqueous phase proceeds through two stages: initial homogeneous reaction followed by a stage with significant contribution by the surface-catalyzed pathway.

To thoroughly assess the efficiency of Cr(VI) immobilization by H_2S treatment, we need to understand how various soil components affect Cr(VI) reduction and H_2S consumption. Important components include clay minerals and metal (hydr)oxides because of their widespread distribution and high specific surface areas. The effects could come from direct Cr(VI) reduction by the soil components or indirectly by the catalysis of mineral components for Cr(VI) reduction. Eary and Rai (1989) observed Cr(VI) reduction by hematite and biotite over a wide pH range from 3.5 to 11. They proposed that the dissolution of ferrous iron from solid phases into the aqueous phase should take place prior to Cr(VI) reduction and the redox reaction occurred in the solution phase rather than at surface sites. Dissolution, however, may not be needed for some other minerals. For example, Patterson and Fendorf (1997) demonstrated that freshly prepared ferrous sulfide (FeS) reduced Cr(VI) quite effectively in the pH range of 5.0 – 8.0 and reaction took place at surface-solution interface. In addition to Cr(VI) reduction directly by ferrous species in soils, it is known that minerals such as aluminum oxide (γ-Al_2O_3), goethite (α-FeOOH), and titanium dioxide (TiO_2) can catalyze Cr(VI) reduction by many types of organic compounds (Deng and Stone, 1996a; b). Buerge and Hug (1999) showed that the rate of Cr(VI) reduction by ferrous iron was also increased by some metal oxides.

In this section, effects of clay minerals (illite, montmorillonite, and kaolinite) and metal oxides (Al_2O_3, SiO_2 and TiO_2) on Cr(VI) reduction by sulfide were examined.

MATERIALS AND METHODS

Chemicals: Chemicals were obtained from Aldrich/Sigma (potassium dichromate, elemental sulfur(S_8), diphenyl carbazide, acetone, N, N-dimethyl-1,4-phenylene-diamine oxalate, ferrozine, and HEPES) and Fisher Scientific (boric acid, sodium phosphate, sodium hydroxide, sodium sulfide ($Na_2S \bullet 9H_2O$), sulfuric acid, hydrogen chloride, ferric chloride, and diammonium hydrogen phosphate). All chemicals were at least ACS reagent grade and used without further purification, except sodium sulfide crystals that was rinsed with degassed water to remove the oxidized surface layer. Stock solutions of chromate and sulfide were prepared by Milli-Q water (Q-H_2O, with18.2 MΩ-cm resistivity, Millipore Corp.) purged thoroughly with high purity nitrogen gas and stored in amber bottles and placed in an anaerobic chamber (Models 855-AC, PLAS-LABS, INC.) prior to use. Stock solution of elemental sulfur was prepared by dispersing crystalline elemental sulfur (S_8) powder in acetone. Glassware was cleaned by soaking in 1M HCl for at least 3 hrs and then thoroughly rinsed.

Minerals: Kaolin (KGa-2), montmorillonite (STx-1), and illite (IMt-2) were obtained from the Source Clay Minerals Repository, University of Missouri-Columbia (U.S.A), and aluminum oxide, silicon oxide, and titanium oxide, Degussa Corporation. Point of zero charge (PZC) and BET specific surface area (SSA) of minerals is listed in Table 4-1.

Table 4-1. Point of Zero Charge and BET special surface aera of minerals.

Minerals	pH_{PZC}	SSA(m^2/g)
Aluminum oxide	8.9[a]	90.1[a]
Silicon oxide	2.3[a]	90.0[a]
Titanium oxide	6.5[d]	40.5[a]
Montmorillonite	5.9[f]	99.0[f]
Kaolin	4.5-5.0[e]	22.4[b]
Illite	3.5[b]	24.0[b]

a--Degussa (1991), b--this work, c--, d--Torrents and Stone (1991), e--Zhou (1996), f--Buerge and Hug (1999)

Experimental procedure: Most of experiments reported in this study, including experimental setup and chemical analyses, were performed in an anaerobic chamber (N_2, balanced by 10% H_2) with a temperature of 24.0 ± 0.5°C. Solution pH was controlled by 0.10 M borate buffer (adjusted with 0.1M boric acid and sodium hydroxide). No strong electrolytes were applied to control ionic strength in this study, because both earlier studies (Pettine, et al, 1994 and 1998) and our preliminary experiments indicated that the reaction was independent of ionic strength in the range from 0.0 and 1.0 M. The actual ionic strength in the experimental systems was controlled largely by the borate buffer, which had a total concentration of 0.10 M.

Kinetics experiments examining the effect of minerals on Cr(VI) reduction began with purging an adequate amount of borate buffer solution in a 40 ml amber bottle with high purity nitrogen gas for 20 min. The vessel was then closed immediately by a screw cap with Teflon/silicon septum and moved into the anaerobic chamber. Variable amounts of minerals and 0.80 ml of 2.00 mM K_2CrO_4 stock solution were added into the bottle, followed by hand-mixing for 30 min. Adequate amounts of sulfide stock solution and Q-H_2O were introduced afterwards to keep a final slurry

volume at 40.00 ml. The final concentrations of Cr(VI) and sulfide were 40.0 μM and 800μM, respectively, and concentrations of minerals were 0, 0.5, 1.5, 3.0, 5.0 g/L. Approximately 1 ml of slurry was periodically withdrawn by a 3ml plastic syringe and immediately filtered through a 0.22 μm membrane filter and the filtrate was measured for Cr (VI) analysis. Due to the strong effect observed for illite and kaolinite on Cr(VI) reduction, these two minerals were selected for further study at a 3.0 g/L solid loading and pH from 7.67 to 9.07. Other conditions were maintained the same.

Several types of experiments were performed at pH 8.27 to evaluate whether ferrous iron produced from illite could alter the reaction rate of Cr(VI) reduction by sulfide: (1) addition of 5.0 μM Fe(II) into the homogeneous system with Cr(VI) and sulfide only; (2) addition of phenanthroline into the homogenous system with Cr(VI) and sulfide; (3) addition of a strong Fe(II) chelating agent, phenanthroline, into the illite system with Cr(VI), sulfide, and illite. Fe(II) and phenanthroline were introduced before Cr(VI) and sulfide were transferred into the reaction system.

Cr(VI) and sulfide adsorption: The adsorption of Cr(VI) and sulfide onto illite and kaolin surfaces at pH 7.87 was assessed by monitoring the concentrations of Cr(VI) and sulfide after solid/solution separation with filtration. Initial concentrations of Cr(VI) and sulfide were 40.0 and 800μM, respectively.

Adsorbed and dissolved Fe(II): The adsorbed and dissolved amounts of Fe(II) in illite suspension at pH 8.27 were monitored in the following three experimental systems: (1) illite + borate buffer; (2) illite + borate buffer + sulfide; (3) illite + borate buffer + sulfide + elemental sulfur. Final concentrations were 800.0 μM for sulfide and 50.0 μM for elemental sulfur. A 3.0 ml suspension was filtered through a 0.10 μm membrane and the filtrate was analyzed for soluble Fe(II). The solids on the membrane were washed with 3 ml Mill-Q water four times to remove the remaining sulfide on the solid surfaces. Afterwards, the solids and the membrane were soaked in a 3.0 ml of 0.1 M HCl solution and stirred with a magnetic Teflon bar for 20min. Then, the suspension was filtered with a 0.22 μm membrane filter and the filtrate was analyzed for the adsorbed Fe(II).

Analytical Methods: Cr(VI) concentration was determined by the diphenylcarbazide colorimetric method, using phosphoric buffer to control pH for the color development (APHA,1998; Deng et al, 1996). The absorbance was measured in a 1-cm cell at 540nm on a spectrophotometer (Spectronic 20 Genesys, Spectronic Instruments) and the method had a detection limit of 0.05 μM. Sulfide concentration in the stock solution was standardized with the standard iodometric titration method (APHA, 1998). Sulfide concentration during the reaction was monitored by a modified methylene blue method (Section III).

Ferrozine method was adopted for Fe(II) analysis (Amonette et al, 2000 and Lovely et al, 1986). It was noticed that borate buffer and sulfide could affect the analytical procedure. If borate buffer was mixed with Fe(II) followed by ferrozine solution, no color development could be observed. Formation of FeS in the system could increase the time needed for full color development. In this study, we added 1.0 ml of 0.50 M HCl into the system with borate buffer, sulfide and Fe(II), followed by ferrozine. This sequence of reagent addition resulted in complete and immediate color development without interference from borate buffer and sulfide. pH ranging from 3.0 to 7.3 did not appear to affect the analysis.

Solution pH was measured before and after the reaction by an Orion 420A pH meter after a 2-point calibration. Dissolved oxygen was analyzed using the HACH dissolved oxygen test kit (HACH Company, Loveland, CO), which was used to evaluate how completely the oxygen was removed

by N_2 purging. The dissolved oxygen in borate buffer was decreased to below the detection limit of 6.3 μM through purging.

RESULTS

Effect of minerals on reaction rate: Clay minerals (illite, kaolinite and montmorillonite) and metal oxides (Al_2O_3, SiO_2 and TiO_2) were used to study the effect of mineral surfaces on the reduction of Cr(VI) by sulfide. The initial concentrations of Cr (VI) and sulfide were 40 and 800 μM, respectively, and the solution pH was 7.87 (borate buffer). Sulfide concentration was at least 20 times as much as that of Cr (VI) during the reaction. Since sulfide in our specific experimental setup was near constant and the overall reaction was pseudo first-order with respect to Cr (VI) (Sections II and III), the kinetic data were expressed by ln[Cr(VI)] versus time plots as shown in Figure 4-1(a-f).

In the presence of illite, the reduction of Cr (VI) by sulfide was faster than the control system without mineral and was increased with increasing amount of illite from 0.5 to 5.0 g/L (Fig. 4-1a). For example, with 5.0g/L of illite, the time needed to complete the reaction was about 50% of the reaction time in the control system. The plots of ln[Cr(VI)] versus time were not linear, however, indicating that overall reaction did not follow a first order kinetics. Instead, a slower initial reaction was followed by a faster one, a trend similarly observed in the homogeneous systems (Section III).

For Al_2O_3, no obvious difference was observed between the systems with and without the solid (Fig. 4-1b). Overall, the kinetic data were characterized by a slow initial reaction step, followed by a fast one. In the stage of slow reaction, ln[Cr(VI)] v.s. t plots were linear.

Unlike illite and Al_2O_3, all other minerals including kaolin (Fig. 4-1c), montmorillonite (Fig. 4-1d), SiO_2 (Fig. 4-1e) and TiO_2 (Fig. 4-1f) decreased the rate of Cr(VI) reduction by sulfide as compared to the system without mineral. The effect was more dramatic at higher mineral concentrations. Better linear plots of ln[Cr(VI)] versus time were obtained with higher concentrations of these minerals. The results indicated that these minerals did not catalyze, but inhibit the reaction between Cr (VI) and sulfide. In addition, by comparing the specific surface area (SSA) listed in table 4-1 with the kinetic results shown in Fig.4-1(a-f), it was clear that the large SSA provided by minerals was not the key factor in accelerating the reduction of Cr (VI) by sulfide. For example, illite, with the lowest SSA of the minerals examined, can accelerate the reaction rate, while Al_2O_3 and SiO_2, both with high SSA, displayed different roles in affecting the reaction rates.

Effect of pH: Illite and kaolin were selected for further study because these two minerals exhibited quite different effects on the Cr(VI) reduction reaction, which might provide some insight into the reaction mechanism. The experiments were conducted in the systems initially containing 40μM of Cr(VI), 800μM of sulfide, and 3.0g/L of illite or 3.0g/L of kaolin, and the solution pH was controlled at six levels (pH 7.67, 7.87, 8.07, 8.27, 8.67 and 9.07. The results (figure 4-2(a-f)) indicated that: (1) the reduction rates in various systems followed the order: illite > homogeneous system> kaolin; (2) in illite and homogeneous systems, overall reaction was characterized by a slower initial step, followed by a faster one, while in the kaolin system, all plots

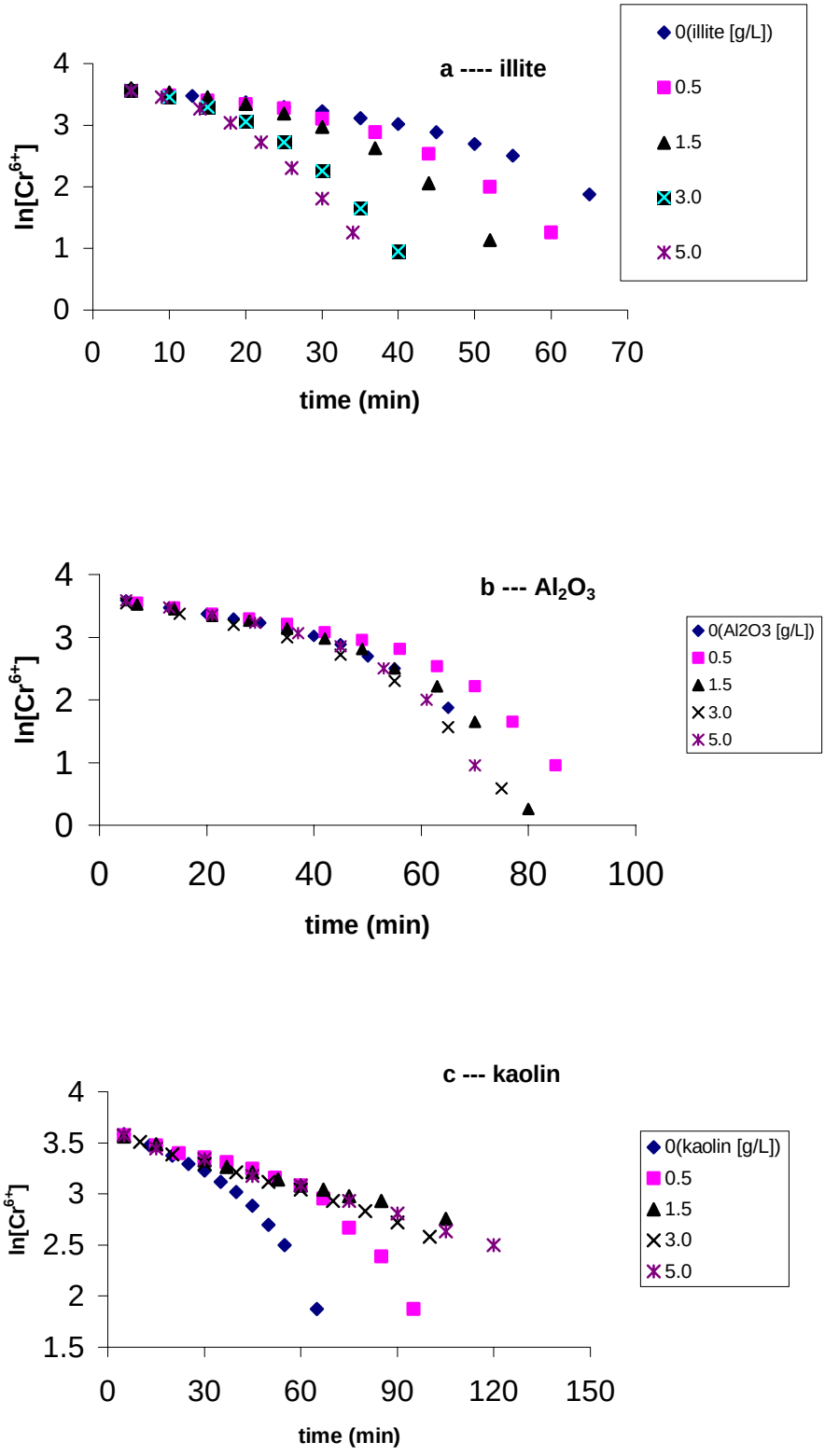

Figure 4-1. Effects of minerals on the reaction between 40µM of Cr(VI) and 800µM of sulfide, with a = illite, b = Al_2O_3, c = kaolin, d = montmorillonite, e = SiO_2 , and f = TiO_2.

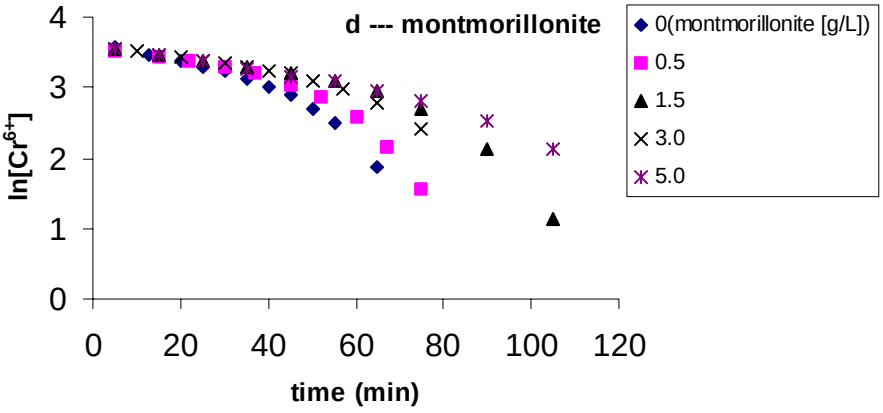

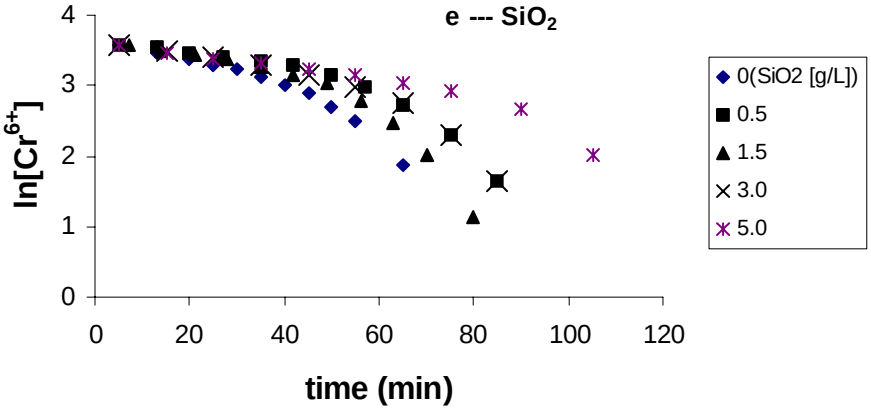

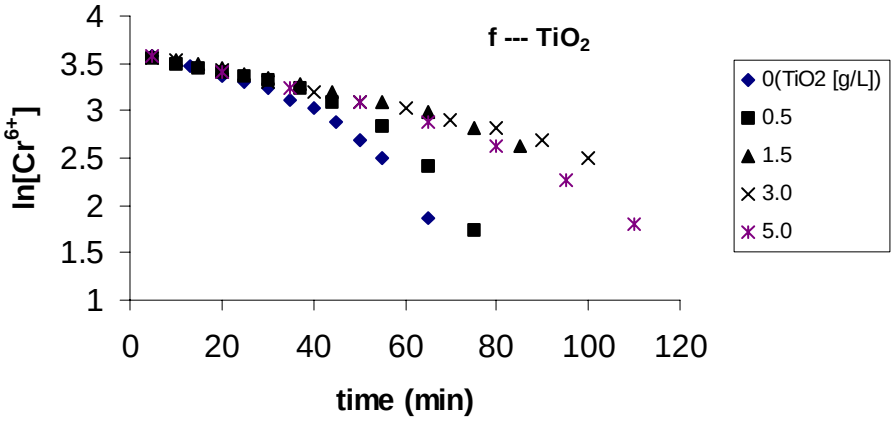

Figure 4-1 (Continued)

of ln[Cr(VI) versus time were linear; (3) in homogeneous system, ln[Cr(VI)] v.s. t in the initial stage displayed a linear trend, but deviated the linear line downwards, representing an accelerated reaction compared to the first order kinetics. If the data before the point of deviation were used in the ln[Cr(VI)] v.s. t plots, which corresponded to about 35% to 50% (i.e., 15 to 20μM) of the initial Cr(VI) was reduced, the derived rate constants for the homogeneous system were almost the same as those in the kaolin system (Figure 4-3). It was clear that with pH increase, the reaction rate was significantly decreased for both types of systems. The relationship between ln k_{obs} and pH was linear with a slope of 2.13 for the kaolin system and 2.05 for the homogeneous system, suggesting the overall reaction order with respect to H^+ was probably 2.

Adsorption of Cr(VI) and Sulfide: In the systems with 40.0 μM Cr(VI) and 3.0 g/l of illite or kaolin, no adsorption of Cr(VI) was observed as tested at pH 7.87. This agreed with previous studies (Buerge et al, 1999). Surfaces of illite and kaolin carried negative charges at this pH (much higher than PZC in Table 1), which reduced the adsorption of anionic Cr(VI) species (mainly CrO_4^{2-}) due to the unfavorable electronic interaction. In addition, borate might inhibit Cr(VI) adsorption because its concentration (0.10 M) was 2500 times as high as Cr(VI) concentration (40μM). Sulfide adsorption pH 7.87 was shown in Figure 4-4. It was clear that sulfide did not adsorb on kaolin, but soluble sulfide decreased approximately 13% or 104μM in the illite system.

Adsorption of Fe(II) on illite: The amount of adsorbed Fe(II) onto illite was assessed in the systems with and without sulfide being present (Figure 4-5). In the control with borate buffer solution but without any sulfide, ferrous iron associated with illite was about 7μM and was constant during a 90 min of testing. In the presence of 800μM of sulfide, the adsorbed Fe(II) was increased by about 4 μM in the first 30 min when compared to the control, then leveled off. The trend was somewhat similar to the adsorption of sulfide on illite. Comparing to the amount of sulfide adsorption of around 105 μM (Fig. 4-4b), this 4 μM of Fe(II), likely produced from the reduction of Fe(III) by sulfide, accounted for any a very small fraction of the sulfide adsorbed on illite. When a 50 μM of elemental sulfur was added into the mixture of illite and sulfide, even more adsorbed Fe(II) was produced than in the system with sulfide alone. The increased amount was about 1.5 to 2 μM. It was likely that the externally added elemental sulfur increased the activity of sulfide, which led to more Fe(III) reduced from the reaction between illite and sulfide.

No dissolved Fe(II) in the filtrate could be detected in all experiments, which indicated that Fe(II) was strongly adsorbed on the surface of illite at pH8.27.

Effect of Fe(II) on the reaction: To investigate whether Fe(II) from illite leads to catalysis of Cr(VI) reduction by sulfide, two types of experiments were designed: (i) addition of Fe(II) into the homogeneous system with Cr(VI) and sulfide and (ii) addition of phenanthroline into the system with Cr(VI), sulfide, and also illite. Phenanthroline is a strong chelating agent for Fe(II) and thus expected to the activities involving Fe(II). The effects of Fe(II) and phenanthroline were assessed against the homogeneous control system with Cr(VI) and sulfide. As shown in Fig. 4-6, addition of low concentration of Fe(II) (5.0 μM) into the homogeneous system dramatically accelerated the Cr(VI) reduction reaction as compared to the control. Kinetic behavior for Cr(VI) reduction was similar to the system with 3.0g/L illite, where about 7 to 11 μM Fe(II) in the adsorbed form was produced during the time period. Phenanthroline did not affect the reduction of Cr (VI) by sulfide in homogeneous system. It was interesting to notice that in the illite system, phenanthroline could

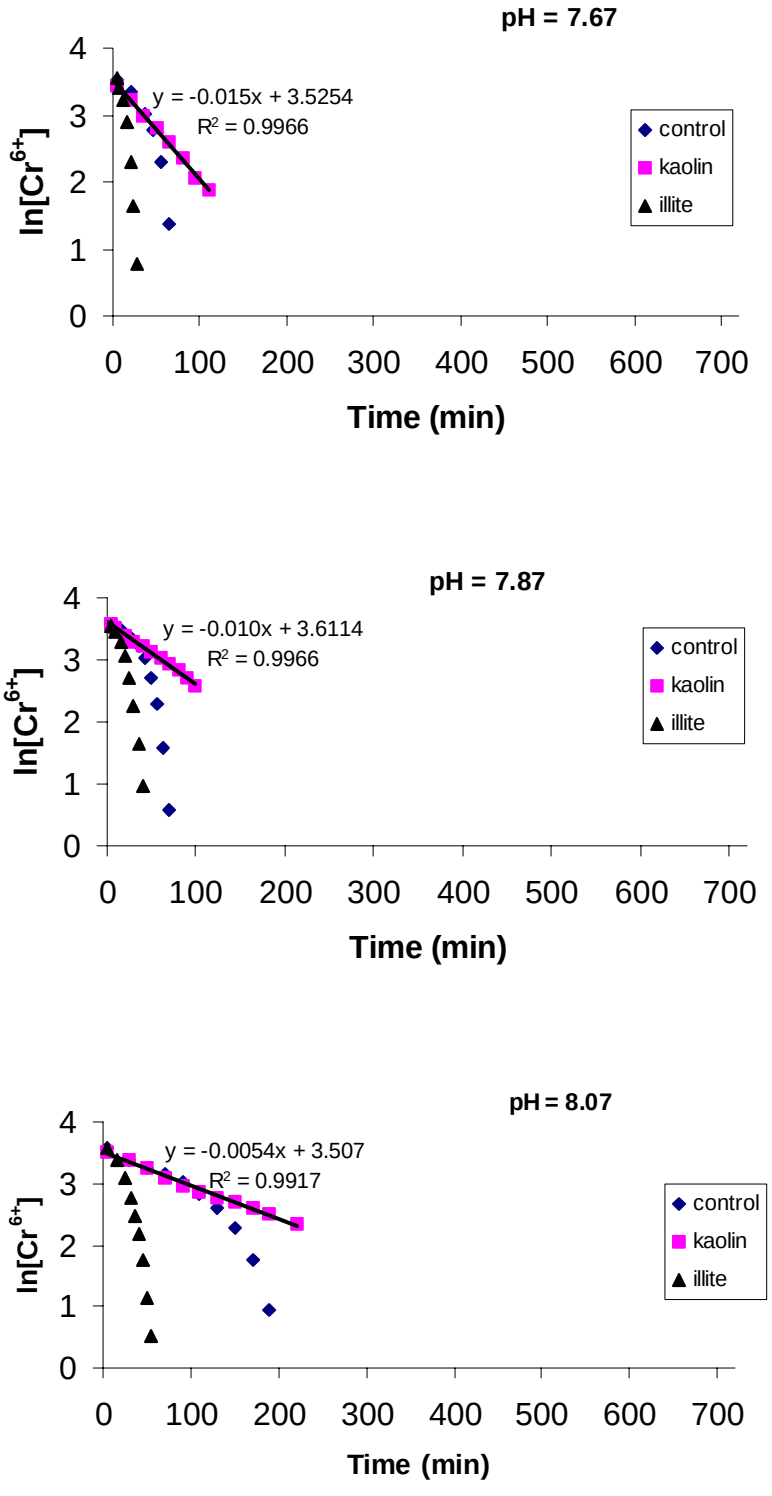

Figure 4-2. Kinetics of Cr(VI) reduction with and without solid surfaces at various pHs ($[Cr(VI)]_0$ = 40.0 40μM; $[sulfide]_0$ = 800μM; $[illite\ or\ kaolin]_0$= 3.0g/L; pH levels: 7.67, 7.87, 8.07, 8.27, 8.67 and 9.07).

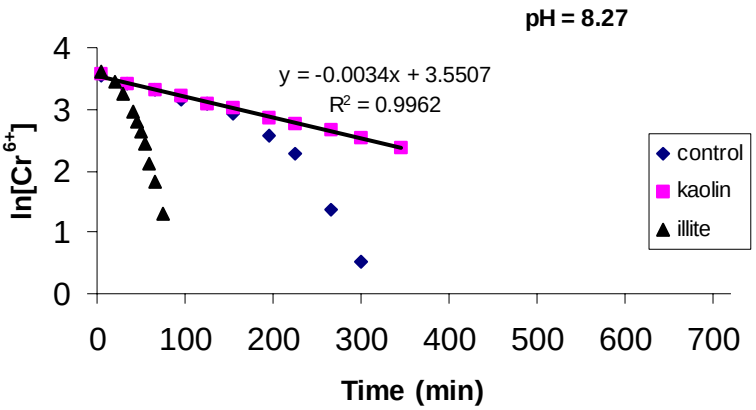

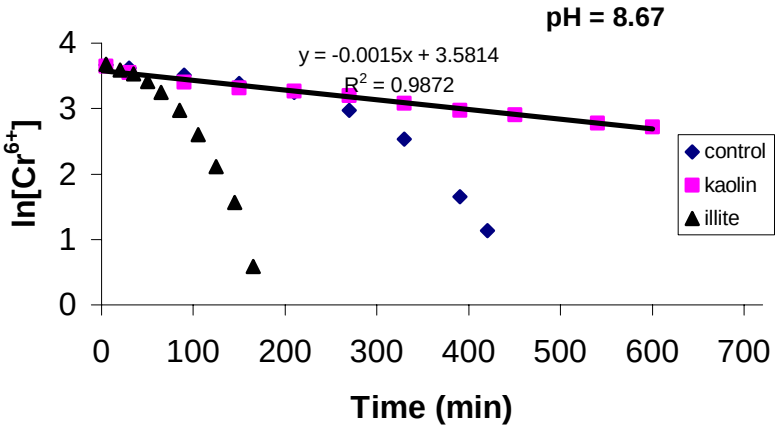

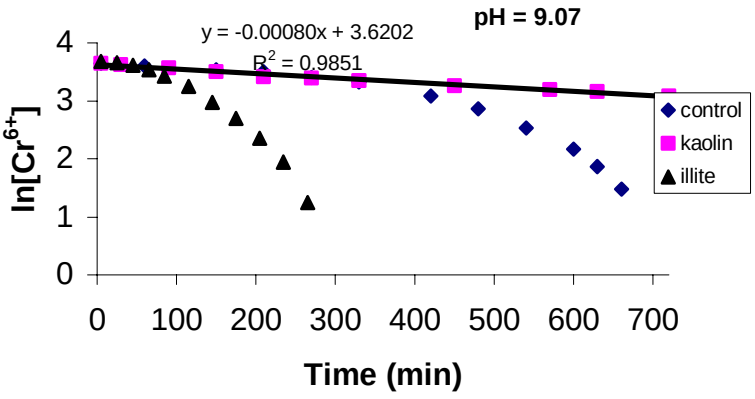

Figure 4-2 (Continued)

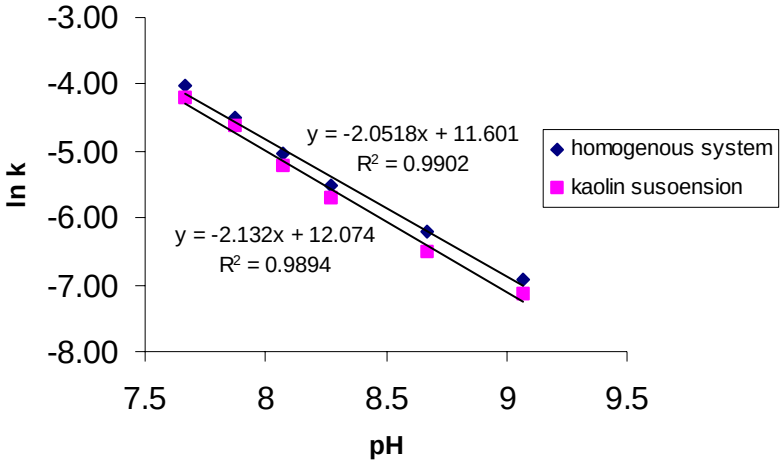

Figure 4-3. ln k_{obs} v.s. pH plots in the homogeneous system and kaolin systems. k_{obs} in the homogeneous system was obtained using the data collected in the initial stage of the reaction, where 35 to 50% of original Cr(VI) was reduced.

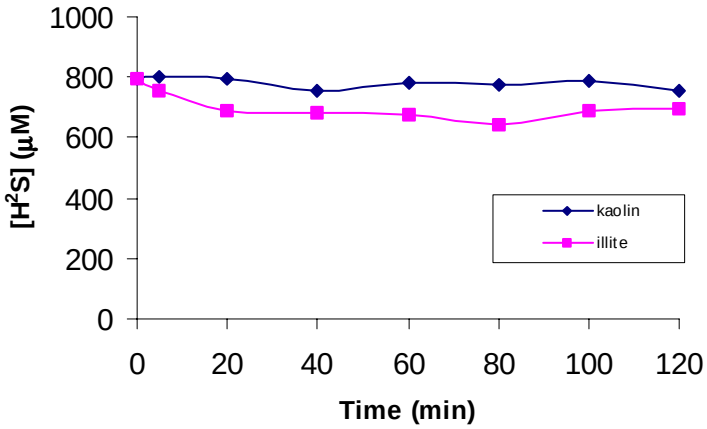

Figure 4-4. Adsorption of sulfide in the illite and kaolin systems at pH 7.87. The initial sulfide concentration is 800.0 µM.

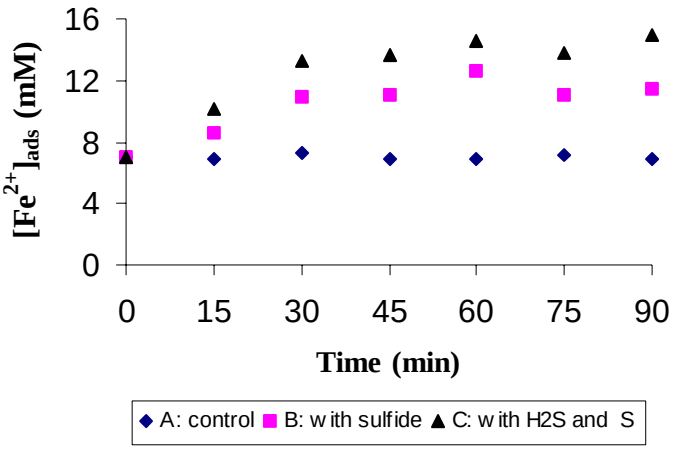

Figure 4-5. Adsorbed amounts of Fe(II) measured in the illite systems at pH8.27 (borate buffer). (A) control, (B) with 800µM sulfide, (C) with 800µM sulfide and 50µM added elemental sulfur.

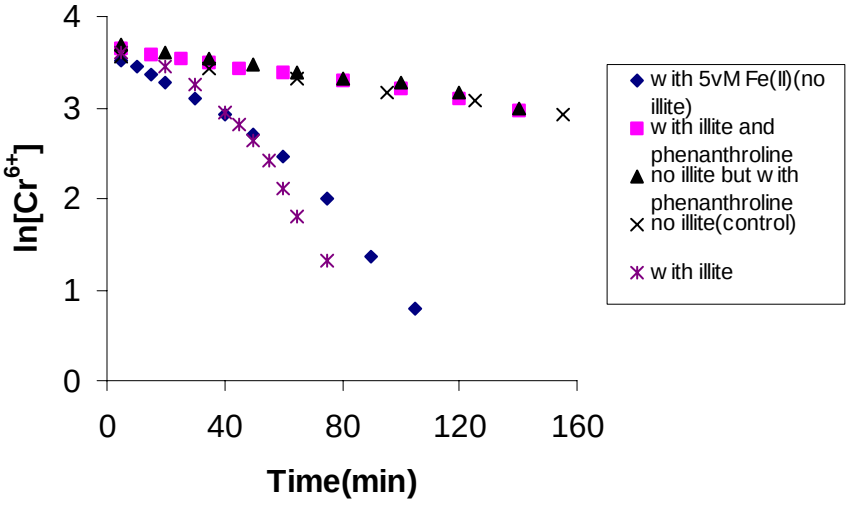

Figure 4-6. Effect of ferrous iron on the reduction of Cr(VI) by sulfide at pH8.27

completely block the effect of illite on the reduction of Cr(VI). In fact, in the following three systems: Cr(VI) + sulfide , Cr(VI) + sulfide+ phenanthroline, and Cr(VI) + sulfide + illite + phenanthroline, the ln[Cr(VI)] versus time plots were all linear with almost the same rate constant. The results suggested that both dissolved Fe(II) and absorbed Fe(II) could catalyze catalyze Cr(VI) reduction by sulfide, but once Fe(II) is in the chelated form with phenanthroline, it's catalytic capability disappeared.

CONCLUSIONS

Experiments in this section showed that the minerals could be categorized into three groups in terms of their effects on Cr(VI) reduction by sulfide. Illite exhibited dramatic catalytic effect on the reduction of Cr(VI) by sulfide. Al_2O_3 showed no obvious effect on the reaction. The third group, which included kaolin, montmorillonite, SiO_2 and TiO_2, inhibited the reduction of Cr (VI) as compared to the control without minerals being present. In the illite suspension, ferrous iron produced from the mineral dissolution, although at low concentration, was likely responsible for the rate acceleration by serving as an electron shuttle. The reaction rate increased with increasing Fe(II) concentration and at the later stage, the effect of elemental sulfur product could also be observed. When a strong Fe(II) chelating agent such as phenanthroline was added into the system, the effect of illite on Cr(VI) disappeared, suggesting Fe(II) bound to the strong ligand could not act as a catalyst. The inhibitive behavior observed for the third group was likely due to the uptake of elemental sulfur product on the mineral surfaces, so the catalytic effect from elemental sulfur was hindered.

V OXIDATION OF H_2S BY IRON OXIDES IN THE VADOSE ZONE

(Kirk J. Cantrell, Steven B.Yabusaki, Mark H. Engelhard,
Alexandre H. Mitroshkov and Edward C. Thornton)

INTRODUCTION

In situ gaseous reduction (ISGR) has been demonstrated to be an effective remediation technology for in situ immobilization of chromate in vadose zone sediments/soils (Thornton et al.1999). This gas phase approach for vadose zone treatment offers significant benefits over liquid phase in situ treatment approaches and excavation methods. For liquid phase in situ treatment, control of the treatment liquid within the desired volume of the vadose zone is difficult and has the potential to cause unintentional mobilization of the contaminants. Excavation is typically expensive, requiring ex-situ treatment, disposal and backfilling. Excavation also can also have practical limitations when the depth of contamination is great. The approach taken with the ISGR technology is to mix H_2S with a carrier gas (typically air or nitrogen) and pump the mixture through a central injection well installed within the contaminated volume of the vadose zone. Surrounding the injection well are a series of extraction wells that use vacuum pumps to draw gas through and treat the desired volume of the contaminated vadose zone. The primary reaction of interest for chromate immobilization is generalized as follows:

$$2CrO_4^{2-} + 3H_2S(g) + 2H_2O = 2Cr(OH)_3(s) + 3S^0 + 4OH^- \quad (1)$$

It is assumed that the chromate is adsorbed or precipitated onto soil surfaces. In this process, the highly mobile chromate anion is reduced to Cr^{3+} that precipitates as the hydroxide with a solubility that is generally less than the drinking water standard for pH values between 6 and 12 (Rai et al. 1987).

At room temperature, the rate of gas phase oxidation of H_2S by oxygen is negligible; however, iron oxides are well-known oxidizing reagents and oxidation catalysts for H_2S (Davydov et al., 1998; Wieckowska, 1995). For most soils the quantity of iron oxides that can act to oxidize H_2S will greatly exceed the quantity of the reducible target contaminants. As a result, it expected that the quantity of H_2S required to remediate a site and the rate of treatment will typically be dependent upon the quantity and form of the iron oxides in the soils and not on the amount of contaminants present. For example at the White Sands Missile Range pilot demonstration, the average Fe^{3+} concentration in the sediments was approximately 1,300 mg/kg, whereas the maximum Cr(VI) concentration was 85 mg/kg (Thornton et al., 1999).

The objective of this work is to develop a mechanistic understanding of the important reactions that occur between H_2S and iron oxides and to determine the reaction rates between H_2S and iron oxides. These reaction rates are required for the development of design and simulation models that can accurately predict the effectiveness of ISGR technology for environmental remediation applications.

BACKGROUND

Interactions between iron oxides or hydroxides H_2S for removal of H_2S from fuel gases such as natural gas and coal gas have been studied for well over a century. Davydov et al. (1998) recently summarized the stoichiometries for reaction of H_2S with ferric hydroxide as follows:

$$2Fe(OH)_3(s) + 3H_2S(g) \rightarrow 2FeS(s) + 1/8S_8(s) + 6H_2O \quad (2)$$

$$2Fe(OH)_3(s) + 3H_2S(g) \rightarrow 2Fe_2S_3(s) + 6H_2O \quad (3)$$

It was indicated that others have proposed that the initial reaction of Fe_2O_3 with H_2S produces Fe_2S_3 (Kattner et al. 1988)

$$Fe_2O_3(s) + 3H_2S(g) \rightarrow Fe_2S_3(s) + 3H_2O \quad (4)$$

and that Fe_2S_3 is thermodynamically unstable and reacts to form pyrite and Fe_3S_4

$$2Fe_2S_3(s) \rightarrow FeS_2(s) + Fe_3S_4(s) \quad (5)$$

As the process proceeds, the iron (hydr)oxides become depleted. To regenerate the iron (hydr)oxides, the sulfides are reacted with oxygen to produce iron (hydr)oxides and sulfur as a byproduct (Kohl and Riesefedl, 1985, Wieckowska, 1995, and Kattner et al, 1988)

$$4FeS(s) + 6H_2O + 3O_2(g) \rightarrow 4Fe(OH)_3(s) + 1/2S_8(s) \quad (6)$$

$$2Fe_2S_3(s) + 6H_2O + 3O_2(g) \rightarrow 4Fe(OH)_3(s) + 3/4S_8(s) \quad (7)$$

$$2Fe_2S_3(s) + 3O_2(g) \rightarrow 2Fe_2O_3(s) + 3/4S_8(s) \quad (8)$$

It should be noted that these equations represent the net stoichiometry of the reactions, other intermediate reaction steps may occur and therefore these reactions may not represent the complete reaction mechanisms, but represent the overall reaction pathways.

EXPERIMENTAL METHODS

Column experiments were conducted by mixing 1% H_2S in nitrogen with a carrier gas to produce a final influent H_2S concentration of approximately 200 ppm_v. Three carrier gases were used: dry nitrogen, dry air (21% oxygen) and 100% oxygen. Electronic gas mass flow controllers/ flowmeters (Aalborg, Orangeburg, New York) were used to control the flow rates of both gas streams. Electronic gas mass flowmeters were used to measure the influent and effluent flow and to verify that no significant leaks occurred in the system. The experiments were conducted at room temperature (20°C to 24°C). The substrate used for most experiments was ferrihydrite coated quartz sand. The procedure used to make the ferrihydrite coated quartz sand is detailed elsewhere (Szecsody et al. 1994). Briefly, acid washed Fisher silica (approximately 1.0 mm to 0.3 mm) was coated with iron oxide gel previously synthesized by hydrolysis of a 0.24 mol L^{-1} ferric chloride solution. The ferric oxyhydroxide gel was equilibrated approximately 24 h at pH 7.5 before mixing with the sand. The mixture was aged for approximately 4 days with pH adjustment to maintain the pH between 6.5 and 7.0, and was washed daily with 0.1 mmol L^{-1} NaCl. The coated material was then filtered in a large Buchner funnel and air-dried. Some darker iron oxide material that did not attach to the sand was removed by rinsing with deionized water over a #45 sieve (354 μm). The final iron concentration of this material was approximately 0.27 % Fe^{3+} by weight. Additional substrates included 1% goethite and 1% hematite coated sand and a < 2mm Hanford sediment.. Preparation of the 1% goethite and 1% hematite coated sands involved adding 1% by weight of dry goethite or hematite powder to dry sand, placing the sand mix in a glass sample jar and rotating overnight. The goethite (α-FeO(OH)) was obtained from Afla Aesar as a powder. The hematite was from Ironton, MN and was crushed to < 106 μm. XRD analysis

of these mineral indicated that the goethite was essentially pure, while the hematite had a minor amount of quartz impurity. The Hanford sediment was sieved to less than 2mm and contained 0.29% ferric iron as determined by 0.5 M HCl extraction. The experiments were conducted in 30.0 cm long x 0.9 cm ID Spectra/Chrom Glass columns. Teflon tubing was used to deliver the gas to and from the columns. Three flowrates were used 102, 204, and 510 standard cubic centimeters per minute (17.6, 35.2, 87.9 pore volumes per minute). H_2S was measured in the influent and effluent with electrochemical gas sensors (EIT, Exton, PA). The sensors were calibrated with certified standards containing 100 ppm_v H_2S in nitrogen. EIT sensors were also used to verify that no $SO_2(g)$ formed during the experiments.

Once the H_2S in the effluent exceeded approximately 90 % of the influent concentration, flow to the column was stopped and the column was transferred to an anaerobic chamber. The iron oxide coated sand was removed from the column and homogenized. Three separate extractions were conducted to determine reaction products. Extractions for sulfate, thiosulfate, and sulfite were conducted by adding 10.0 mls of oxygen free deionized water to 2.00 grams of sand in a centrifuge tube. The tube was placed on a rotator for approximately 24 hours in the anaerobic chamber. The extracts were analyzed by ion chromatography (Dionex, DX-120). An IonPac AS9-HC analytical column and an IonPac AG9-HC guard column were used. The eluent was 9.0 mM solution of Na_2CO_3 with a flow rate of 1.0 mL/min. Complete separation of all observed anions including sulfur-containing anions such as sulfate, sulfite, and thiosulfate was routinely achieved. Elemental sulfur was determined by extracting 1.00 gm of sand with 5.00 mls of benzene followed by Gas Chromatography – Mass Spectrometry (GC-MS) analysis using an HP5890/5970 system. In this procedure, an HP-1 capillary column (L = 30 m, 0.32 mm i.d., 0.17 μm film) was used. The temperature program was 50°C to 250°C @ 15°C/min., with a 5 min. hold time. Each analysis included a four level calibration was conducted using an SV Internal Standard Mix (RESTEK, #31006). Ferrous and ferric iron extractions were conducted by adding 2.00 grams of sand to 10.0 mls of oxygen free 0.5 M HCl and rotating the mixture in tubes in the anaerobic chamber for approximately 24 hours. The iron was analyzed colorimetrically with the phenathroline method (Loeppert and Inskeep, 1996).

Surface analysis of the reacted iron oxide coated sand was conduced with X-ray photoelectron spectroscopy (XPS) to identify reaction products. XPS measurements were made on a Physical Electronics Quantum 2000 Scanning ESCA Microprobe. This system uses a focused monochromatic Al Kα x-ray (1486.7 eV) source for excitation and a spherical section analyzer. The instrument has a 16 element multichannel detection system. The X-ray beam used was a 100W, 100 um diameter beam that is rastered over a 1.4 mm by 0.2 mm rectangle on the sample. The x-ray beam is incident normal to the sample and the x-ray detector is at 45° away from the normal. The survey scans were collected using a pass energy of 117.4 eV. For the Ag 3d 5/2 these conditions produce FWHM of better than 1.6 eV. The high-energy resolution data was collected using a pass energy of 23.5 eV. For the Ag 3d 5/2 these conditions produce FWHM of better than 0.75 eV. The collected data were referenced to an energy scale with binding energies for Cu 2p 3/2 at 932.67± 0.05 eV and Au 4f at 84.0± 0.05 eV. Low energy electrons and argon ions were used for specimen neutralization.

RESULTS AND DISCUSSION

H_2S Reaction with Ferrihydrite: H_2S breakthrough curves for three column experiments with the ferrrihydrite coated sand, using three different carrier gases, conducted at a flowrate of 102 sccm are shown in Figure 5-1. These curves are plotted as the ratio of effluent concentration over influent concentration vs. time. The influent H_2S concentration in each case was approximately

200 ppm_v. The carrier gases used were nitrogen, air (21% oxygen), and 100 % oxygen. The fastest breakthrough occurs when the carrier gas is 100 % oxygen. The second fastest breakthrough occurs when air is the carrier gas and the slowest breakthrough occurs when N_2 is the carrier gas.

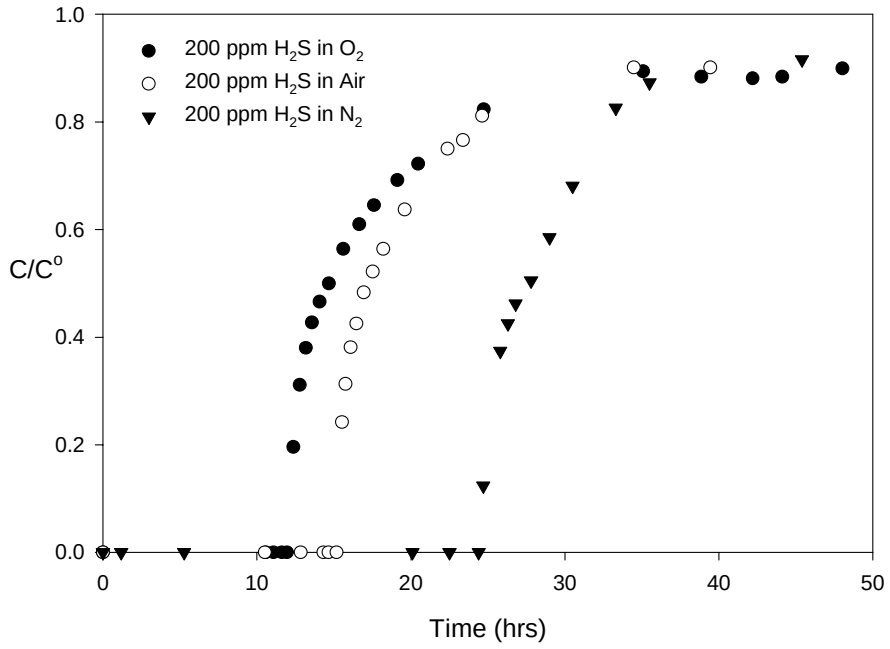

Figure 5-1. H_2S breakthrough curves for ferrihydrate coated sand (0.27 % Fe^{3+}) in various carrier gases (200 ppm H_2S) at a flowrate of 102 sccm.

Column breakthrough curves for three different flowrates, where N_2 was used as the carrier gas, are plotted in Figure 5-2. In this case, the ratio of effluent concentration over influent concentration is plotted against the ratio of the total moles of H_2S reacted over the total moles of Fe^{3+} in the column. The breakthrough curves are shifted to lower H_2S/Fe^{3+} ratios at the flowrate increases. This is consistent with a rate-controlled process. If the reactions occurred as an equilibrium process, these breakthrough curves would be expected to be coincident.

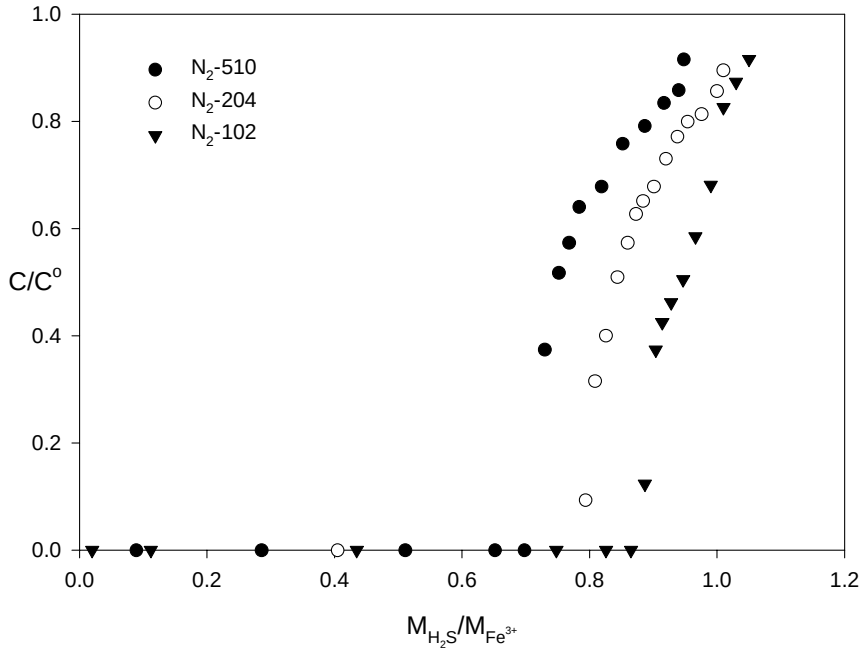

Figure 5-2. H_2S breakthrough curves for ferrihydrite coated sand (0.27 % Fe^{3+}) in nitrogen (200 ppm H_2S) at various flowrates.

Mass balance results (on a molar basis) for each of the column experiments are presented in Table 1. Included in the table is the column name (determined from the carrier gas and flowrate in standard cubic centimeters per minute), the initial (unreacted) ferric iron content determined from the 0.5 M HCl extracts, quantity of H_2S that reacted within the column, the ferrous iron (FeS), sulfur, moles of thiosulfate-sulfur, moles of sulfate-sulfur and moles of FeS_2-sulfur. The 0.5 M HCl extraction will dissolve FeS but not FeS_2 (Heron et al., 1994); therefore, FeS_2 sulfur was determined by assuming that the difference between the total iron before and after the experiment was FeS_2. A breakthrough experiment conducted on the silica sand (with no ferrihydrate) indicated that H_2S adsorption onto the silica surfaces was negligible.

Table 1. Mole balance for column experiments (n.m. – not measured, n.d. – not detected).

Column	**Init. Fe^{3+}**	**H_2S Used**	**Fe^{2+}(FeS)**	**Sulfur-S**	**Thio-S**	**Sulfate-S**	**FeS_2-S**	**Total-S Products**
N_2-102	1.67e-3	1.95e-3	1.33e-3	6.60e-4	7.40e-6	2.60e-6	n.d.	2.00e-3
N_2-204	1.70e-3	1.85e-3	1.33e-3	4.90e-4	n.m.	n.m.	n.d.	1.82e-3
N_2-510	1.69e-3	1.60e-3	1.43e-3	5.30e-4	n.m.	n.m.	n.d.	1.96e-3
O_2-102	1.70e-3	1.31e-3	8.32e-5	5.89e-4	3.64e-5	3.70e-5	4.02e-4	1.15e-3
Air-102	1.64e-3	1.24e-3	1.05e-4	6.30e-4	3.28e-5	4.75e-5	3.91e-4	1.21e-3

For easier comparisons, these values are converted to a percentage basis, relative to the quantity of H_2S (Table 2). For the N_2 experiments, thiosulfate and sulfate were measured in just one experiment because it was determined that these reaction products account for a very small fraction of the total H_2S oxidation products. Note that if equation 2 is the only reaction of significance, the mole balance of FeS and S^0 relative to the moles of H_2S consumed should be 67% and 33% respectively. The results for the N_2 experiments are very close to these theoretical values and indicate that equation 2 is the primary reaction that occurs between H_2S and ferrihydrate in the absence of O_2.

Table 2. Mass balances (percent H_2S basis) for column experiments (n.m. – not measured).

Column	**H_2S Used**	**Fe^{2+}(FeS)**	**Sulfur-S**	**Thio-S**	**Sulfate-S**	**FeS_2-S**	**Total-S Products**
N_2-102	100	68	34	0.4	0.1	0	103
N_2-204	100	72	26	n.m.	n.m.	0	98
N_2-510	100	89	33	n.m.	n.m.	0	122
O_2-102	100	6.3	45	2.7	2.8	31	88
Air-102	100	8.5	51	2.6	3.8	32	98

XPS analyses were conducted on some of the reacted materials to identify the reaction products. Sulfur species results for the N_2-102 column are shown in Figure 5-3. Regression analysis of these results, indicate that the reaction products are consistent with FeS, and S^0, with a small amount of sulfate. The XPS results indicate 60% FeS (mackinawite, $Fe_{1+x}S$ (x = 0.01 – 0.08)), and 34% S^0, and are very close to the theoretical values. The formation of mackinawite is consistent with results obtained in low temperature aqueous systems. Lennie and Vaughan (1996) indicate that the iron monosulfides mackinawite and amorphous FeS are the first formed iron sulfides in aqueous systems at low temperature and amorphous FeS is rapidly converts to mackinawite. The XPS results also indicated a sulfate concentration of 4.5%. This value is significantly higher than that determined by analysis of the water extracts. The likely explanation for this discrepancy is that a small amount of FeS oxidation at the surface occurred as a result of brief exposure to air that occurred during the transfer of the sample from the inert atmosphere storage to the XPS sample chamber. Because XPS is a surface technique (sensitive to a depth of approximately 5 to 50 Å), the measured concentration of sulfate in this surface zone is likely to be elevated relative to the bulk sulfate content determined from the water extracts.

The results of the experiments in which oxygen and air were used as carrier gases (Tables 1 and 2) indicate that equation 2 alone cannot explain these results. A significantly higher degree of oxidation is apparent in the reaction products. For example, FeS makes up only a small fraction of the reaction products (6-9%). Although the amount of H_2S consumed in the experiments that had oxygen in the carrier gas was about 70% of that consumed in the nitrogen carrier gas experiments, the quantity of sulfur that was produced was nearly the same or slightly higher. This suggests that reaction 6 is important when oxygen is in the carrier gas. When oxygen is in the carrier gas, a small fraction of thiosulfate and sulfate were also produced. Although the concentrations of these reaction products make up only a relatively small fraction of the total sulfur balance, they are significantly higher than observed in the nitrogen carrier gas experiments. A number of possible reaction pathways are possible for these two oxidation products; however, because of the dominance of reaction 2 in the absence of oxygen, the following reaction pathways are assumed:

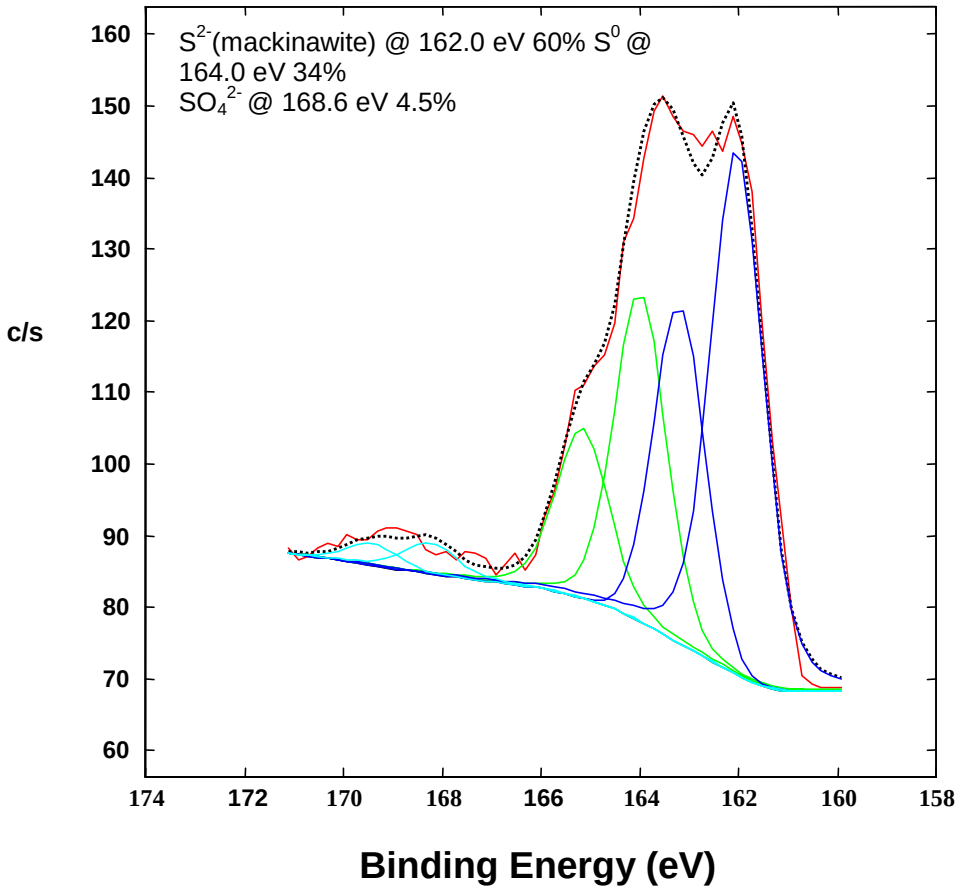

Figure 5-3. XPS spectra (dotted line) and best fit (red) for sample from column N_2-102. The best fit was determined using S^{2-} (blue), S^o (green), and SO_4^{2-} (aqua).

$$FeS(s) + 9/4O_2(g) + 5/2H_2O \rightarrow H_2SO_4 + Fe(OH)_3(s) \quad (9)$$

$$FeS(s) + 5/2O_2(g) + 4H_2O \rightarrow H_2S_2O_3 + Fe(OH)_3(s) \quad (10)$$

The most significant reaction product, for the experiments that had oxygen in the carrier gas, besides sulfur, is FeS_2. As indicated earlier, previous workers have indicated that FeS_2 could be produced through the reaction pathway shown in equation 3, followed by equation 5. If this were true, it would be expected that these reactions would also occur in the absence of oxygen; however, no FeS_2 is produced under these circumstances in our experiments. It should be pointed out that it is possible that not all of the reactions pathways that have been put forth in the

literature for reaction of H_2S with iron (hydr)oxides (equations 2 though 8) are necessarily applicable to our low temperature conditions. Based on reasoning suggested earlier for the formation of thiosulfate and sulfate, it is suggested that FeS_2 is produced through oxidation of FeS as follows:

$$FeS(s) + 1/2O_2(g) + H_2S(g) \rightarrow FeS_2(s) + H_2O \qquad (11)$$

A variety of alternative reaction pathways could be suggested, for example, mackinawite is known to readily oxidize to greigite ($Fe_3S_4(s)$) (Lennei et al, 1997). In our system this could occur as follows;

$$3FeS(s) + 1/2O_2(g) + H_2S(g) \rightarrow Fe_3S_4(s) + H_2O \qquad (12)$$

Greigite might then dissociate as proposed by Hallberg (1972);

$$Fe_3S_4(s) \rightarrow 2FeS(s) + FeS_2(s) \qquad (13)$$

this reaction is known to be thermodynamically favorable (Berner, 1967). The net reaction of equations 12 and 13; however, is equation 11. Work conducted in aqueous systems suggests that FeS reacts rapidly with sulfur to produce FeS_2 (Rickard, 1975; Luther, 1991; Lennie et al., 1997):

$$FeS(s) + 1/8S_8(s) \rightarrow FeS_2(s) \qquad (14)$$

however, if equation 14 was significant for the conditions of our experiments, then it should have also occurred in the absence of oxygen (nitrogen carrier gas experiments), which it did not.

Based on this analysis it is concluded that the primary reactions of interest, for H_2S in a carrier gas containing oxygen, with ferrihydrate are equations 2, 6, and 11. Equations 9 and 10 will play a minor role. The mass balance results of Table 2 indicate that the majority of the FeS that forms in the oxygen containing carrier gas experiments is further oxidized and that both reactions 6 and 11 are important. For example, if all the sulfur that was formed occurred only as a result of equation 2, then a percent sulfur of 33% would be expected; however, from Table 2 it is apparent that the fraction of H_2S that becomes oxidized to sulfur is significantly higher. XPS analysis was conducted on a sample from column Air-102 in an attempt to confirm the mole balance results shown in Table 1. The results indicated that the distribution of sulfur species at the surface was 55 mole % sulfate, 34 mole % sulfur, 7 mole % sulfite, and 5 mole % S_2^{2-} (probably marcasite). When air is in the gas phase, it can be expected that greatest degree of oxidation would occur at the surface relative to the bulk. Therefore, these results do not provide useful quantitative results to confirm the mass balance data in Tables 1 and 2, but it does confirm that a S_2^{2-} phase (presumably marcasite) does form.

H_2S Reaction with Other Iron Oxides and Natural Sediments: A comparison of H_2S column breakthrough results for one-percent goethite coated sand (0.63% Fe^{3+}) and one-percent hematite coated sand (0.70% Fe^{3+})(200 ppm H_2S in N_2 at a flowrate of 102 sscm) is shown in Figure 5-4. By comparing these results with the results for ferrihydrite coated sand (containing only about half as much ferric iron) in Figure 5-1, it is clear that goethite and hematite are much less reactive than ferrihydrite. In addition, hematite is much less reactive than goethite, with very little reactivity at all. Mass balance results for these two experiments indicate that only 11% of the available ferric iron in the goethite and 0.6% of the available iron in the hematite were reduced in

these experiments. This is sharp contrast to the ferrihydrite (N_2 carrier gas) experiments, in which approximately 80% of the available ferric iron was reduced.

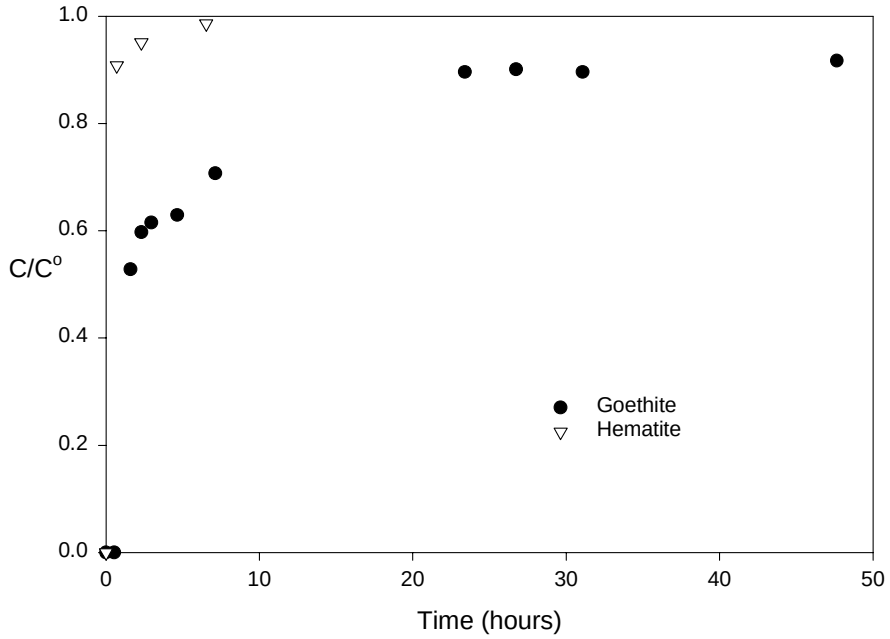

Figure 5-4. H_2S breakthrough curves for 1% goethite (0.63% Fe^{3+}) and 1% hematite (0.70% Fe^{3+}) coated sand in nitrogen (200 ppm H_2S) at a flowrate of 102 sccm.

Figure 5-5 shows results for two H_2S column breakthrough curves for Hanford sediments. Both experiments were conducted at a flowrate of 102 sscm and an H_2S concentration of 200 ppm; however, one experiment was conducted using N_2 as the carrier gas and the other using air as the carrier gas. Similar to the ferrihydrite experiments shown in Figure 5-1, the experiment in which air was used for the carrier gas broke through before the experiment using N_2 as the carrier gas. No significant delay prior to breakthrough occurs in these experiments. This behavior is more consistent with that observed for the goethite experiments than the ferrihydrite experiments. In the experiment in which N_2 was used as the carrier gas, 64% of the available ferric iron was reduced during the experiment. These results indicate that oxidation of H_2S by iron oxides in Hanford sediments has characteristics that are similar to both ferrihydrite coated sand and goethite. The amount of available ferric iron that actually gets reduced is more similar to ferrihydrite coated sand, but the characteristics of the breakthrough curve is more similar to goethite coated sand. Further studies are required to determine the mechanism responsible for these differences in behavior.

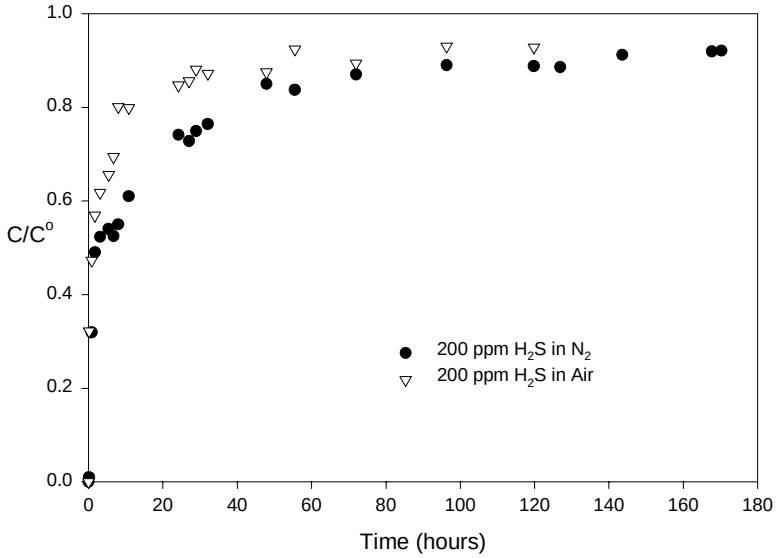

Figure 5-5. H_2S breakthrough curves for Hanford sediment (0.29 % Fe^{3+}) in nitrogen and air (200 ppm H_2S) at a flowrate of 102 sccm.

Determination of Reaction Rates and Transport Modeling: Based on the postulated sets of reactions for the nitrogen and oxygen cases, our conceptual model is based on the initial availability of $Fe(OH)_3$ that can react instantaneously with H_2S. H_2S entering the column reacts with the first $Fe(OH)_3$ it encounters to form FeS and S. Without any constraints on the reactivity of the $Fe(OH)_3$, a reaction "front" with FeS and S behind it and unreacted $Fe(OH)_3$ ahead would slowly propagate down the column with eventual breakthrough at 1.6 days. Because it is known that the actual H_2S breakthrough is considerably earlier in both nitrogen and air experiments, our conceptual model must account for the reduction in iron oxide reactivity due to the formation of secondary minerals at the surface, specifically sulfur.

The ferrihydrite precipitated on the surfaces of the quartz sand contained an average concentration of 0.269%. Visually, the ferrihydrite appeared to coat the sand grains but the SEM images (Fig. 5-6) show that the ferrihydrite does not uniformly coat the sand and, in fact, exists as "patches" of varying sizes. The interpretation here is that the surfaces of these ferrihydrite "patches" are initially directly accessible to the H_2S gas and account for the bulk of the initial ferrihydrite reactivity. While the formation of secondary minerals on the ferrihydrite surfaces can eventually limit the transport of H_2S to the underlying active ferrihydrite, it is the larger and/or thicker patches with lower surface area to volume ratios that will be more susceptible to this surface "suffocation." Over time, in this conceptual model, bulk ferrihydrite reaction rates will range from essentially instantaneous down to nearly zero.

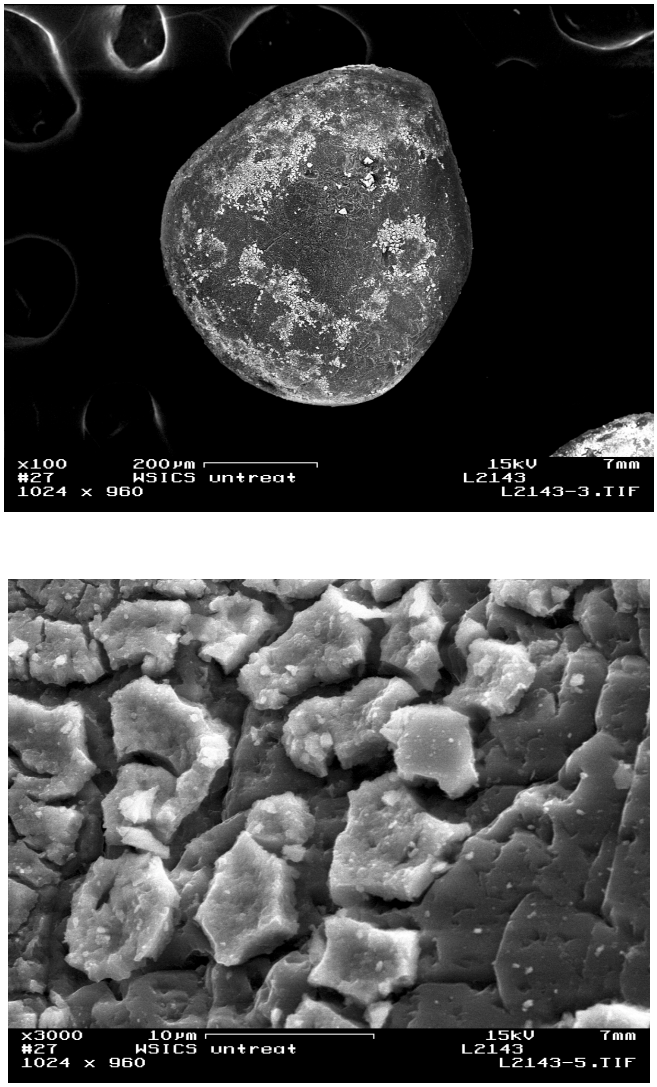

Figure 5-6. SEM Images of the Ferrihydrite Coated Sand.

The multiple reaction rates can be modeled in many ways. Two general approaches were explored: 1) parallel reactions with different reaction rates for different ferrihydrite fractions, and 2) evolving ferrihydrite reactivity dependent on the sulfur mineral volume. Testing of the different conceptual models was performed with the RAFT simulator (Chilakapati, 1995, Chilakapati, et al. 1998, 2000). In this case, RAFT was used to model transport and reactions in the 1-D column experiments. RAFT uses an operator split, sequential, non-iterative approach based on second-order total variation diminishing transport and a differential algebraic equation solution of the system of equilibrium and kinetic reactions. Estimation of reaction rates and ferrihydrite fractions to fit the column breakthrough behavior was performed with UCODE (Poeter and Hill, 1999).

Actual measured influent H_2S concentrations were modeled for all experiments to capture the effects of variability that were observed. The 30-cm columns were treated as initially

homogeneous soils (uniform porosity and initial ferrihydrite distributions) resolved with 25 1.2 cm grid cells.

Nitrogen Carrier Gas Case

Initial modeling and testing of parallel ferrihydrite reactions with first-order kinetics indicated that reaction 2 would have to be assigned to four ferrihydrite fractions with different rates to match the breakthrough behavior. While the dominant fraction would be the ferrihydrite associated with the instantaneous reaction rate, three additional first-order kinetic mass action reactions were necessary to match the breakthrough behavior of H_2S effluent concentrations.

With the knowledge that the H_2S breakthrough could not be addressed simply with one or two first-order kinetic reactions, we began investigating more mechanistic approaches consistent with our conceptual model of evolving reactivity. The first approach tested was the shrinking core model (Levenspiel, 1998), which accounts for diffusion-limited H_2S access to the active ferrihydrite surface through formation of secondary minerals on the idealized spherical particles. In this case, an increasing volume of reaction products continually increases the diffusion length, which effectively decreases the transport rate of H_2S to the reactive iron surfaces. The diffusive length between the particle surface and the active iron surface continually increases with time as the ferrihydrite is reacted. In this approach, the reaction rate gradually evolves from instantaneous to slower diffusion-limited rates.

It was found that additional particle sizes would have to be introduced to capture the post-breakthrough H_2S behavior. This is because once the particle surface diffusion coefficient is specified, the particle size is the only remaining parameter that can significantly alter the transport-limited reaction rate. It also became apparent that the initial breakthrough of H_2S could be effectively controlled by the specification of a fixed fraction of the iron that reacts instantaneously with H_2S gas.

To gain better control of the diminishing ferrihydrite reactivity, we investigated a surface poisoning rate law that inhibits reactivity as the formation of reaction products approaches a critical concentration/volume (Perry and Chilton, 1973).

$$\frac{d[H_2S]}{dt} = -k_{f1}\left(1 - k_{s1}[S^0]\right)[H_2S]$$

where

$$k_{f1} = \textit{forward rate}\left(s^{-1}\right)$$

$$k_{s1} = \textit{inhibition cons}\tan t\left(cm^3 / \textit{Moles}\right)$$

In this rate law, the irreversible reaction rate of H_2S with ferrihydrite is dependent on the H_2S and sulfur (S^0) concentrations. As the sulfur concentration at a given location in the column increases from zero, the rate is linearly reduced until the sulfur concentration approaches the inverse of the inhibition constant, k_{s1}, whereupon the rate goes to zero. Note that although $Fe(OH)_3$ is not explicitly included in the rate law, reaction 2 will not proceed when either reactant [i.e., H_2S and $Fe(OH)_3$] is not present.

To accommodate this conceptual model, we employ two quantities of $Fe(OH)_3$ that sum to the total ferrihydrite in the system: highly reactive "fast" ferrihydrite and diffusion-limited iron. The

fast ferrihydrite reaction is reaction 2 treated as an equilibrium reaction with an arbitrarily high stability constant (log K = 12) that essentially drives the reaction to completion (i.e., until one of the reactants is depleted). For the diffusion-limited ferrihydrite, reaction 2 is treated as a kinetic reaction using the surface poisoning rate law to dynamically account for the increasing elemental sulfur volume fraction that limits the transport of H_2S to the reactive surface.

The UCODE parameter estimation framework was used to fit 1) initial distribution between "fast" and diffusion-limited iron, 2) inhibition constant, k_s, and 3) intrinsic rate, k_f. The approach was to fit these parameters for the two parallel reactions in the slowest of the three nitrogen experiments, 102 sccm, and test the fit against the faster experiments at 204 and 510 sccm. The result was a reasonably good simulation of the reactive transport behavior (Fig. 5-7) under a range of flow rates. The model simulations were also in general agreement with measurements at the end of the three nitrogen column experiments for moles of H_2S consumed and moles of FeS and S^0 produced (Fig. 5-8). Most simulated components were within 10% of the observed. It was concluded that the prevailing dynamics of reaction and transport had been adequately captured for this case. The fitted parameters were: 8.07×10^{-5} moles/cc of fast ferrihydrite, 1.96×10^{-4} moles/cc of diffusion-limited ferrihydrite, and 9.57×10^{3} cc/mole sulfur inhibition (k_{s1}).

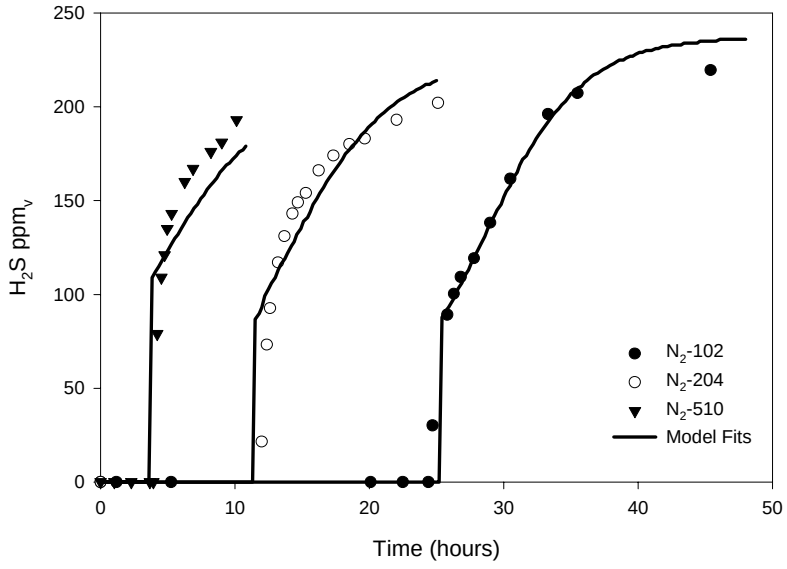

Figure 5-7. Comparison of Measured Effluent Concentrations of H_2S with Model Fits for Columns N_2-102, N_2-202, and N_2-510.

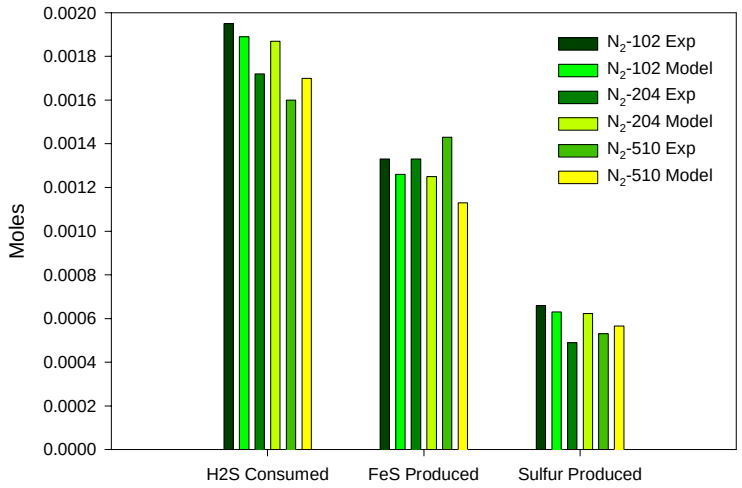

Figure 5-8. Comparison of Measured Values for H_2S Consumed, FeS Produced and S^0 Produced with Model Determined Values for Columns N_2-102, N_2-202, and N_2-510.

Air Carrier Gas Case

The modeling approach to the air case builds on the two parameterized parallel reactions from the nitrogen case and adds in the two oxidation reactions (reactions 6 and 11). From the standpoint of controlling the initial breakthrough of H_2S, reaction 6 is critical to the enhanced production of elemental sulfur (as compared to the nitrogen case) that reduces the reactivity of the available ferrihydrite and results in the H_2S breakthrough at 0.65 days compared with 1.03 days for the nitrogen case. The amount of fast ferrihydrite determined from the nitrogen experiments is still consistent with the earlier breakthrough; i.e., if fast ferrihydrite alone controlled the breakthrough, it would occur at 0.47 days. Consequently, we continued to use the initial fast ferrihydrite mole fraction as well as the intrinsic rate and inhibition constant from the iron surface poisoning reaction rate law.

Our initial application of UCODE to the air case focused only on identifying reaction rates for the oxygen reactions (reactions 6 and 11). The modeling provided considerable insight on the interplay between the reactions. The enhanced production of elemental sulfur in reaction 6 must be fast enough to accumulate enough sulfur in addition to sulfur created by reaction 2 to inhibit ferrihydrite reactivity leading to early H_2S breakthrough. Additionally, the pool of FeS provided by the equilibrium (i.e., fast ferrihydrite) reaction 2 will eventually lead to three times the sulfur produced in the nitrogen case, which is not consistent with the experimental measurement. It was clear that simple mass action kinetics for reaction 6 was not sufficient to describe the observed behavior. Once again we invoked the surface poisoning rate law, this time for reaction 6. Nominally, the reaction rate should be dependent on the oxygen concentration; however, the relatively high concentration of oxygen (210,000 ppm) remains essentially constant during the reactions. Consequently, we eliminated oxygen dependence from the rate laws for reactions 6 and 11, essentially incorporating the constant concentration into the intrinsic rate constant.

$$\frac{d[FeS]}{dt} = -k_{f2}\left(1 - k_{s2}[S^0]\right)[FeS]$$

where

$k_{f2} = forward\ \ rate\left(s^{-1}\right)$

$k_{s2} = inhibition\ \ constan\ t\left(cm^3 / Moles\right)$

$$\frac{d[FeS]}{dt} = -k_{f3}[H_2S][FeS]$$

where

$k_{f3} = forward\ \ rate\left(s^{-1}\right)$

UCODE was subsequently applied to the air case to identify the intrinsic rate constants for reactions 6 and 11, as well as an additional sulfur inhibition constant for reaction 6. The comparison of the model and observed concentrations for the Air-102 experiment are shown in Fig. 5-9. While the model simulation of the initial H_2S gas breakthrough was 1.8 hours later than the experimental observation at 15.5 hours, much of the general behavior was captured. Furthermore, the comparison between simulated and measured moles of consumed and produced components at the end of the experiment were very good (Figure 5-10). The principal discrepancy was that 1.57E-4 moles of FeS were predicted to be produced compared with the 8.32E-5 moles

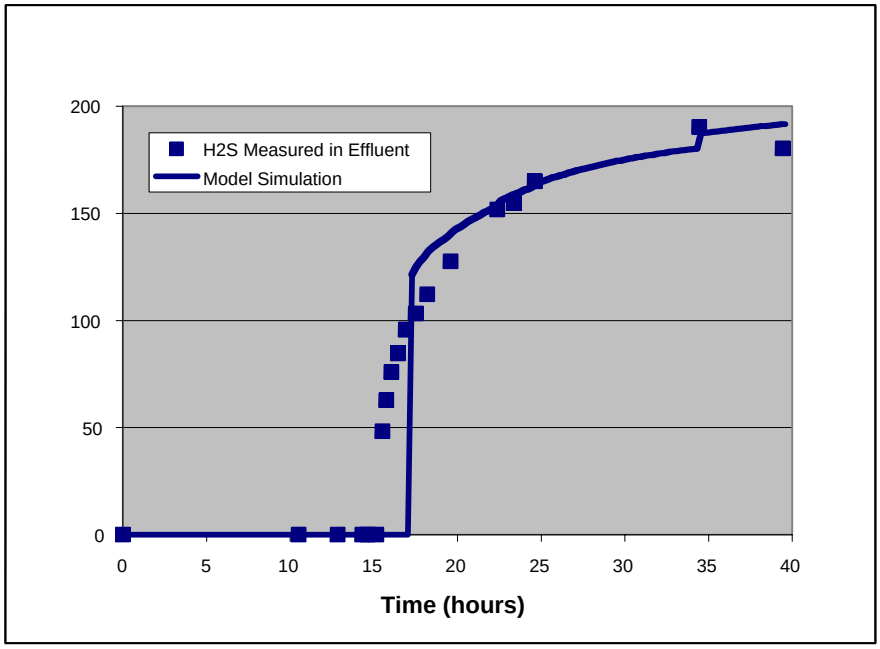

Figure 5-9. Comparison of Measured Effluent Concentrations of H_2S with Model Fits for Air-102 Experiment.

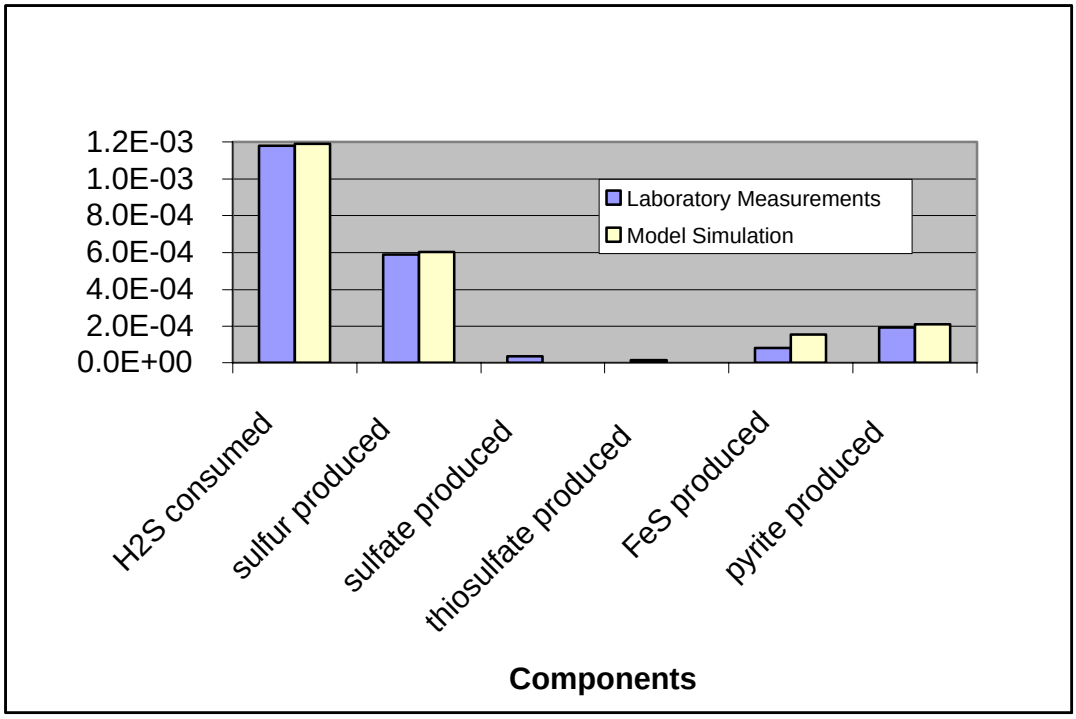

Figure 5-10. Measured and Simulated Component Moles at Experiment End.

that were measured. This might be explained by our omission of reactions 9 and 10 which produce sulfate and thiosulfate, respectively, from the oxidation of FeS. The 3.70E-5 moles of sulfate and the 1.82E-5 moles of thiosulfate measured at the end of the experiment represent the oxidation of 7.34E-5 moles of FeS that are not captured in the model. This is essentially the discrepancy between the simulated and measured FeS.

As mentioned previously, the calibration of the oxygen reaction rates and inhibition contant was performed while maintaining the rates and contant for reaction 2 determined from the nitrogen carrier gas experiment. The fitted parameters were:
intrinsic irreversible rate for reaction 6 (k_{f2}) = 8.75 x 10^1 (1/day)
intrinsic irreversible rate for reaction 11 (k_{f3}) = 8.72 x 10^7 (1/day)
FeS inhibition constant (k_{s2}) = 1.07 x 10^4 (cc/mole)

The model appears to capture the salient features of the H_2S breakthrough. More importantly the model provided significant insights on the processes controlling the H_2S breakthrough.

- The fast (equilibrium reaction 2) iron fraction must be completely depleted before H_2S breakthrough takes place.
- $Fe(OH)_3$ reactivity, which regulates the H_2S breakthrough behavior through kinetic reaction 2, is ultimately inhibited by the formation of elemental sulfur

- The rate of elemental sulfur formation in reaction 6 must be sufficiently fast to accelerate the inhibition of the $Fe(OH)_3$ reactivity that results in the earlier H_2S breakthrough in the air case; however, the production of sulfur through reaction 6 must diminish significantly prior to H_2S breakthrough to allow kinetic reaction 2 to control the shape of the breakthrough.
- Reaction 11 provides a slow but continuous conversion of the available FeS to pyrite in the presence of H_2S and O_2. Post-breakthrough H_2S behavior is also regulated by the consumption of H_2S in this reaction.

CONCLUSIONS

An understanding of the processes determining the consumption of H_2S during interaction with sediments is important with regard to the design of ISGR field remediation activities. The primary sediment component involved in these interactions is ferric (hydr)oxides, which are reduced by H_2S. The results of the study presented here illustrate that the reactions involving the ferric oxide ferrihydrite with H_2S under anaerobic and aerobic conditions are largely understood from a mechanistic standpoint. Future work will focus on extending this work to develop a better understanding of the reaction and diffusional processes determining H_2S consumption by sediments under natural conditions.

VI. IMMOBILIZATION OF CHROMIUM, TECHNETIUM, AND URANIUM IN SOILS FROM THE HANFORD SITE, WASHINGTON

(E.C. Thornton, V. Legore, and K. Olsen)

INTRODUCTION

The objectives of testing activities summarized in this section are to determine (i) if Tc- and U-contaminated sediments can be effectively treated by exposure to diluted hydrogen sulfide gas and (ii) if H_2S-treated sediments can effectively retard the migration of Cr, Tc, and U in solutions that may potentially infiltrate through the treated zone. If so, In Situ Gaseous Reduction (ISGR) may have broad applications for reducing the migration of Cr, Tc, and U in the vadose zone. Both contaminated and uncontaminated soil samples from the Hanford Site are used for assessing the treatment efficiencies. Possible applications at the Hanford Site include the treatment of contamination existing beneath several single-shell tanks and the prevention of further release of contamination during closure of the tanks.

Previous field and laboratory testing activities have shown that Cr(VI) species in soil can be efficiently reduced to Cr(III) forms by ISGR treatment and thereby immobilized (Thornton et al. 1999). It is unclear whether Tc and U can be similarly immobilized by H_2S reduction. In addition, while Cr is likely to remain in the immobilized forms once reduced, Tc and U are subject to reoxidation. Thus permanent immobilization of Tc and U by reduction may not be possible. However, reaction of hydrogen sulfide with sediments also results in the reduction of the sediment matrix. In particular, ferric iron is reduced to ferrous iron. A significant increase in the reductive capacity of the sediment can potentially serve as a vadose zone permeable reactive barrier (PRB). If the reductive capacity of the treated zone is sufficiently high, the oxidation potential may remain low enough to immobilize technetium and uranium, as well as chromium, for years. Previous testing activities have also revealed that immobilization of contamination occurs after gaseous treatment due to the formation of coatings on grain surfaces (Thornton and Amonette 1999; see also Szecsody et al. 1998).

ISGR treatment of the vadose zone under the waste tanks thus can have two different applications. The first is to immobilize or stabilize pre-existing contamination present in the vadose zone. This process involves reduction of Cr, Tc, and U, and possible sequestration by development of treatment product coatings or precipitates. It is known that Cr(VI) can be immobilized through reduction. Here we report the preliminary studies on the reduction of Tc and U and possible sequestration in the contaminated soils at the Hanford site.

A second possible application is to create a permeable reactive barrier, which arises from the reduction of the ferric iron component of vadose zone sediments to the ferrous state. This provides a means for capturing contamination that may subsequently enter the treated zone owing to possible future releases of contamination from a waste tank. Thus, emplacement of the permeable reactive barrier by in situ gaseous treatment can be undertaken as part of a leak mitigation program. The work reported here focuses on assessing the effectiveness of a vadose zone ISGR PRB for capturing contaminants that may be released from a tank as the result of a containment failure.

Assessing the longevity of the treatment for the contaminant immobilization is a critical issue. A test lasting 835 days was performed to see whether reoxidation of Cr could occur in H_2S-treated soils from the Hanford site.

GASEOUS TREATMENT OF Tc-CONTAMINATED SEDIMENT

Approach and testing procedure: To assess the viability of immobilizing technetium, it is necessary to address several questions. It must be determined, first, if technetium in a sediment sample can be immobilized and reduced from the +VII to +IV oxidation state by treating with diluted hydrogen sulfide. Secondly, it is necessary to determine if technetium will remain immobilized as the sediment is reoxidized. If the technetium is remobilized, it is necessary to determine the rate of release of technetium during the oxidative process. Finally, it is also important to determine if technetium can be efficiently removed from solutions that may later pass through the treated sediment. The testing approach used to answer the first question posed above involved conducting column tests with Tc-contaminated sediment, as described below. In these tests, technetium-contaminated sediment was treated with diluted hydrogen sulfide. Treated and untreated sediments were then leached with water and the rate of sediment reoxidation and technetium release was monitored.

The Tc-contaminated sediment used in these tests was provided by the CH2M Hill Hanford Group and was collected from borehole 299 W23-19 (B8809), located at the south end of the Waste Management Area (WMA) S-SX Tank Farm at the Hanford Site (Serne et al. 2002). Sediment was taken from four sleeves collected in the interval between 126 and 130 ft below ground surface and composited. The sediment in this interval of the borehole has been determined to contain 0.02 to 0.03 ug/g (350 to 500 pCi/g) technetium-99. The sediment also contains high concentrations of soluble nitrate (700 to 4,000 ug/g) and calcium (10,000 to 15,000 ug/g).

The testing performed involved packing four columns with the Tc-contaminated sediment. The columns were 2.5 cm in diameter and 12 cm in length. One of these columns was the untreated control and was leached with oxygenated water at a flow rate of 0.4 ml/min (approximately one pore volume per hour) using a Gilson HPLC pump. Effluent samples were collected and analyzed for technetium by ICP-MS to determine the total leachable technetium and the rate of release of technetium from untreated sediment.

The second column was treated with hydrogen sulfide diluted in air and the third and fourth with hydrogen sulfide diluted in nitrogen through the use of flow controllers (Figure 6-1). Gas sources included cylinders of nitrogen and air and a small cylinder of 1% hydrogen sulfide in nitrogen. A 200-ppm hydrogen sulfide mixture was prepared by dilution and passed through the column being treated at a flow rate of 300 ml/min. Breakthrough of hydrogen sulfide at the column outlet was monitored using an EIT hydrogen sulfide sensor. The treated columns were then leached and reoxidized with aerated water (Figure 6-2) that was equilibrated with a gas standard containing 21% oxygen in nitrogen. The column effluent was passed through an oxygen electrode to obtain the oxygen content of the effluent and samples were collected for analysis by ICP-MS. The concentration of technetium in the effluent from the treated columns was compared to that of the untreated column to determine the degree of immobilization associated with gas treatment.

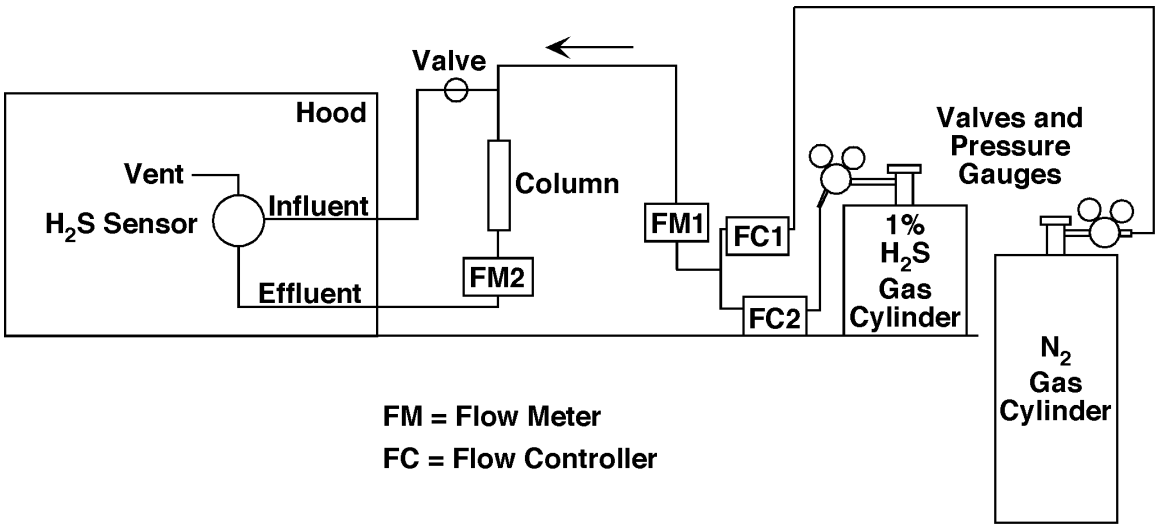

Figure 6-1. Schematic of the Gas Treatment System

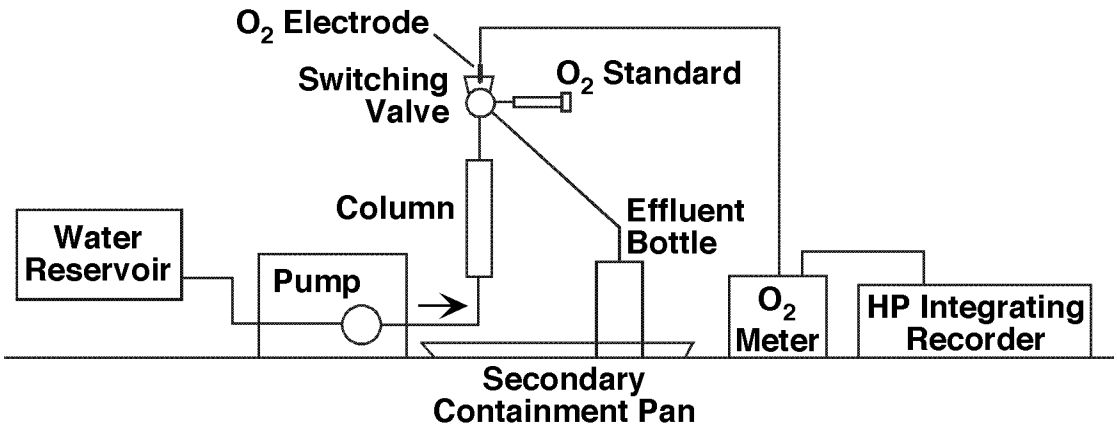

Figure 6-2. Schematic of the Reoxidation System

Results: The release of technetium during leaching of the untreated sediment (test Tc1) is illustrated in Figure 6-3, where the concentration of technetium in the column effluent is plotted versus time. Note that a concentration of 155 ug/l technetium was measured in the first sample, which represented the first 0.4 column pore volumes, and was much lower in subsequent samples. Technetium was not detected in samples collected after 6 hours (6 column pore volumes) into the test, which continued for two weeks. A cumulative amount of 0.020 ug technetium was leached per gram of sediment. About 98% of this was leached from the column in the first sample (0 to 0.4 column pore volumes).

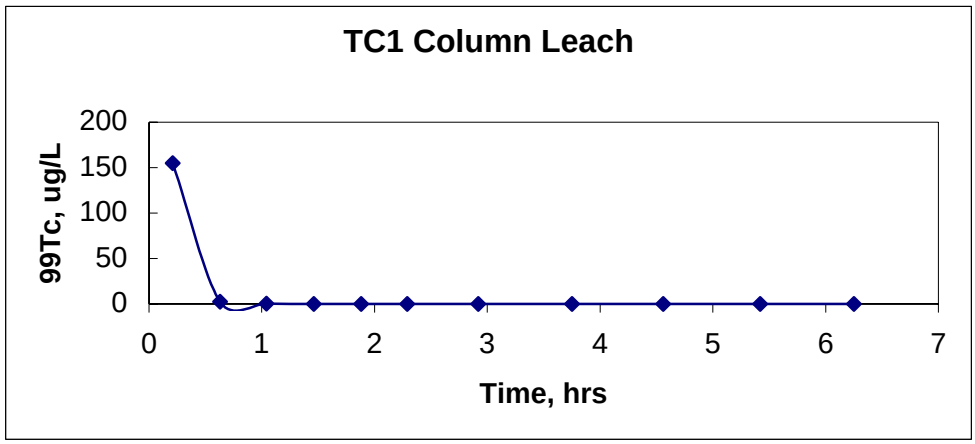

Figure 6-3. Release of Tc-99 from the Untreated Sediment

The second column was treated with 200-ppm hydrogen sulfide in air at a gas flow rate of 300 sccm during test TcA1. The breakthrough of hydrogen sulfide is illustrated in Figure 6-4 as the ratio of effluent concentration, C, to influent concentration, C_o. Gas treatment was performed over period of 73.5 hours, although most of the consumption of hydrogen sulfide occurred in the first 24 hours. A cumulative amount of 1.24 x 10^{-5} moles of hydrogen sulfide was consumed per gram of sediment. The treated sediment was then leached with aerated water. The oxygen concentration of the effluent from the column was similar to that of the influent, indicating that no reductive capacity was generated in the sediment as the result of H_2S/air treatment.

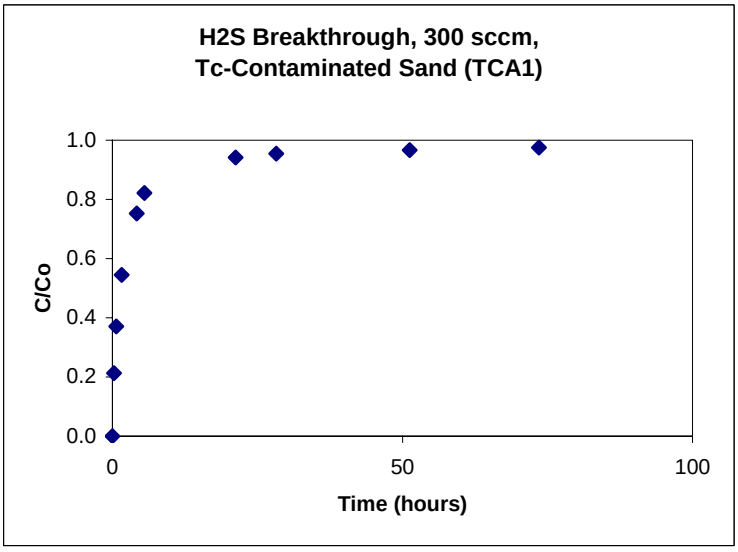

Figure 6-4. Breakthrough of Hydrogen Sulfide During Treatment Test TcA1

The release of technetium from the column during the water-leaching step is shown in Figure 6-5. The concentration of technetium in the first effluent sample (0.4 column pore volumes) was 34.4 ug/L, about 22% of that of the first sample collected from test Tc1. Technetium continued to be

released over much of the two-week duration of leaching but was below the limits of detection (0.02 ug/l) by the end of the test. A cumulative amount of 0.0107 ug technetium was leached per gram of sediment. Thus about 49% of the technetium was immobilized as a result of gas treatment, based on the amount of technetium released in this test relative to water-leaching results obtained for the test with the untreated sediment.

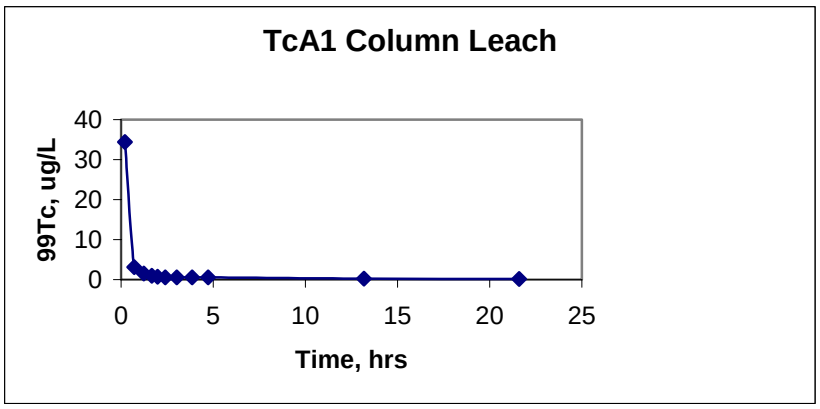

Figure 6-5. Release of Tc-99 During Leaching of the H_2S/Air Treated Sediment

The third and fourth columns were treated with 200-ppm hydrogen sulfide in nitrogen at a gas flow rate of 300 sccm during duplicate tests TcN1 and TcN2. Gas treatment was conducted over a period of 69.33 hours in test TcN1 with most of the consumption of hydrogen sulfide again taking place within the first 24 hours (Figure 6-6). A cumulative total of 9.26×10^{-6} moles of hydrogen sulfide were consumed per gram of sediment. The reoxidation of the treated sediment is illustrated in Figure 6-7 for test TcN2 and illustrates that a significant amount of reductive capacity was generated as a result of treatment of the sediment with the H_2S/N_2 gaseous mixture. The release of technetium from the column during the water-leaching step is shown in Figure 6-8 for test TcN1. The concentration of technetium in the first effluent sample (0.4 column pore volumes) was 10.1 ug/L, about 6.5% of that of the first sample collected from test Tc1. Technetium continued to also be released from this experiment over the two-week duration of leaching, but decreased to a concentration of only 0.03 ug/l by the end of the test. A cumulative amount of 0.00947 ug technetium was leached per gram of sediment. Thus about 51% of the technetium was immobilized as a result of gas treatment, based on the amount of technetium released in this test relative to water-leaching results obtained for the test with the untreated sediment.

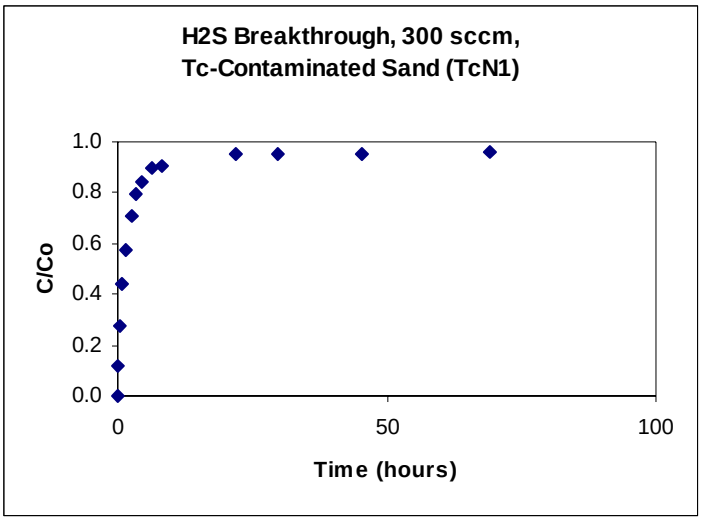

Figure 6-6. Breakthrough of Hydrogen Sulfide During Treatment Test TcN1

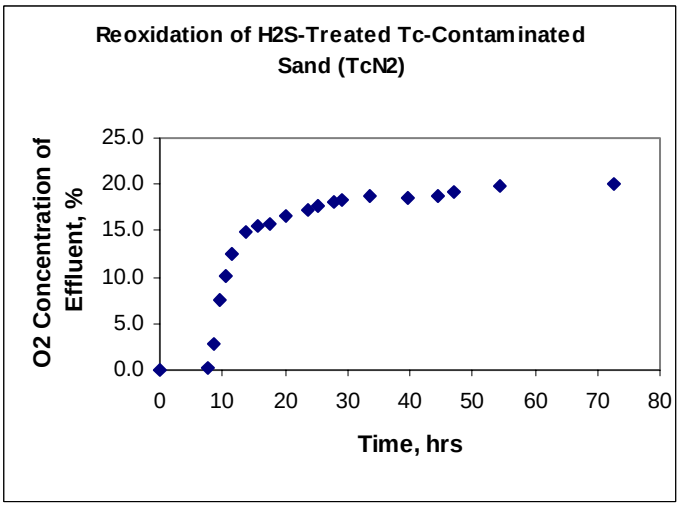

Figure 6-7. Oxygen Breakthrough During the Reoxidation Step of Test TcN2

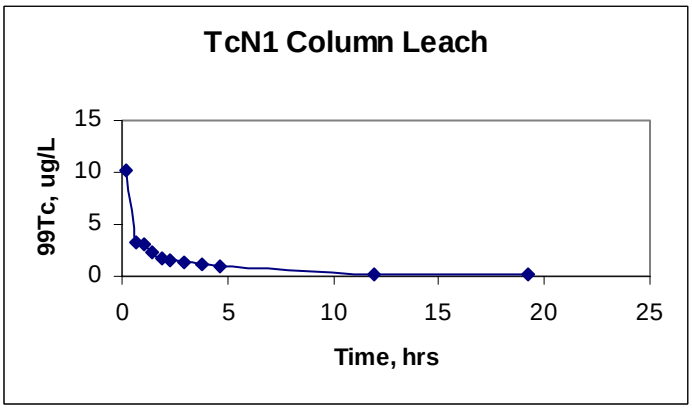

Figure 6-8. Release of Tc-99 During Leaching of the H_2S/N_2 Treated Sediment

Conclusions: The results obtained during this study indicate that ~50% of the technetium present in the contaminated sediment was immobilized by treatment with diluted hydrogen sulfide. The amount released in the first 0.4 column pore volumes during water leaching of the sediment treated with H_2S/air was about 22% of the untreated control. About 6.5% was released from the sediment treated with H_2S/N_2 relative to the control. No reductive capacity was produced as a result of treatment of the sediment with H_2S/air. A limited amount of reductive capacity was generated by treatment with H_2S/N_2, but oxygen breakthrough resulted in only about 8 hours. The relatively low reductive capacity of the H_2S/N_2 treated sediment may be related to a low available iron content for the sediment. Previous tests with Hanford sediment typically indicates that about 30 column pore volumes of aerated water can be pumped through H_2S/N_2 treated sediment prior to oxygen breakthrough. The color of this sediment is pale gray, suggesting that the iron oxide content is low. The relatively high flow rate (0.4 ml/min) used during the reoxidation/leaching stage of test TcN2 may also have resulted in a measured reductive capacity less than the true reductive capacity.

It is concluded that treatment of the vadose zone with H_2S/air could provide a means of partially stabilizing technetium contamination present beneath a tank. The partial immobilization of technetium observed in the H_2S/air treatment test may be due to the incorporation of reduced technetium in iron oxide product phases or perhaps through formation of a coating (e.g., elemental sulfur). These processes would result in the retardation of transport of technetium through the vadose zone and lowering of the concentration levels ultimately reaching groundwater. Thus, the level of risk to groundwater associated with technetium would be reduced because concentration levels and total mass of technetium ultimately reaching the groundwater would be reduced. Treatment of the vadose zone with H_2S/air would not be useful in generating a permeable reactive barrier, however, since no reductive capacity appears to result from treatment of sediment with this mixture.

Treatment with H_2S/N_2, however, may serve to stabilize technetium contamination present in the vadose zone as well as creating a permeable reactive barrier. Stabilization of existing contamination could occur owing to the reduction of technetium and the generation of products sequestering technetium. The generation of a permeable reactive barrier would result from the reductive capacity generated by reduction of the iron component present in vadose zone sediments, as indicated by the testing results presented above. The longevity of the barrier would be a function of the reducible iron content of the sediment and the rate of barrier reoxidation. Barrier reoxidation will occur in response to the flux of oxygen through the barrier, which is related to water infiltration rates and the diffusion of oxygen through the vadose zone. Thus an estimate of barrier lifetime can be obtained based on a laboratory-measured reductive capacity of treated sediment in conjunction with information regarding vadose zone characteristics at a site where gaseous treatment is to be undertaken.

GASEOUS TREATMENT OF U-CONTAMINATED SEDIMENT

Approach and testing procedure: To assess the viability of immobilizing uranium, it is necessary to address several questions. It must be determined, first, if U in a sediment sample can be immobilized and reduced from the +VI to +IV oxidation state by treating with diluted hydrogen sulfide. Secondly, it is necessary to determine if U will remain immobilized as the sediment is reoxidized. If U is remobilized, it is necessary to determine the rate of release of U during the oxidative process. Finally, it is also important to determine if U can be efficiently removed from solutions that may later pass through the treated sediment. The testing approach used to answer the first question posed above involved conducting column tests with U-

contaminated sediment, as described below. In these tests, U-contaminated sediment was treated with diluted hydrogen sulfide. Treated and untreated sediments were then leached with water and the rate of sediment reoxidation and uranium release was monitored.

The U-contaminated sediment used in these tests was provided by the CH2M Hill Hanford Group and was collected from borehole BX102, located in Waste Management Area (WMA) BX Tank Farm at the Hanford Site. Sediment was taken from a composite of sleeves 78A, 78B, 78C, and 78D collected in the depth range of 159 to 161 below ground surface and located in the Hanford formation H2 Unit middle sand sequence. The total uranium content of the sediment is about 150 ug/g. The sediment contains low to non-detect concentrations of water-extractable Tc-99 (<0.001 ug/g) and Cr (<0.05 ug/g).

The testing performed involved packing three columns with the U-contaminated sediment. The columns were 2.5 cm in diameter and 12 cm in length. One of these columns was an untreated control and was leached with aerated water at a flow rate of 0.4 ml/min (approximately one pore volume per hour) using a Gilson HPLC pump. Effluent samples were collected and analyzed for uranium by ICP-MS to determine the total leachable uranium and the rate of release of uranium from untreated sediment.

The second column was treated with hydrogen sulfide diluted in air and the third with hydrogen sulfide diluted in nitrogen through the use of flow controllers. Gas sources included cylinders of nitrogen and air and a small cylinder of 1% hydrogen sulfide in nitrogen. A 200-ppm hydrogen sulfide mixture was prepared by dilution and passed through the column being treated at a flow rate of 300 ml/min. Breakthrough of hydrogen sulfide at the column outlet was monitored using an EIT hydrogen sulfide sensor. The treated columns were then leached and reoxidized with aerated water. The column effluent was passed through an oxygen electrode to obtain the oxygen content of the effluent, and samples were collected for analysis by ICP-MS. The concentration of uranium in the effluent from the treated columns was compared to that of the untreated column to determine the degree of immobilization associated with gas treatment.

Results: The release of uranium during leaching of the untreated sediment (test U2) is illustrated in Figure 6-9, where the concentration of uranium in the column effluent is plotted versus time. A concentration of 7928 ug/l uranium was measured in the first sample, which represented the first 0.7 column pore volumes, and gradually declined in subsequent samples. Uranium was detected in samples collected for the duration of the test, which continued for two weeks. However, a steady state concentration of about 40 ug/L U-238 was observed after the first six days of leaching. A cumulative amount of 9.05 ug uranium was leached per gram of sediment. Thus, most of the uranium appears to be present in mineral phases of low solubility (the total uranium content is about 150 ug/g).

The second column was treated with 200-ppm hydrogen sulfide in air at a gas flow rate of 300 sccm during test UA1. The breakthrough of hydrogen sulfide is illustrated in Figure 6-10 as the ratio of effluent concentration, C, to influent concentration, C_o. Gas treatment was performed over period of 102.9 hours, although most of the consumption of hydrogen sulfide occurred in the first 24 hours. A cumulative amount of 8.55×10^{-6} moles of hydrogen sulfide was consumed per gram of sediment. The treated sediment was then leached with aerated water. The oxygen concentration of the effluent from the column was similar to that of the influent, indicating that no reductive capacity was generated in the sediment as the result of H_2S/air treatment. The release of uranium from the column during the water-leaching step is shown in Figure 6-11. The concentration of technetium in the first effluent sample (0.7 column pore volumes) was 8741 ug/L, similar to that of the first sample collected from test U2. Uranium continued to be released

over much of the two-week duration of leaching and was at a level of about 25 ug/L by the end of the test. A cumulative amount of 7.66 uranium was leached per gram of sediment. Thus only about 15% of the uranium was immobilized as a result of gas treatment, based on the amount of uranium released in this test relative to water-leaching results obtained for the test with the untreated sediment.

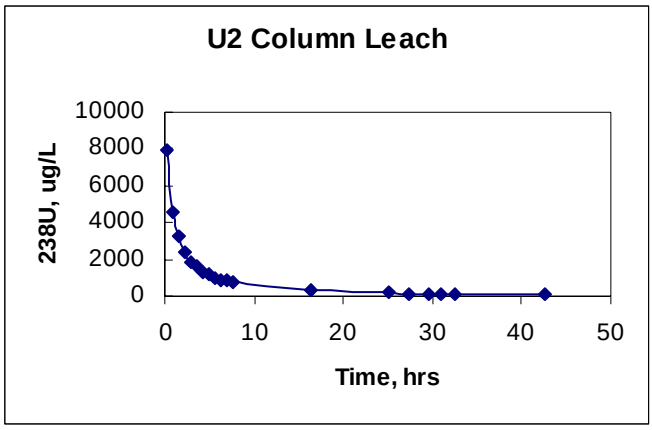

Figure 6-9. Release of U-238 from the Untreated Sediment during Water Leaching

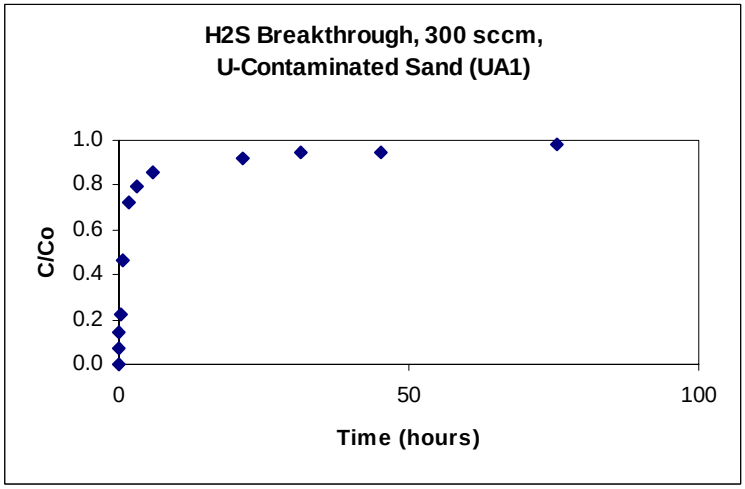

Figure 6-10. Breakthrough of Hydrogen Sulfide During Treatment Test UA1

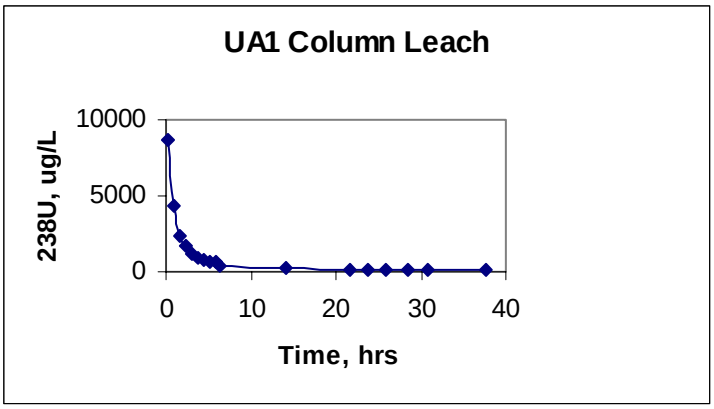

Figure 6-11. Release of U-238 During Leaching of the H_2S/Air Treated Sediment

The third column was treated with 200-ppm hydrogen sulfide in nitrogen at a gas flow rate of 300 sccm during test UN1. Gas treatment was conducted over a period of 102.3 hours in test UN1 with most of the consumption of hydrogen sulfide again taking place within the first 24 hours (Figure 6-12). A cumulative total of 1.26 x 10^{-5} moles of hydrogen sulfide were consumed per gram of sediment. The reoxidation of the treated sediment is illustrated in Figure 6-13 for test UN1 and illustrates that a significant amount of reductive capacity was generated as a result of treatment of the sediment with the H_2S/N_2 gaseous mixture (1.58 x 10^{-6} moles of O_2 was consumed per gram of sediment during reoxidation). The release of uranium from the column during the water-leaching step is shown in Figure 6-14 for test UN1. The concentration of uranium in the first effluent sample (0.7 column pore volumes) was 2349 ug/L, about 30% of that of the first sample collected from test U2. Uranium continued to be released over the two-week duration of leaching and appeared to reach a steady state level of about 40 ug/L at the end of the test. A cumulative amount of 8.24 ug of uranium was leached per gram of sediment versus 9.05 for the untreated sample. Thus less than 10% of the uranium was immobilized as a result of gas treatment, based on the amount of technetium released in this test relative to water-leaching results obtained for the test with the untreated sediment.

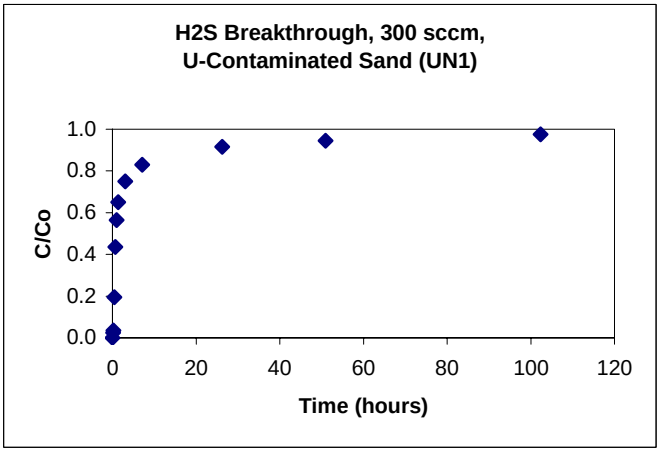

Figure 6-12. Breakthrough of Hydrogen Sulfide During Treatment Test UN1

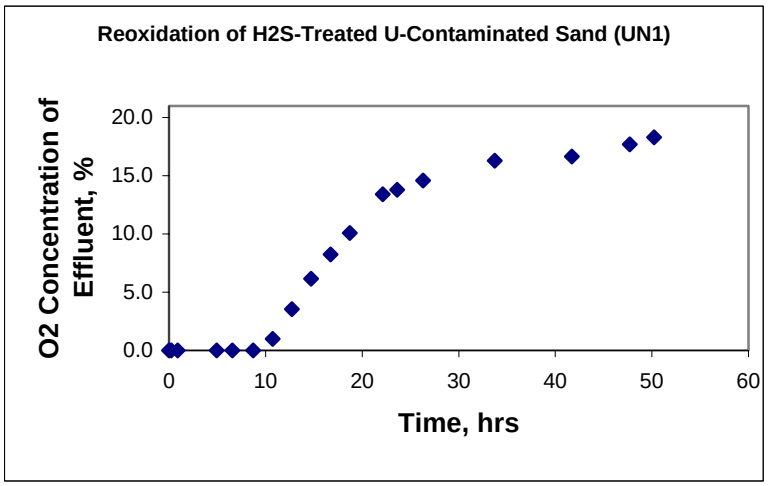

Figure 6-13. Oxygen Breakthrough During the Reoxidation Step of Test UN1

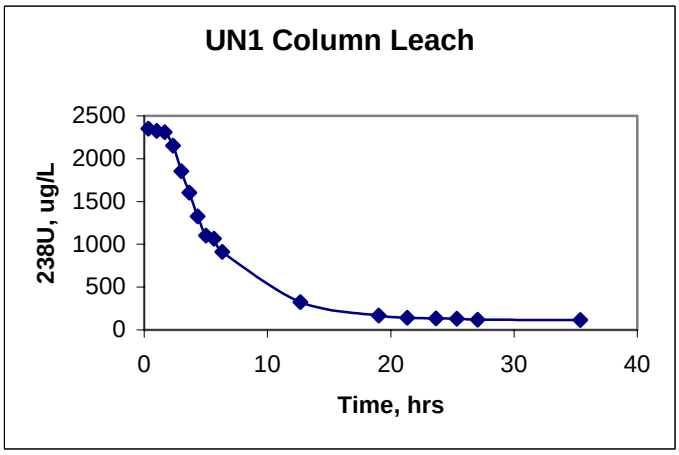

Figure 6-14. Release of U-238 During Leaching of the H_2S/N_2 Treated Sediment

Conclusions: The results obtained during this study indicate that only about 10% of the uranium present in the contaminated sediment was immobilized by treatment with diluted hydrogen sulfide. The amount released in the first 0.7 column pore volumes during water leaching of the sediment treated with H_2S/N_2 was about 30% of the untreated control, however. No reductive capacity was produced as a result of treatment of the sediment with H_2S/air. A limited amount of reductive capacity was generated by treatment with H_2S/N_2, though oxygen breakthrough resulted in only about 10 hours. The relatively low reductive capacity of the H_2S/N_2 treated sediment may be related to a low available iron content for the sediment. In addition, a relatively high flow rate (0.4 ml/min) was maintained during the reoxidation/leaching stage of test UN1 and the total reductive capacity may be larger than was measured.

It is concluded that treatment of the vadose zone with H_2S/air would probably not provide a means of stabilizing uranium contamination present beneath a tank. Treatment with H_2S/N_2, however, may serve to stabilize uranium contamination present in the vadose zone to some extent

as well as creating a permeable reactive barrier. Stabilization of existing contamination could occur owing to the reduction of uranium and the generation of products sequestering uranium. The generation of a permeable reactive barrier would result from the reductive capacity generated by reduction of the iron component present in vadose zone sediments, as indicated by the testing results presented above. The longevity of the barrier would be a function of the reducible iron content of the sediment and the rate of barrier reoxidation. Barrier reoxidation will occur in response to the flux of oxygen through the barrier, which is related to water infiltration rates and the diffusion of oxygen through the vadose zone. Thus an estimate of barrier lifetime can be obtained based on a laboratory-measured reductive capacity of treated sediment in conjunction with information regarding vadose zone characteristics at a site where gaseous treatment is to be undertaken.

EVALUATION OF THE ISGR PRB CONCEPT FOR IMMOBILIZATION OF CHROMIUM, TECHNETIUM, AND URANIUM IN THE VADOSE ZONE

Approach and testing procedure: The uncontaminated sediment used in these tests was provided by the CH2M Hill Hanford Group and is referred to as the "borehole fine sand". It was collected during the drilling of well 299-W22-50, located just southeast of the Waste Management Area (WMA) SX Tank Farm in the 200 West Area of the Hanford Site (Serne et al. 2002). The sediment was collected in the depth range of 62.5 to 97 feet below ground surface in Hanford formation sand.

The testing performed involved packing two columns with the uncontaminated sediment. The columns were 2.5 cm in diameter and 12 cm in length. One of these columns was used as an untreated control, while the second column was treated with a diluted hydrogen sulfide gas mixture. Gas sources included a cylinder of nitrogen and a small cylinder of 1% hydrogen sulfide in nitrogen. A 200-ppm hydrogen sulfide mixture was prepared by dilution with flow controllers and passed through the column being treated at a flow rate of 300 ml/min. Breakthrough of hydrogen sulfide at the column outlet was monitored using an EIT hydrogen sulfide sensor.

An aerated solution (21.5% O_2) was prepared containing 1 ppm of Cr(VI), 2.4 ppm of Tc(VI), and 0.9 ppm of U(VI) at a pH of 3. This solution was pumped at a flow rate of 0.4 ml/min (approximately one column pore volume per hour) through both columns using a syringe pump for about six days (untreated test) and ten days (treated test). The column effluent was passed through an oxygen electrode to obtain the oxygen content of the effluent. Effluent samples were collected and analyzed for Tc-99 and U-238 by ICP-MS, Cr(total) by ICP-OES, and Cr(VI) by spectrophotometry using EPA Method 7196 (EPA 1992). The concentrations of chromium, technetium, and uranium in the effluent from the treated column were compared to that of the untreated column to determine the degree of immobilization associated with gas treatment.

Results: The concentration of Cr(total), Tc-99, and U-238 in the effluent from the column containing the untreated sediment (test SSC1) is illustrated in Figure 6-15, where the concentration of these constituents is plotted versus time over the period of the test (155 hours). The concentration of Cr in the untreated column effluent ranged from 732 to 1002 ug/L, which was similar to the influent concentration (1 ppm or 1000 ug/L). The samples that were analyzed for Cr(VI) also yielded values in the range from 890 to 980 ug/L, indicating that essentially all of the chromium in the influent and effluent samples was in the hexavalent oxidation state. The

concentration of Tc-99 in the column effluent was also similar to that of the influent (2400 ug/L Tc-99) throughout the test, indicating no adsorption or precipitation processes were occurring. The concentration of U-238 in the untreated column effluent was initially low, <20 ug/L, but increased to about 300 ug/L after several weeks (versus about 900 ug/L U-238 in the influent). It is suggested that U(VI) may have precipitated as a carbonate phase in the column. The pH of the column effluent was near neutral through most of the experiment, due to the high buffering capacity of the sediment, but decreased slowly with time.

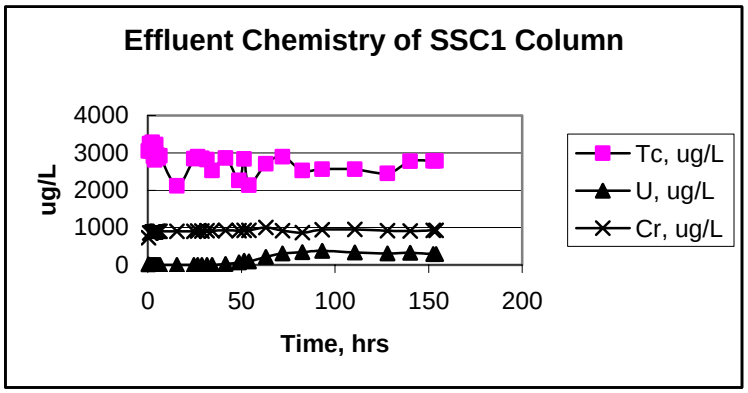

Figure 6-15. Concentration of Cr(total), Tc-99, and U-238 in the Effluent of the Untreated Sediment Column

The second column was treated with 200-ppm hydrogen sulfide in nitrogen at a gas flow rate of 300 sccm (test SSC2). The breakthrough of hydrogen sulfide is illustrated in Figure 6-16 as the ratio of effluent concentration, C, to influent concentration, C_o. Gas treatment was performed over a period of 102.3 hours, although most of the consumption of hydrogen sulfide occurred in the first 24 hours. A cumulative amount of 2.70 x 10^{-3} moles of hydrogen sulfide was consumed per gram of sediment.

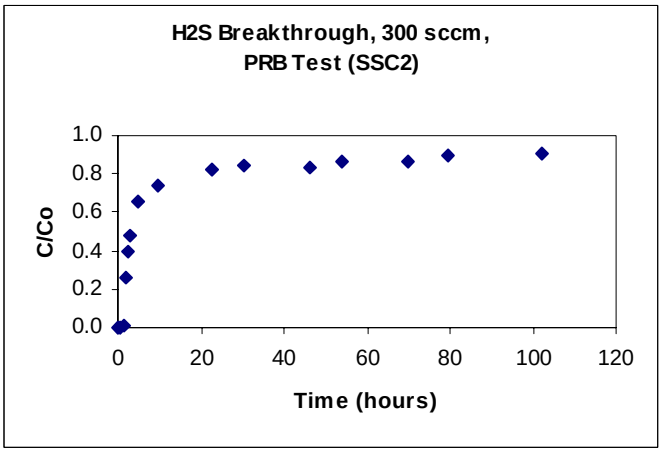

Figure 6-16. Breakthrough of Hydrogen Sulfide During Treatment Test SSC2

The reoxidation of the treated sediment by the aerated solution is illustrated in Figure 6-17 for test SSC2 and illustrates that a significant amount of reductive capacity was generated as a result of treatment of the sediment with the H_2S/N_2 gaseous mixture.

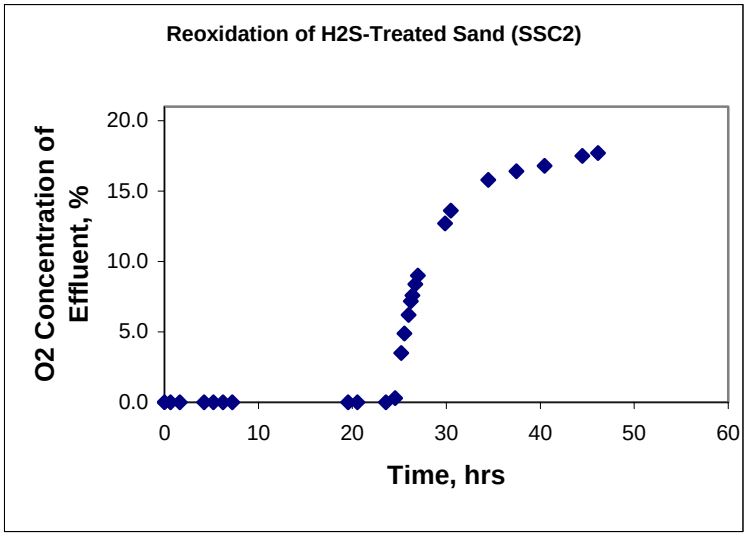

Figure 6-17. Oxygen Breakthrough During the Reoxidation Step of Test SSC2.

The composition of the column effluent is presented in Figure 6-18 for the first 60 hours of the period when the aerated water was pumped through the treated column in test SSC2 (total period = 235 hours). Note that the concentration of Cr(VI) and Cr(total) was low during the period when the system was reduced (prior to 25 hours or about 25 column pore volumes) but increased subsequent to reoxidation (compare figures 6-17 and 6-18). Thus Cr(VI) was reduced and precipitated while the system was depleted of oxygen, but was unaffected once the system became oxygenated. The concentration of technetium in the effluent was only 107 ug/L in the first sample at 0.7 hours but increased as reoxidation progressed and was approximately equal in concentration to the influent (2400 ug/L) at 25 hours. Uranium concentration trends in the column effluents of both tests were similar.

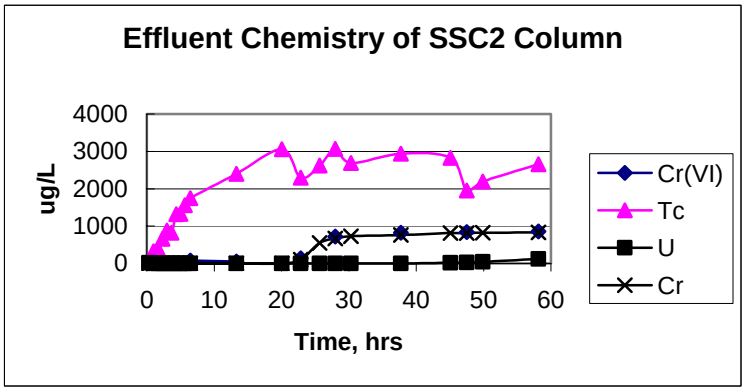

Figure 6-18. Concentrations of Cr(VI), Cr(total), Tc-99, and U-238 in the Effluent of the Treated Sediment Column

Conclusions: The results obtained during this study suggests that a PRB generated by treatment with an H_2S/N_2 gas mixture would be very effective at immobilizing Cr(VI) present in solutions released into the vadose zone. This results from the ease with which Cr(VI) is reduced to Cr(III), which is essentially insoluble. Once reduced, chromium is not readily reoxidized or remobilized. However, the barrier would no longer be effective for reducing additional Cr(VI) once the sediment is reoxidized. The barrier lifetime is estimated to be hundreds to several thousands of years depending on sediment iron content, barrier thickness, and transport rates of oxygen through the vadose zone.

These results also indicate that limited immobilization can be achieved for Tc(VII) using an ISGR vadose zone PRB. It appears the degree of immobilization is high when the reductive capacity of the treated sediment is great, but decreases as the sediment is reoxidized. This is related to the lower oxidation potential of the Tc(VII)/Tc(IV) couple relative to that of chromium. It is also important to note that the Tc couple is reversible under natural conditions and thus Tc could be remobilized from the barrier once it is reoxidized. This suggests that an ISGR PRB could be useful as a short term measure for capturing Tc(VII) that might be released during waste tank closure operations. The long-term viability of the barrier, however, is difficult to assess. It is possible that a mid to long-term barrier useable lifetime could be achieved if the barrier is periodically recharged by treatment with additional H_2S.

Uranium was immobilized to a similar extent in both the untreated and treated column tests. The mechanism responsible for the relatively low mobility of U(VI) in these tests is not clear. It is suggested that uranium may have precipitated in the columns as a carbonate or hydroxide phase. Further work is obviously needed to assess the mobility of uranium in terms of the application proposed here.

The results of the proof-of-principle tests performed during this study thus suggest that an ISGR vadose zone PRB could be very effective in immobilizing chromium and, to a lesser extent, technetium. It should be noted that reduction processes are often relatively slow, so a better understanding of barrier effectiveness could be developed if information is gathered regarding the kinetics of the reduction processes involved. In particular, the flow rates utilized in these experiments were relatively high. Performance of additional tests under lower flow rates and a better knowledge of the reaction kinetics involved in immobilization could greatly help in assessing the performance of an ISGR PRB. This is particularly important for assessing the potential for immobilizing technetium in the vadose zone. Assessment of the mobility of uranium with respect to the barrier appears to require a better knowledge of the oxidation-reduction processes and aqueous and solid species involved.

EVALUATION OF THE POTENTIAL FOR LONG-TERM CHROMIUM REOXIDATION IN AN H_2S-TREATED SEDIMENT

Hexavalent chromium in soil is readily reduced to the trivalent oxidation state by reaction with hydrogen sulfide. It is generally regarded as stable in this form in the natural environment and relatively insoluble. In this study, a long-term test has been conducted to provide information regarding whether or not reoxidation of chromium can occur after Cr(VI) is reduced in a contaminated sediment by gas treatment.

In this test, a chromate-contaminated sediment sample collected from the 100K Area at the Hanford Site was treated with diluted hydrogen sulfide gas and then exposed to air under humid conditions. Analysis of the Cr(VI) content of sediment samples was conducted by water leaching for one hour and measurement of Cr(VI) in the leachate by the diphenylcarbazide spectrophotometric method. The untreated sample contains about 110 mg/kg leachable Cr(VI), while the treated sediment was determined to contain 3.3 mg/kg Cr(VI). Characterization of Cr(VI) sediment samples collected in the 100D Area at Hanford suggests that a portion of the Cr(VI) in Hanford Site contaminated sediments may be coprecipitated or sequestered in calcite cement and also as barium chromate. The results of the gas treatment test indicates that immobilization of Cr(VI) to Cr(III) is essentially quantitative despite the fact that a portion of the chromate may be contained in solid waste phases.

The treated sample was exposed to air under humid conditions and sampled periodically and analyzed to determine if the concentration of Cr(VI) changes with time. Results obtained during 835 days of testing are shown in Figure 6-19. Levels of hexavalent chromium in the sediment dropped from about 3.3 mg/kg in the first year to a level ranging from 2.1 to 2.6 mg/kg. Samples collected at 492, 653, and 835 days all contained about 2.1 mg/kg, suggesting a steady state concentration was attained. Data obtained from this test, which exceeded two years in duration, thus suggests that reduced chromium will not reoxidize to the hexavalent state.

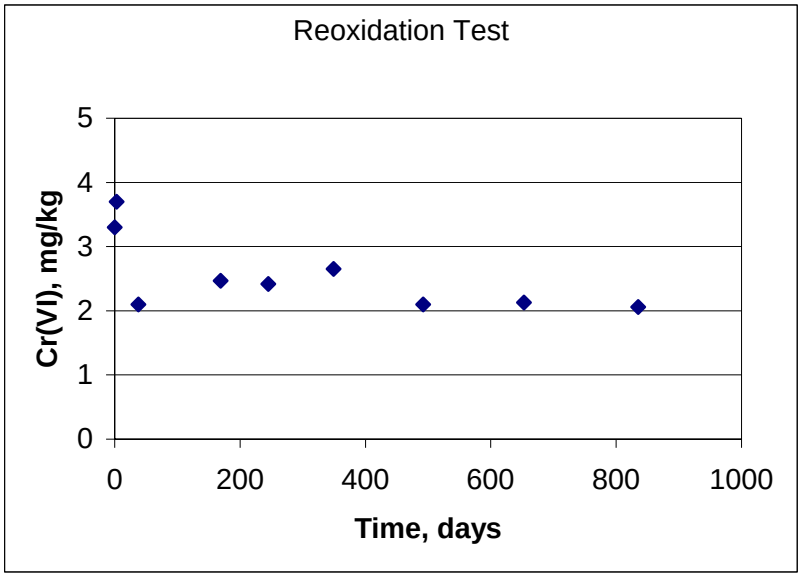

Figure 6-19. Leachable Cr(VI) from a H_2S-treated soil sample as a function of time. The sample contained about 110 mg/kg of leachable Cr(VI) prior to the H_2S treatment.

Information Access

Journal papers:

Kim, C.; Zhou, Q.; Deng, B.; Thornton, E. C.; Xu, H. (2001) "Chromium (VI) Reduction by Hydrogen Sulfide in Aqueous Media: Stoichiometry and Kinetics ", *Environ. Sci. Technol*, Vol. 35, 2219 - 2225.

Deng, B.; Lan, L.; Houston K.; Brady, P. (2002) "Effects of clay minerals on Cr(VI) reduction by organic compounds", *Environmental Monitoring and Assessment*, (in press).

Lan Y.; Kim, C.; Deng, B.; Thornton, E. C. "Chromium(VI) Reduction by Sulfide under Anaerobic Conditions: Catalysis by Elemental Sulfur Product" (In preparation).

Kirk J. Cantrell, Steven B.Yabusaki, Mark H. Engelhard, Alexandre H. Mitroshkov and Edward C. Thornton "Oxidation of H_2S by Iron Oxides in the Vadose Zone" (in preparation).

Lan Y.; Kim, C.; Deng, B.; Thornton, E. C "Influence of mineral surfaces on Chromium(VI) Reduction by Sulfide under Anaerobic Conditions" (in preparation).

Kim, C.; Lan Y.; Deng, B.; Amonette, J. E.; Thornton, E. C. "Cr(VI) reduction in the Cr(VI) goethite-H_2S systems" (in preparation).

Presentations:

Cantrell, K. J.; Yabusaki, S. B.; Mitroshkov, A. V.; Amonette, J. E.; Thornton, E. C. (2001) "H2S Oxidation by Iron Oxide: Experimental Determination of Mechanisms and Rates for Modeling Gas Phase Treatment of the Vadose Zone", Platform Presentation at the 222th ACS National Meeting, Chicago, IL, August 26-30, 2001

Deng, B.; Kim, C.; Lan, Y. and Thornton, E. C. (2001) "Chromium (VI) reduction by hydrogen sulfide in aquatic systems", Platform Presentation at the 222th ACS National Meeting, Chicago, IL, August 26-30, 2001.

Thornton, E. C.; Deng, B.; Cantrell, K. J.; Olsen, K. B.; Amonette, J. E.; Kim, C., Lan, Y. (2001) "Interfacial Reduction-Oxidation Mechanisms Governing Fate and Transport of Contaminants in the Vadose Zone", Poster Presentation at the 222th ACS National Meeting, Chicago, IL, August 26-30, 2001.

Deng, B. (2001) "Redox Processes in the Aquatic Environment: Applications to Site Remediation", EMSL, Pacific Northwest National Laboratory, June 12, 2001.

Deng, B. Kim, C.; Lan, Y.; Thornton, E. C. (2001) "Kinetics Of Cr(VI) Reduction By Hydrogen Sulfide In Aquatic Systems: Direct And Catalyzed Reactions", (Oral Presentation), 11th Goldschmidt Conference, Hot Spring, Virginia, May 20 – 24, 2001

Kim, C.; Lan, Y.; Deng, B.; Thornton, E. C. (2001) "Catalytic Effects of Goethite on Chromium(VI) Reduction by Hydrogen Sulfide in Anaerobic Aqueous Phase", (Oral Presentation), The 221th ACS National Meeting, San Diego, April 1-5, 2001.

Lan, Y.; Kim, C.; Deng, B.; Thornton, E. C. (2001) "Chromium(VI) Reduction by Sulfide under Anaerobic Conditions: Catalysis of Elemental Sulfur Product", (Oral Presentation), The 221th ACS National Meeting, San Diego, April 1-5, 2001.

Zhou, Q.; Kim, C.; Deng, B.; Thornton, E. C. (2000) "Effects of Mineral Surfaces on Chromium(VI) Reduction by Hydrogen Sulfide", Preprints of the Extended Abstracts, Division of the Environmental Chemistry, The 220th ACS National Meeting, Washington D.C. August 20-24, 2000., pp 592 – 593.

Kim, C.; Zhou, Q.; Deng, B.; Thornton, E. C. (2000) "Chromium (VI) Reduction by Hydrogen Sulfide in the Aqueous Phase" Preprints of the Extended Abstracts, Division of the Environmental Chemistry, The 220th ACS National Meeting, Washington D.C. August 20-24, 2000., pp 669-670.

Thornton, E. C.; Cantrell, K. L.; Olsen, K. B.; Amonette, J. E.; Yabusaki, S. B.; Deng, B. (1999) "Laboratory Evaluation of Surface-Catalyzed Reduction Mechanisms in the H_2S-O_2-

Cr(VI)-Sediment System" (Oral Presentation), Geological Society of America Annual Meeting, Denver, CO.

References

Amonette, J. E.; Workman, A.J.;Kennedy, D. W.;Fruchter, J. S.;Gorby, Y. A. *Environmental Science & Technology* 2000, 34, 4606-4613.

Anderson, L. D.; Kent, K. B.; Davis, J. A. *Environ. Sci. Technol.* 1994, *28*, 178-185.

ASME (1999) *Technical Peer Review Report in Assessment of Technologies Supported by the Office of Science and Technology, Department of Energy,* The American Society of Mechanical Engineers.

APHA; AWWA; WPCF *Standard Methods for the Examination of Water and Wastewater*, 20 ed.; American Public Health Association: Washington, D. C., 1998.

Berner R. A. *Am. J. Sci.* 1967, *265*, 773.

Blowes, D. W.; Ptacek, C. J.; Jambor, J. L. *Environ. Sci. Technol.* 1997, *31*, 3348-3357.

Buerge, I. J.; Hug, S. J. *Environ. Sci. Technol.* 1997, *31*, 1426-1432.

Buerge, I. J.; Hug, S. J. *Environ. Sci. Technol.* 1998, *32*, 2092-2099.

Buerge, I. J.; Hug, S. J. *Environ. Sci. Technol.* 1999, *33*, 4285-4291.

Chen, K. Y.; Morris, J. C. *Environ. Sci. Technol*. 1972, *6*, 529-537.

Chilakapati, A. 1995, RAFT A Simulator for ReActive Flow and Transport of Groundwater Contaminants. PNL-10636, Pacific Northwest Laboratory, Richland, Washington.

Chilakapati, A. Ginn, T., Szecsody J. 1998, Water Resour. Res., 34(7), 1767-1780.

Chilakapati, A. Yabusaki, S., Szecsody J., MacEvoy, W. 2000, J. Contamin. Hydrol., 43(3-4), 303-325.

Cline, J. D.; Richards, F. A. *Environ. Sci. Technol.* 1969, *3*, 838-843.

Connett, P. H.; Wetterhahn, K. E. *J. Am. Chem. Soc.* 1985, *107*, 4282-4288.

Costa, M. *Crit. Rev. Toxicol*. 1997, *27*, 431-442.

Davydov, A. D.; Chuang, D. T.; Sanger, A. R. *J. Phys. Chem.* 1998, 102, 4745-4752.

Deng, B. *Chromium(VI) reduction by naturally-occurring organic compounds-Kinetics of direct and surface catalyzed reactions*, Ph.D. thesis, The Johns Hopkins University, 1995.

Deng, B.; Stone, A. T. *Environ. Sci. Technol*. 1996, *30*, 2484-2494.

Deng, B.; Stone, A. T. *Environ. Sci. Technol.* 1996, *30*, 463-472.

Dixon, D. A.; Dasgupta, T. P.; Sadler, N. P. *J. Chem. Soc. Dalton* 1995, *13*, 2267-2271.

Eary, L. E.; Rai, D. *Am. J. Sci.* 1989, *289*, 180-213.

Eary, L. E.; Rai, D. *Environ. Sci. Technol.* 1988, *22*, 972-977.

Eary, L. E.; Rai, D. *Soil Sci. Soc. Amer. J.* 1991, 55, 676-683.

Fendorf, S. E.; Li, G. *Environ. Sci. Technol.* 1996, *30*, 1614-1617.

Fude, L.; Harris, B.; Urrutia, M. M.; Beveridge, T. J. *Appl. Environ. Microbiol*. 1994, *60*, 1525-1531.

Goodgame, D. M. L.; Hayman, P. B. *Inorganica Chimica Acta* 1984, *91*, 113-115.

Hallberg, R. O. *Neues Jahrb. Mineralogie* 1972, *11*, 481.

Heron, G.; Crouzet C.; Bourg, A. C. M.; Christensen, T. H. *Environ. Sci. Technol*. 1994, 28, 1698.

Ilton, E. S.; Veblen, D. R. *Geochim. Cosmochim. Acta* 1994, *58*, 2777-2788.

Ilton, E. S.; Veblen, D. R.; Moses, C. O.; Raebur, S. P. *Geochim. Cosmochim. Acta* 1997, *61*, 3543-3563.

James, B.; Bartlett, R. J. *J. Environ. Qual.* 1983, *12*, 177-181.

Kattner, J. E.; Samuels, A.; Wendt, R. P. *J. Petr. Technol.* 1988-(Sept), 1237.

Katz, S. A.; Salem, H. *The biological and environmental chemistry of chromium*, VCH: New York, NY, 1994.

Kohl, A. L.; Riesefedl, F. S. *Gas Purification;* Gulf: Houston, 1985: Chapter 4.

Lennie, A. R.; Redfern, R. A. T.; Champness, P. E.; Stoddart, C. P.; Schofield, P. F.; Vaughan, D. J. *Am. Mineral.* 1997, *82*, 302.

Lennie, A. R.; Vaughan, D. J. In *Mineral Spectroscopy: A Tribute to Roger G. Burns*; Dyar, M. D.; McCammon, C.; Schaefer, M. W., Eds.; Special Publication No. 5, The Geochemical Society, 1996; p 117.

Levenspiel, O. 1998, Chemical Reaction Engineering, 3rd Ed., John Wiley & Sons, New York, NY.

Loeppert, R. L.; Inskeep, W. P. In *Methods of Soil Analysis, Part 3 – Chemical Methods;* Soil Science Society of America: Madison, WI, 1996; pp 639-664.

Lovley, D.R.; Philips, E. J. P. *Appl. And Environ. Microbiol* 1986, 52, 751-757.

Luther, G. W. III *Geochim. Cosmochim. Acta* 1991, *55*, 2839.

Morse, J. W.; Millero, F. J.; Cornell, J. C.; Rickard, D. *Earth Sci. Rev*. 1987,24,1.

Nriagu, J. O.; Nieboer E. *Chromium in the Natural and Human Environments*, Wiley & Sons: New York, NY, 1988.

O'Brien, D. J.; Birkner, F. G. *Environ. Sci. Technol.* 1977, *11*, 1114-1120.

Patterson, R. R and Fendorf , S. *Environ. Sci. Technol* 1997, 31, 2039-2044.

Perry R. H. and Chilton C. H. Chemical Engineer's Handbook 1973 Fifth Ed. Pg. 4-33, McGraw-Hill, New York.

Peterson, M. L.; Brown, G. E.; Parks, G. A. *J. Phys.* IV 1997, *7(C2)*, 781-783.

Pettine, M.; Barra, I.; Campanella, L.; Millero, F. J. *Wat. Res*. 1998, *32(9)*, 2807-2813.

Pettine, M.; D'Ottone, L.; Campanella, L.; Millero, F. J.; Passino, R. *Geochimica et Cosmochimica Acta* 1998, *62*, 1509-1519.

Pettine, M.; Millero, F. J.; Passino, R. *Marine Chemistry* 1994, *46*, 335-344.

Poeter E. P. and Hill M. C. *Computers and Geosciences* 1999, 25(4), 457-462.

Pratt, A. R.; Blowes, D. W.; Ptacek, C. J. *Environ. Sci. Technol.* 1997, *31*, 2492-2498.

Rai, D.; Sass, B. M.; Moore D. A. *Inorg. Chem.* 1987, 26, 345-349. Chromium(III) hydrolysis constants and solubility of Chromium(III) hydroxide.

Rethmeier, J.; Rabenstein, A.; Langer, M.; Fischer, U. *J. Chrom. A* 1997, *760*, 295-302.

Rickard, D. T. *Am. J. Sci.* 1975, *275*, 636.

Saleh, F. Y.; Parkerton, T. F.; Lewis, R. V.; Huang, J. H.; Dickson, K. L. *Sci. Total Environ.* 1989, 86, 25-41.

Schroeder, D. C.; Lee, G. F. *Water, Air, Soil Pollut.* 1975, *4*, 355-365.

Seaman, J. C.; Bertsch, P. M.; Schwallie, L. *Environ. Sci. Technol.* 1999, *33*, 938-944.

Sedlak, D. L.; Chan, P. G. *Geochim. Cosmochim. Acta* 1997, *61*, 2185-2192.

Serne RJ, HT Schaef, BN Bjornstad, BA Williams, DC Lanigan, DG Horton, RE Clayton, VL LeGore, MJ O'Hara, CF Brown, KE Parker, IV Kutnyakov, JN Serne, AV Mitroshkov, GV Last, SC Smith, CW Lindenmeier, JM Zachara, and DB Burke. 2002. *Characterization of Uncontaminated Vadose Zone Sediment from the Hanford Reservation - RCRA Borehole Core Samples and Composite Samples*. PNNL-13757-1, Pacific Northwest National Laboratory, Richland, Washington.

Shi, X. L.; Chiu, A.; Chen, C. T.; Halliwell, B.; Castranova, V.; Vallyathan, V. *J. Toxicol. & Environ. Health B-Crit. Rev.* 1999, *2*, 87-104.

Smillie, R. H.; Hunter, K.; Loutit, M. *Water Res*. 1981, *15*, 1351-1354.

Stumm, W.; Morgan, J. J. *Aquatic chemistry; Chemical equilibria and rates in natural waters,* 3rd Ed. Wiley Interscience, 1996.

Szecsody J. E, K. J. Cantrell, K. M. Krupka, C. T. Resch, M. D. Williams, and J. S. Fruchter. 1998. *Uranium Mobility During In Situ Redox Manipulation of the 100 Areas of the Hanford Site.* PNL-12048, Pacific Northwest Laboratory, Richland, Washington.

Szecsody, J. E.; Zachara J. M.; Bruckhart P. L. *Envir. Sci. Tech.* 1994, 28(9), 1706-1716.

Thornton, E. C.; Amonette, J. E. *Environ. Sci. Technol*. 1999, *33*, 4096-4101.

Thornton, E. C.; Amonette, J. E. *Gas treatment of Cr(VI)-contaminated sediment samples from the north 60's pits of the chemical waste landfill*; PNNL-11634, Pacific Northwest National Laboratory: Richland, WA, 1997.

Thornton, E.C., J.T. Giblin, T.J. Gilmore, K.B. Olsen, J.M. Phelan, and R.D. Miller (1999) *In Situ Gaseous Reduction Pilot Demonstration – Final Report*. PNNL-12121, Pacific Northwest National Laboratory.

U.S. Environmental Protection Agency (1992) *Test Methods for Evaluating Solid Wastes: Physical/Chemical Methods, 3rd ed.* SW-846, Office of Solid Waste and Emergency Response, Washington, D.C.

Wieckowska, J. *Catalysis Today 1995, 24, 405-465.*

Wittbrodt, P. R.; Palmer, C. D. *Environ. Sci. Technol.* 1995, *29*, 255-263.

Xu, F. ;Wang, Y. J. Nuclear Materials, 2000, *279*, 100-1-6.

Zhang, J.; Millero, F. J. *Geochim. Cosmochim. Acta* 1993, *57*, 1705-1718.